The International Journal of Advanced Manufacturing Technology (2023) 127:987–1043
https://doi.org/10.1007/s00170-023-11566-z

CRITICAL REVIEW

Surface roughness of as-printed polymers: a comprehensive review

Ali Payami Golhin[1] · Riccardo Tonello[2] · Jeppe Revall Frisvad[2] · Sotirios Grammatikos[1] · Are Strandlie[1]

Received: 6 January 2023 / Accepted: 5 May 2023 / Published online: 27 May 2023

Abstract
Surface roughness is gaining increasing recognition in the processing design methods of additive manufacturing (AM) due to its role in many critical applications. This impact extends not only to various AM product manufacturing but also to indirect applications, such as molding and casting. This review article discusses the role of processing on the surface roughness of AM-printed polymers with limited post-processing by summarizing recent advances. This review offers a benchmark for surface quality improvement of AM processes, considering the surface roughness of polymeric parts. For this purpose, it lists and analyzes the key processes and various printing parameters used to monitor and adjust surface roughness under given constraints. Four AM techniques for manufacturing polymeric parts are compared: fused filament fabrication (FFF), selective laser sintering (SLS), vat photopolymerization (VPP), and material jetting (MJT). A review and discussion of recent studies are presented, along with the most critical process parameters that affect surface roughness for the selected AM techniques. To assist in selecting the most appropriate method of 3D printing, comparable research summaries are presented. The outcome is a detailed survey of current techniques, process parameters, roughness ranges, and their applicability in achieving surface quality improvement in as-printed polymers.

Keywords Additive manufacturing · 3D printing parameters · Polymer · Surface roughness · Surface quality

Abbreviations

3DP	3D printing
ABS	Acrylonitrile butadiene styrene
AM	Additive manufacturing
ANN	Artificial neural networks
ANOM	Analysis of means
ANOVA	Analysis of variance
ASA	Acrylonitrile styrene acrylate
BJT	Binder jetting
CAD	Computer-aided design
CAM	Computer-aided modeling
CB	Carbon black
CLIP	Continuous liquid interface production
CLSM	Confocal laser scanning microscope
CMYK-W	Cyan, magenta, yellow, black, and white
DfAM	Design for additive manufacturing
DIW	Direct-ink-writing
DLP	Digital (direct) light processing
DM	Digital material
DMD	Digital micromirror device
DoE	Design of experiment
DTAM	Digital thread in additive manufacturing
ED	Energy density
FDM	Fused deposition modeling
FEP	Fluorinated ethylene propylene
FFF	Fused filament fabrication
FPT	Fringe projection technique
FR	Flame retardant
FV	Focus variation
GF	Glass fiber
GLM	Generalized linear model

✉ Ali Payami Golhin
ali.p.golhin@ntnu.no

Riccardo Tonello
rict@dtu.dk

Jeppe Revall Frisvad
jerf@dtu.dk

Sotirios Grammatikos
sotirios.grammatikos@ntnu.no

Are Strandlie
are.strandlie@ntnu.no

[1] ASEMlab - Laboratory of Advanced and Sustainable Engineering Materials, Department of Manufacturing and Civil Engineering, NTNU - Norwegian University of Science and Technology, Gjøvik, Norway

[2] Department of Applied Mathematics and Computer Science, DTU - Technical University of Denmark, Kgs. Lyngby, Denmark

HDDA	Hexanediol diacrylate
HDPE	High-density polyethylene
HL	Hot lithography
LCD	Light crystal display
LOM	Laminated object manufacturing
LW	Laser writing
MCDM	Multi-criteria decision-making
MEX	Material extrusion additive manufacturing
MJF	Multi jet fusion
MJP	Multi jet printing
MJT	Material jetting
MW	Mask-based writing
PA	Polyamides
PAEK	Polyaryletherketone
PBF	Powder bed fusion
PBS	Polybutylene succinate
PC	Polycarbonate
PCL	Polycaprolactone
PDMS	Polydimethylsiloxane
PE	Polyethylene
PEEK	Polyetheretherketone
PEI	Polyetherimide
PEKK	Polyetherketoneketone
PET	Polyethylene terephthalate
PLA	Polylactic acid
PMMA	Polymethyl methacrylate
PP	Polypropylene
PPFT	Post-production finishing techniques
PPP	Primary processing parameters
PPSF	Polyphenylsulfone
PRISMA-ScR	Preferred reporting items for systematic reviews and meta-analyses extension for scoping reviews
PS	Polystyrene
PSO	Particle swarm optimization
PTFE	Polytetrafluoroethylene
PVC	Polyvinyl chloride
QAs	Quality attributes
RRP	Roughness reduction percentage
RSM	Response surface methodology
SEM	Scanning electron microscope
SHL	Sheet lamination
SHS	Selective heat sintering
SLA	Stereolithography
SLS	Selective laser sintering
SOS	Symbiotic organism search
TPP	Two-photon photopolymerization
TPU	Thermoplastic polyurethane
UAV	Unmanned aerial vehicle
VPP	Vat photopolymerization
XMT	X-ray micro-computed tomography

1 Introduction

Additive manufacturing (AM), often known as 3D printing, combines materials to fabricate products from 3D model data, typically in a layer-upon-layer process [1]. AM has continued its exponential growth in many applications because of its attributes, such as mass customization, waste minimization, and on-demand design revisions [2]. However, AM parts cannot precisely replicate 3D CAD models due to the inherent surface roughness and accuracy limitations of the AM process. In-process enhancing the quality of the surface in AM technology is presently one of the most significant challenges of advanced manufacturing. It is a critical element for compatibility with surface coatings, the fatigue resistance of the products, liquid trapping, and the presence of moving particles [3].

Recently, the influence of the primary processing parameters (PPP) on the quality assessment of 3D-printed (3DP) objects has received considerable attention from academia and industry, mainly because optimizing these PPPs provides more fabrication competence based on mass customization, on-demand design revisions, and waste minimization. Enhancing the 3D model, material and process selection, and surface modification can satisfy the performance constraints of the 3DP parts, such as tooling [4], jewelry [5], sensors [6], performance improvement, production, personalization and customization, spare parts, maintenance, repair, art, design, and architecture [7]. Considering the growing applications of personal 3D printers (shortened form as "printer") and the small-scale market for AM technologies, it is increasingly essential to thoroughly understand the surface morphology created by various 3DP methods. Not surprisingly, most post-processing machines are currently either unavailable or high-priced to most AM users.

Polymers have been the center of attention in fabricating 3D parts because of their cost, availability, ease of production, and appearance options, particularly in the case of entry-level 3DP machines [8, 9]. The Wohlers Report 2021 [10] reported 7.5% growth in AM industry. It shows almost half of AM service providers offer polymer 3D printing, and 29% provide polymers besides other materials, such as metals and ceramics. As a result, over 80% of the AM market is involved with polymeric materials. In addition, polymer powder consumption is mentioned as rising by 43.3% in 2021, overtaking photopolymers as the most commonly used additive manufacturing material. In total, the polymer 3DP market is expected to increase to $24 billion in 2024 and $55 billion in 2030 [11]. Since 2012, 14,150 out of 54,275 (26.1%) publications in the field of additive manufacturing applied to polymer-based techniques (data from Web of Science, 2023). As almost 80% of the AM

market is dedicated to polymer-containing materials, this is still growing, and there is significant potential for future research and development of polymeric AM objects.

The polymeric AM parts suffer from poor surface finish and geometric deviation. Among textural appearance attributes, surface roughness is a critical indicator for assessing the quality of a product and the manufacturing process. For many direct and indirect applications, the surface of the printed object must meet specific criteria and properties such as mechanical [12], physical [13], tribological [12], and other quality attributes (QAs) [14].

Surface roughness is a metric relating to the QAs of AM parts because of its impact on the aesthetic appearance and the integrity of the piece in terms of its ability to interface with other components. It influences not only the appearance but also the functional properties of a part [15].

In most circumstances, the finishing process is rarely used to modify the part dimensions except for reducing the surface roughness via sandblasting and polishing or for structural applications [16]. In some cases, various painting and coating methods are used to achieve the required surface finish. These practices are insufficient to form the printing process and must overcome several challenges. For instance, material accumulation in fused filament fabrication (FFF), as a material extrusion (MEX) AM process, occurs along the edges and inside the products, which cannot be resolved by painting or coating [17, 18]. To choose a process based on the specifications of a part, Gordon et al. [19] provided a decision tree as a framework. They suggested the appropriate design modifications considering the desired surface to account for the selected techniques.

Various kinds of polymers are primarily supplied for AM in the shape of filaments, pellets, resin, or powder [20]. Furthermore, composite polymers reinforced by fibers and particles offer a favorable combination for almost all the existing AM methods [20]. While there are many choices of available AM processes to 3D print polymers, the mechanisms of the different AM methods distinctly differ from one another. Polymers are sensitive to printing parameters, mainly changes in temperature. Hence, the printing process and material should be carefully considered according to the end-user applications [11]. Several review papers have previously discussed roughness in AM processes, including material extrusion [18, 21], vat photopolymerization [22, 23], material jetting [24, 25], and selective laser sintering [26, 27] techniques. However, the reviews have not yet observed a thorough study of methods and quality evaluation trends in AM polymer products.

The AM process for polymers presents different challenges in surface quality than conventional manufacturing. A uniform standard for evaluating the roughness and dimensional accuracy of 3D-printed objects does not exist at present. Studying the surface roughness issues and the various PPP techniques for improving surface quality is also lacking in the literature. The roughness of AM technologies differs considerably, as was reported in this study and in the studies that compared 3DP methods [3, 16, 28].

This study focuses on recent advances in investigating the roughness of 3D-printed surfaces. It describes the primary AM processes for polymers and the corresponding PPP in the pre-processing and printing steps. The next section provides an overview of the AM processes for polymers and the research methodology. This is followed by an explanation of roughness measurements and metrics in the next section. For each of the AM methods studied, including FFF, selective laser sintering (SLS), vat photopolymerization (VPP), and material jetting (MJT), the main process parameters as well as surface roughness studies have been presented in separate sections. Furthermore, a discussion on the issues surrounding the setting up of polymer key AM processes. In another section, studies on several AM methodologies and their results were compared. This review study concludes with a summary, as well as a discussion of future trends and capabilities in the later sections.

2 Overview

2.1 AM processes for polymers

This work defines AM techniques by ISO 52900 – 2021 [29] and their generally accepted terms. A wide range of advanced manufacturing techniques is available, from the nanoscale to the macroscale. Part size is primarily determined by the working volume afforded by the system of motion of the machine. This literature review is focused on manufacturing at the meso- and micro-scales, where surface roughness can significantly affect the visible quality of parts [30]. Table 1 lists relative characteristics overview of AM techniques for polymers and their most relevant AM applications, including prototypes, medical devices, and precision mechanisms.

In many applications, AM is still in its infancy and requires post-production finishing techniques (PPFTs), which include post-processing and surface finishing [17]. The process can either be used as the primary manufacturing process or as part of a chain of manufacturing processes. Figure 1 classifies finishing as a critical step and quality assurance information flow in a digital thread in additive manufacturing (DTAM). A series of pre- and/or post-processing is available to alter the surface and significantly enhance the appearance of AM parts. However, some of these methods are limited in changing the surface morphology of complex shapes inexpensively and reliably over time [31]. The following sections will provide a detailed description of AM key processes.

Table 1 Characteristic overview of polymer AM categories. Data extracted from references [9, 32]

Process category*	Key process	Basic AM principle	Material feedstock and key materials	Remarks	Applications
Material extrusion	FDM/FFF, DIW	Extrusion of melted or liquid material through a nozzle	Thermoplastic filament (PLA, ABS, PEI, TPU, PETG, PC, ASA, HiPS), Ink	Low build speed Low build cost High surface roughness Poor surface finish Full-color and multi-material available Relatively high mechanical properties Can build fully functional parts Feasible and accessible Vertical anisotropy Generally low resolution Typical part size constraint: ~ 0.01–10 m Smallest feature size: ~ 0.2–10 mm (~ 2 × path width) *XY* resolution: ~ 100 µm (FFF) and ~ 1–100 µm (DIW) Part tolerance: ± 0.5 mm	Electrical housings/enclosures, prototypes, jigs and fixtures, investment casting patterns, solid monolithic parts, scaffolds, biologically compatible tissue implants, tailored composite materials
Material jetting	MJ PolyJet, MJP	Reactive curing/fused agent with energy	Photopolymer and thermoset resins (acrylates, PMMA)	Relatively high build speed Medium build cost Low surface roughness Good surface finish Full-color and multi-material available Developed for visual appearance Medium mechanical properties Low waste Limited to certain resins High dimensional accuracy Typical part size constraints: ~ 0.01–1 m Smallest feature size: ~ 100–500 µm (*XY*) and 10 µm (*Z*) High resolution: ~ 10–25 µm Minimum part tolerance: ± 0.1 mm (depending on part size)	Full-color product prototypes, injection mold-like prototypes, low-run injection molds, medical models

Table 1 (continued)

Process category*	Key process	Basic AM principle	Material feedstock and key materials	Remarks	Applications
Powder bed fusion	SLS MJF	Selective fusion of material in a powder bed	Thermoplastic powder bed (PA6, PA11, PA12, PEEK)	Relatively low build speed Large build volume High build cost and energy consumption Rough surface roughness with grainy surface texture High mechanical and chemical properties Complex geometries Self-supporting 3D Printing Less anisotropy Typical part size constraint: ~ 0.005–1 m Smallest feature size: ~ 0.5–1 mm *XY* resolution: ~ 100 nm -100 µm Minimum part tolerance: ± 0.2 mm (depending on part size)	Functional polymer parts, complex ducting (hollow designs), low-run part production
Binder jetting	BJT	Reactive curing with a binding agent	Liquid binding agent Powder bed (metals, sand, ceramics, and polymer)	Relatively high build speed Large build volume Relatively high build cost Rough and grainy surface roughness Relatively low mechanical properties Shaping process at room temperature and atmosphere Self-supporting 3D Printing Multi-step process: PPFTs are necessary High surface roughness and low dimensional accuracy Typical part size constraints: ~ 5–50 mm Smallest feature size: ~ 50–120 µm Typical resolution: ~ 100 µm Mainly dedicated to ceramics and metals, but recently developed for printing thermoplastic polymers and polyamides	Full-color models, sacrificial models for sand casting

Table 1 (continued)

Process category*	Key process	Basic AM principle	Material feedstock and key materials	Remarks	Applications
Vat photopolymerization	SLA, DLP, CLIP	Light reactive photopolymer curing	Photopolymer resin (acrylates and epoxides; standard, castable, transparent, high temperature)	Moderate build speed Relatively high build cost Low surface roughness Good surface finish and accurate dimensions Developed for aesthetic purposes and biocompatible parts Relatively low mechanical properties and shelf life Large parts Limited to photopolymers Post-processing and post-curing are necessary Typical part size constraints: ~ 0.01–1 mm (Ultra-precision systems), ~ 5–300 mm (Inverted systems), up to ~ 1000 mm (Upright systems) Smallest feature size: ~ 0.03–0.75 mm High resolution: ~ 0.1–100 µm Part tolerance: ± 0.1 mm and less	Injection mold-like, polymer prototypes, jewelry (investment casting), dental applications, hearing aids
Sheet lamination	UAM, LOM	Fusion of stacked sheets	PVC sheet	Relatively high build speed Medium build cost High surface roughness Full-color and multi-material available Relatively high mechanical properties Typical minimum part size constraints: ~ 500 mm Smallest feature size: ~ 0.07–0.2 mm Typical resolution: ~ 200–300 µm	Composite parts

*According to ISO/ASTM 52900 standard

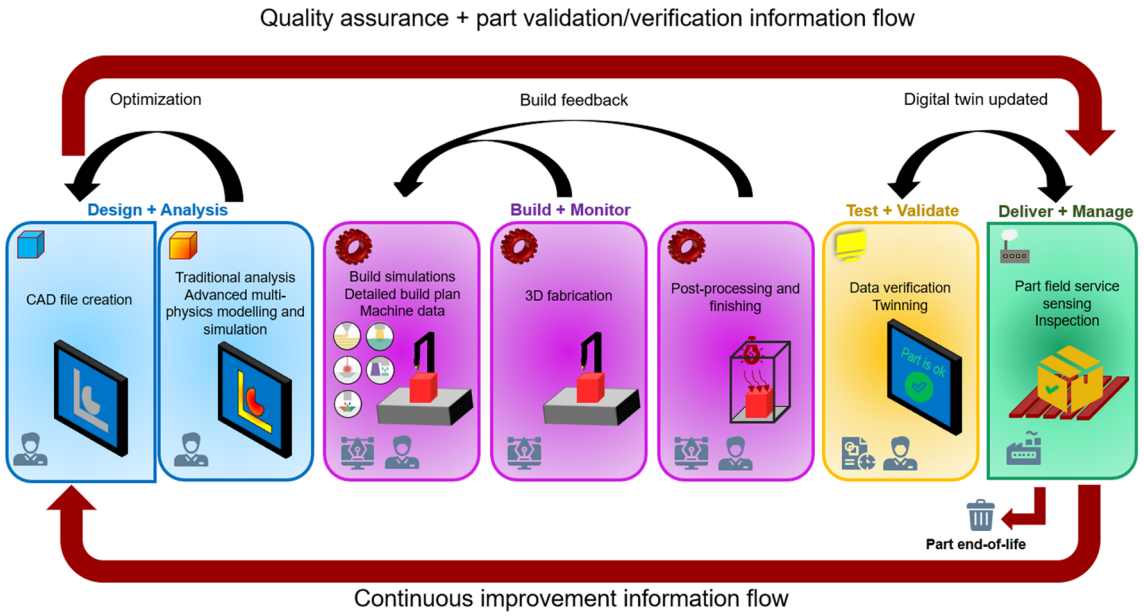

Fig. 1 Stepping through the digital thread in additive manufacturing (DTAM)

Table 2 Characteristic overview of different unfilled AM polymers for general purposes

Materials	AM technology*	Material properties					Ref
		Tensile strength (MPa)	Tensile modulus (MPa)	Elongation at Yield (%)	Flexural strength (MPa)	Heat deflection temperature (°C)	
ABS	FFF, SLA, BJT, MJT	15–68	1500–4000	1.6–6	48–110	51–99	[35–37]
ASA	FFF, BJT	29–52	1510–2340	2–9	48	91–98	[35, 36]
PA (Nylon) 6, 11, 12	FFF, SLS, BJT, MJT, SHS	45–76	944–1350	4–8	37–85	55–182	[35, 36]
PBS	FFF	16–27	46–50	22–27	3.3–5.6	50–65	[36, 38]
PC	FFF, SLA, SLS, BJT, MJT	61–72	2200–2500	3.5–7	92–160	48–55	[35–37]
PCL	FFF, SLS, BJT	5–42	343–441	3.5–8	23–117	41–50	[39, 40]
PE (HDPE)	FFF, MJT, SLS	25–31	1070–1550	6–15	22–28	34–42	[32, 41]
PEEK	FFF, SLS	80–110	2843–3950	4–6	165–185	51–107	[32, 42]
PEKK	FFF, SLS	88–112	2900–3790	3–8	128–168	60–98	[42]
PETG (PET, PETT)	FFF	55–86	2800–3710	3.8	80–116	65–80	[37, 43]
PLA	FFF, SLS, BJT	15–72	2020–3600	3.5	48–115	49–52	[35, 36, 44]
PMMA transparent	FFF, SLA, BJT, MJT	38–72	1940–2250	2–10	73–76	41–48	[43, 45]
PP	FFF, SLA, SLS, MJT	19–58	1600–1950	6–25	55–58	46–122	[37, 46]
PPSF/PPSU	FFF	36–52	2068–2100	1–3	110	100–135	[35, 36]
PS	FFF, SLS, MJT	14–53	1900–3500	1–4	62–100	62–80	[37, 47]
PVC	FFF	37–55	2450–4700	2–6	67–96	30–75	[48, 49]
TPU (Flexible Polyurethane)	FFF, SLA, SLS, MJT	21–44	8–36	N/A	6–10	85–110	[50, 51]

*Data are compiled from various sources, including material datasheets and publications

Thermoplastics and their composites are the primary polymer materials used for AM [33], which can be divided into crystalline and amorphous states. Table 2 lists some of the main polymers and their specifications used in the AM process. The publication share of main AM polymers is shown in Fig. 2. Most of these polymers are mixed and enhanced by manufacturers under various commercial market trademarks, especially resin-based feedstocks. Besides, many other polymeric compounds are used in specific AM processes, such as polydimethylsiloxane, ethylene vinyl acetate (EVA) [34], and commercial digital materials from 3DP machine manufacturers.

2.2 Research method

This literature review focused on the current state of academic investigation with the broadest possible analysis of all recently published articles on surface roughness and 3D printing parameters. The review process was based on the content analysis of 55 articles. This review paper benefited from the preferred reporting items for systematic reviews and meta-analyses extension for scoping reviews method (PRISMA-ScR) for reporting scoping reviews as a general guide [52].

By utilizing the PRISMA-ScR method, a systematic and comprehensive scoping review approach is provided. A clear reporting framework facilitates transparency and replication of the review process, and a reduction of bias in the selection and interpretation of findings is achieved. It should be noted, however, that the method used had a few limitations. The scoping review methodology used may not provide a comprehensive review of all literature on surface roughness for polymer AM, particularly considering the broadness of the topic. A review process may have been limited by the quality of the selected articles and their generalizability for some methods. Thus, the content analysis of the articles may have been influenced by subjective judgments [52, 53]. For instance, available MJT papers in the studied field were considerably fewer than those for FFF (Fig. 3), resulting in more challenges for generalizations of the results. Besides, there were a variety of hand-made and tweaked 3D printers studied in the literature that may affect the review procedure.

The publications were explored on Web of Science and Scopus to be as comprehensive as possible, as these scientific databases have high coverage of reputed high-impact publications.

Figure 3 shows the most common terminology and methods for polymers mentioned in the literature. Based on the number of publications in each AM category, 5 key processes are determined to be studied further. Accordingly, the authors selected the FFF process for MEX, SLA, and DLP processes for VPP, the SLS process for powder bed fusion (PBF), and the MJT category, including the PolyJet process. Other AM methods which generally use polymers in the fabrication of different materials and composites have been excluded, such as binder jetting (BJT) and sheet lamination (SHL). The market report on polymer 3DP machine sales [33] also confirms the same trend and technological share for selected key processes. Other techniques which were not mainly dedicated to polymers or rarely used for research are not included in our study. As AM growth is dynamic on a daily basis, their capabilities are sporadically mentioned.

Various generic keywords, such as "3D*print," "additive manufacturing," and "additive tech*," were employed as criteria in the search section of the title, abstract, and

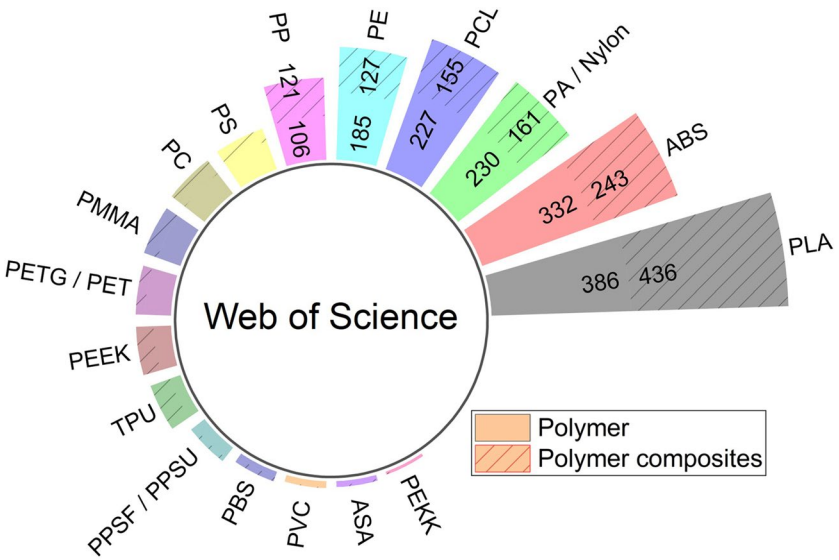

Fig. 2 Total number of publications corresponding to polymers and their composites in additive manufacturing since 2012 (data from Web of Science, 2023)

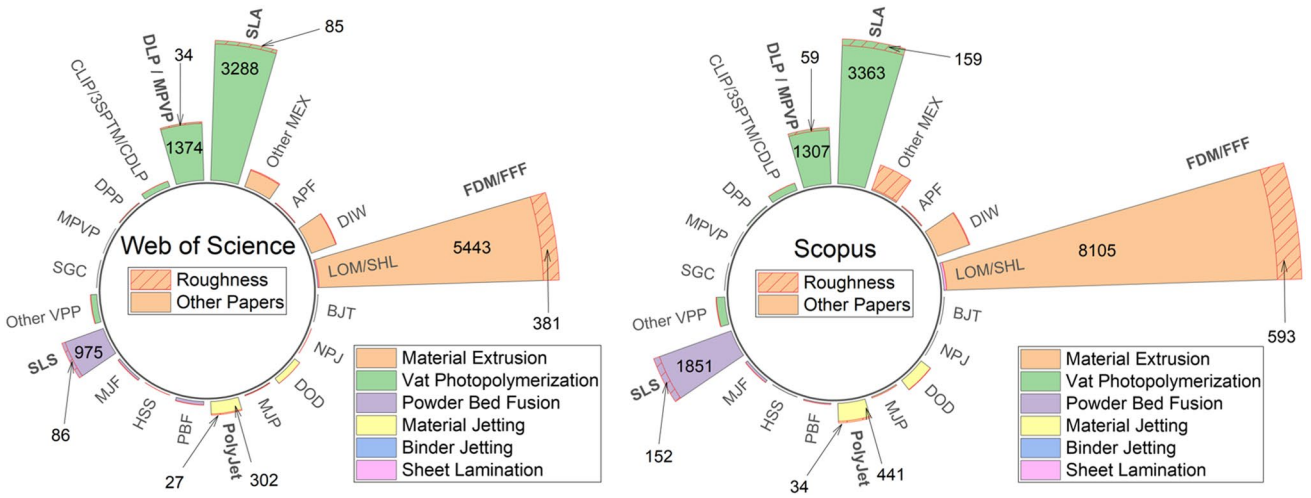

Fig. 3 The most widely used polymer AM technologies and the total number of publications since 2012 (data from Scopus and Web of Science, 2023)

keywords. The following is a formulation of research key strings for AM processes:

(("3d*print*" OR "advanced manuf*" OR "additive manuf*" OR "additive fabric*" OR "additive proces*" OR "additive tech*" OR "additive method*" OR "additive layer* manuf*"))

To examine the role of PPP on roughness, the post-processing of samples should be restricted to 1st level processes, as suggested by the Wohlers report [54]. It secures a minimal impact of post-processing on the roughness of the as-printed samples compared to the slightly post-processed replicas. It is usually less than a 20% deviation, depending on the specific needs of the project or application. Most studies reviewed here limited the PPFTs to a minimum number of steps to minimize the dimensional variations.

This work considered journal articles and conference proceedings to obtain a broader understanding of the topic. Upon eliminating duplicates, the titles and abstracts, availability of full text, and English language were screened before the full-text review. Following this, papers were controlled by their relevance to the present review paper, their originality in providing roughness evaluation for polymers, and their comprehensiveness and uniqueness in terms of the studied parameters and reported roughness metrics. Thus, papers that were out of these criteria were excluded from the study, which resulted in 55 articles separately being exported to Endnote and OriginPro 9.9.5 for in-depth analysis. Figure 4 summarizes the selection procedure used in the current study. The authors have 3D-printed several specimens for each AM category to visualize the surface roughness and texture conditions discussed.

3 Roughness measurements and metrics

Additively manufactured surfaces are composed of various spatial frequency components, including profile, form, waviness, and roughness (Fig. 5). Each of these components has different origins and influences the appearance and functional performance of products differently. The waviness may reveal machine vibration, the form is usually produced by the poor performance of the manufacturing system, and the profile can be ascribed to layer-by-layer manufacturing. Roughness, however, is generated by surface irregularities due to printing and material removal errors. The waviness appears as a signal noise because of the planarity of the motion system and any deformations caused by weight or residual stress [55]. As a result of the specific printing process and materials used, there may be other sources of waviness, including defects in the printing process, thermal distortion, poor adhesion between layers, inadequate support structures, and mechanical deformation during post-processing [56, 57].

Specifically, surface roughness is a critical texture component for assessing the quality of manufactured items by investigating the distribution of topographical features on the surface. Different metrics describe surface roughness because different industry sectors refer to various measures. Due to uncertainty in the surface quality of 3D-printed products, using several metrics would also be efficient [58]. For instance, Triantaphyllou et al. [59] concluded that average area roughness (S_a) and area root mean squared height (S_q) are appropriate metrics for measuring area surface roughness, as they were not sensitive to measurement parameters such as sampling length and evaluation length. In contrast, area height distribution skewness

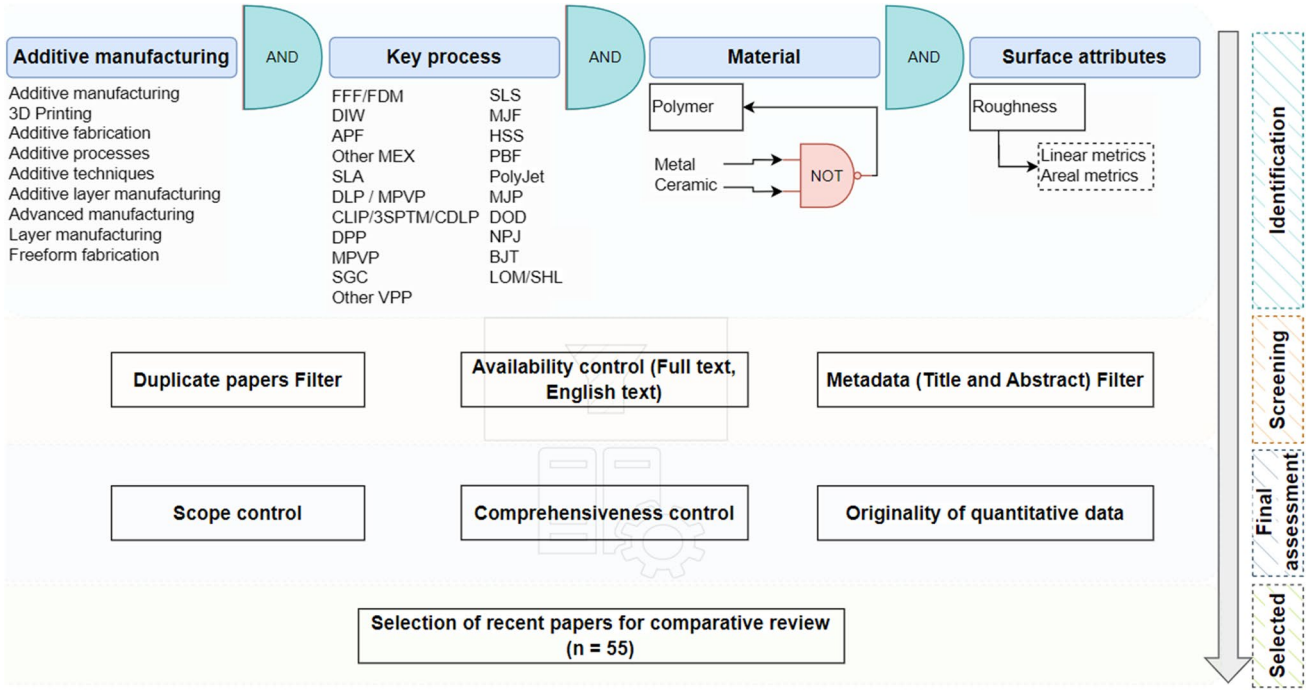

Fig. 4 An overview of the screening procedure employed in this study

(S_{sk}) was found to sufficiently characterize the upside and downside surfaces from SLM parts.

Surface topography measurements based on data obtained from the 3D scanned images of a sample surface are either reported from a linear measurement, referred to by *R*, or from an aerial surface measurement indicated by *S*. The *R* and S metrics are defined and parameterized in ISO 21920–2 [60] and ISO 25178 [61], respectively. Area ratio, or the overall real surface area over the theoretical area of a smooth surface, can reveal how rough a surface is. Generally, the standard height-based metrics employed to describe surface roughness based on a linear profile can be derived from Eqs. (1)–(10) in Table 3. On the other hand, area roughness parameters are sometimes used to describe the roughness variation on a surface (Table 4).

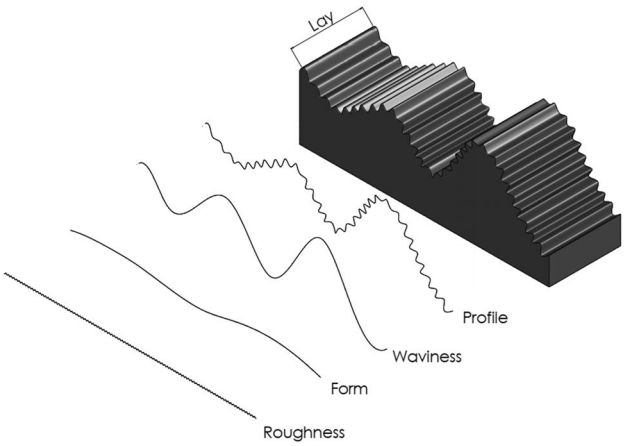

Fig. 5 General spatial frequency components of additively manufactured surfaces

The roughness parameter R_a is widely used by researchers in AM studies as a straightforward metric to define and measure. Considering height variation as a general concept makes it easier to understand, but R_a is insensitive to wavelength variations [63]. Li et al. [64] revealed that the highest peak-to-valley distance parameter (R_z) was superior to R_q and R_a as standard metrics for measuring surface roughness. Li et al. reached a more significant correlation between R_z, tactile evaluation outcomes, and visual assessment results. Other appearance factors, however, influence sensory judgments, such as surface texture and color of the build material. Therefore, R_z alone is insufficient to comprehensively characterize the differences in human perception and surface QAs among samples.

Extraction of the roughness profile is not a common reproducible method because it depends highly on the operational instrument, shape, rotation, and displacement speed [3], as reported in several studies [3, 65]. While 2D profile measurements based on the stylus, according to ISO 4287, are still popular, there is a growing interest in X-ray computed tomography (CT) scan and contactless 3D optical profilometry, according to ISO 25178–2, to obtain more information without scratching the surface.

Table 3 Surface roughness metrics based on linear measurement [60, 62]

Parameter	Description	Equation*	
R_a (roughness average)	The arithmetic average of the absolute values of the roughness profile ordinates	$R_a = \frac{1}{l_e}\int_0^{l_e} \lvert z(x)\rvert dx$	Equation 1
R_q	Root Mean Squared of measured microscopic peaks and valleys	$R_{\mathrm{q}} = \sqrt{\frac{1}{l_{\mathrm{e}}}\int_0^{l_{\mathrm{e}}} z^2(x)\mathrm{d}x}$	Equation 2
R_t (total height of profile)	The vertical distance between the maximum profile peak height and the maximum profile valley depth along the evaluation length	$R_{\mathrm{t}} = \underset{x\in X}{max}(z(x)) - \underset{x\in X}{min}(z(x))$	Equation 3
R_{sk} (skewness)	Positive skewness indicates that the surface is made up of peaks and asperities, whereas negative R_{sk} refers to dominant valleys on the surface	$R_{\mathrm{sk}} = \frac{1}{R_{\mathrm{q}}^3}\frac{1}{l_{\mathrm{e}}}\int_0^{l_{\mathrm{e}}} z^3(x)\mathrm{d}x$	Equation 4
R_{ku} (kurtosis)	A measure of the sharpness of profile peaks	$R_{\mathrm{ku}} = \frac{1}{R_{\mathrm{q}}^4}\frac{1}{l_{\mathrm{e}}}\int_0^{l_{\mathrm{e}}} z^4(x)\mathrm{d}x$	Equation 5
R_zDIN	The average distance of peaks to valleys (German Standard)	$R_{zDIN} = \frac{1}{s}\sum_{i=1}^{s} R_{t_i}$	Equation 6
R_zJIS	The average distance of peaks to valleys (Japanese Standard)	$R_{zJIS} = \frac{1}{5}\sum_{i=1}^{5} R_{t_i}$	Equation 7
η	Asperity-peak density	$\eta = \frac{\frac{m_4}{m_2}}{6\pi\sqrt{3}}$	Equation 8
ρ	Asperity-peak radius	$\rho = 0.375\sqrt{\frac{\pi}{m_4}}$	Equation 9
σ_s	The standard deviation of asperity-peak heights	$\sigma_s = \sqrt{1 - \frac{0.8968}{\alpha}}\sqrt{m_0}$	Equation 10

*$X = \{x \in \mathbf{R} \mid 0 \le x \le l_{\mathrm{e}}\}$, $m_0 = AVG(Z^2)$, $m_2 = AVG\left(\left(\frac{dZ}{dx}\right)^2\right)$, $m_4 = AVG\left(\frac{d^2Z}{dx^2}\right)^2$, $\alpha = \frac{m_0 m_4}{m_2^2}$

Table 4 Area roughness parameters [28, 65, 66]

Parameter	Description	Equation	
S_a	Deviations in the height of the surface points concerning the Mean Reference Plane of the measurement area (A)	$Sa = \frac{1}{A}\iint_A \lvert z(x,y)\rvert dxdy$	Equation 11
S_z	Sum of the largest peak height value and the largest pit depth value within the defined area	$Sz = max(z(x,y)) + min(z(x,y))$	Equation 12
S_q	Root mean square surface height	$S_q = \sqrt{\frac{1}{\mathrm{A}}\iint_A z^2(x,y)\mathrm{dxdy}}$	Equation 13
S_{sk}	The skewness of the surface	$S_{\mathrm{sk}} = \frac{1}{S_q^3}\frac{1}{\mathrm{A}}\iint_A z^3(x,y)\mathrm{dxdy}$	Equation 14
S_{ku}	The kurtosis of the surface	$S_{\mathrm{ku}} = \frac{1}{S_q^4}\frac{1}{\mathrm{A}}\iint_A z^4(x,y)\mathrm{dxdy}$	Equation 15
RRP	The reduction in surface roughness	$RRP = \frac{S_a^i - S_a^f}{S_a^i} \times 100$	Equation 16

Launhardt et al. [66] evaluated four alternative methods for evaluating the surface roughness of Polyamide 12 components produced by SLS. According to them, stylus-based techniques scratch the surface somewhat without substantially altering its roughness. Despite being unable to measure the valley depth, the tactile method was the most reproducible among other studied techniques.

On the other hand, optical methods do not physically alter the surface but are hypersensitive to light reflection and surface transparency, leading to defect detection [67]. The advantages of this method, such as contactless measurement and a comparable R_a and roughness trend to tactile systems in the focus variation mode, make it a viable technique for smooth polymeric surfaces. The focus variation is a vertical scanning method with a shallow depth of focus. It simultaneously allows the measurement of steep flanks, form, and surface roughness [68]. Optical methods could also detect a three-dimensional topography of the surface and its roughness.

The focus variation method suffers from error because of the translucent polymer. The fringe projection and confocal laser scanning microscope represent higher roughness values and more sensitive measurements prone to outliers and faults [66]. The lower wear resistance of polymers in tactile methods and the possibility of the semi-translucent appearance in optical techniques make them more sensitive to method selection in roughness measurement.

Beitz et al. [69] used a confocal laser scanning microscope (CLSM) and X-ray micro-computed tomography (XMT) to measure surface roughness. They reported that roughness resulting from XMT data diverged substantially from those obtained from CLSM data. Due to the inability to level peaks, smaller measuring lengths result in higher arithmetic roughness values. The method also has a smaller sample size, resulting in lower surface roughness along the measurements section. Thus, assessing the roughness metrics of AM polymeric surfaces requires identifying the roughness evaluation method.

Regarding test artifacts for quality surface evaluation, most studies have used the twisted pillar (truncheon) [24, 65, 70], sloped surfaces [70–72], standard test artifact [65], or faceted sphere [24, 73] to measure roughness (Fig. 6). The design of an AM artifact should consider adaptability to various AM processes and machine sizes, as well as its ability to perform non-contact and contact measurements, editable geometry, and minimal material, and energy consumption. The twisted pillar is the preliminary design for this purpose which consists of a sequence of square segments rotated 0 to 90° around a central axis with 3° or 5° increments. The design is appropriate for measuring the surface roughness of an angled plane in the range of 0 to 360° [24]. Yet, it cannot meet all the above requirements of the measurement. Understanding the measurement process is an essential step in interpreting the results.

4 Fused filament fabrication (FFF)

Even though FFF 3DP has made significant advances so far, the fabricated parts tend to have a poor surface finish, including rough surfaces, voids, and prominent striations [2]. The morphology is relatively rough due to various limiting factors such as phase transformations, fast cooling, and exhaustive energy (Fig. 7). Although FFF is attractive for demanding applications, printed parts deviate from their initial designed geometry, volumetric error, and hardware settings in translating a CAD file to a physical object [74, 75]. To control the shape deviation, the corresponding

Fig. 7 Appearance and accuracy of gradient lattice-based structures in as-printed FFF samples using PLA filament and Prusa i3 mk3s + (scale bar represents 1 cm)

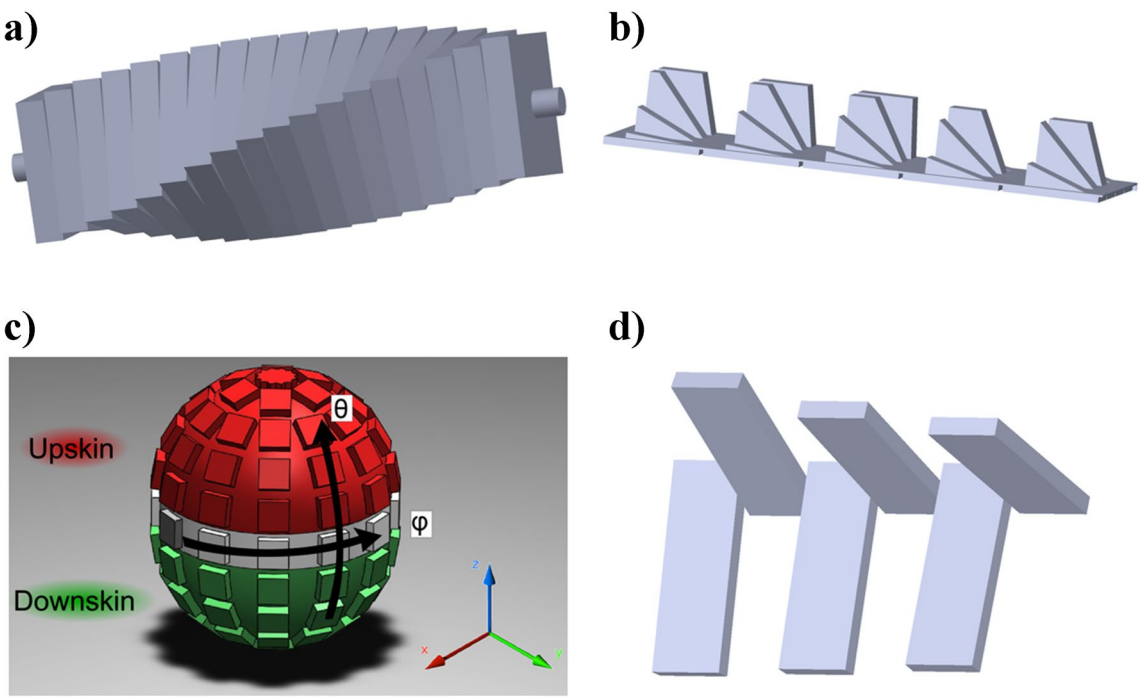

Fig. 6 3DP designs for studying build orientation (wedge angles): **a** Twisted tower, **b** tilted surfaces, **c** faceted sphere, and **d** Standard Test Artifact (STAR)

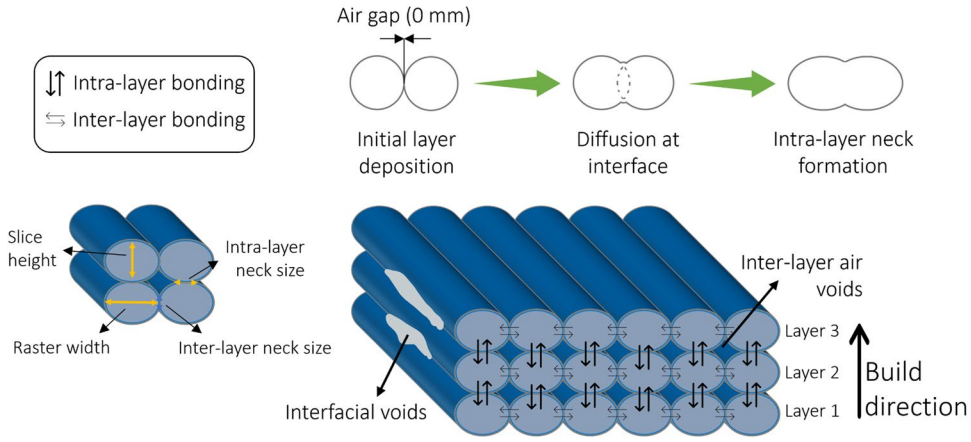

Fig. 8 Bonding and stages of neck formation in the FFF process

allowances are approximately estimated before printing [76]. However, the FFF parts still required PPFTs to meet the market [17]. For instance, temperature variation during the layer-by-layer part fabrication procedure undesirably affects the printing quality [2].

Generally, there are two types of bonding in the FFF process: inter-layer and intra-layer (Fig. 8). The high thermal expansion in polymers can play an important role in the weak bonding among the layers during the build process, leading to staircase (stairstep) formation. As an inherent issue, the formation of staircases has a considerable negative impact on the surface quality of FFF components [18, 75].

Among literature reviews on the process parameters of FFF, Turner et al. in 2014 [77] summarized the process design and modeling of FFF. They reviewed the bonding of the raster, the model spread of the deposited raster, and the motor torque and power. Chohan et al. [21] have reported a literature review on pre- and PPFTs to improve surface characteristics of FFF parts. In 2018, Singh et al. gathered results from studies on the effect of pre- and post-processing procedures on FFF patterns to develop biomedical implants from the route of AM and investment casting (IC) [78]. Several AM materials and their mechanical performance have been reviewed by Popescu et al. (2018) [79]. In addition, deliberately structuring the polymeric surfaces using FFF 3D printing has become a popular choice for AM processes. Cuan-Urquizo et al. [17] reviewed the literature on the characterization and projection of the mechanical behavior of FFF products using analytical and computational approaches (2019).

4.1 Process parameters

In FFF, pre-processing includes instructions generated by a slicer software to gain data, slice the design file into layers of 3D pixels (voxel), model construction, optimization of the toolpath for the printing process, and material preparation. Parameters directly affecting the process are categorized based on operation, geometry, material, and machine-specific parameters [80]. Generally, the accuracy of the motion system limits the precision of the part. To minimize the issues due to the design and pre-production phase, each voxel must have accurate position information and print-process parameters in tool pathing. In the following, the main process parameters influencing the surface roughness of FFF polymeric surfaces are discussed.

4.1.1 Filament material

The growing interest in using polymers ranging from rubber-like materials to rigid plastics leads to new applications in vehicle parts, shoe soles, and biomedical applications [81]. While high surface quality and desired roughness are advantages for 3DP parts, other material properties and manufacturing features are usually considered in the selection of the AM method. Figure 9 illustrates a general cumulative performance score based on the comparative scoring of each parameter on a scale between 1 and 9. PLA and ABS are the most well-known feedstock among other materials for FFF. Since PLA filaments can provide better surface quality and biodegradable polymer derived from corn, it is considered more eco-friendly than petroleum-based ABS [82].

In most cases, materials are already enhanced for optimum performance. Their parameters are challenging to alter later in the production stage, but choosing the appropriate material to improve surface roughness is crucial. This may prevent the usage of FFF prototypes in some cases where the surface should be smooth. An overview of the major polymers used in FFF is presented in Table 5.

4.1.2 Print temperature

In FFF 3D printing, print temperature and cooling speed play an important role as it affects the quality of the 3D-printed object. The model temperature should be high

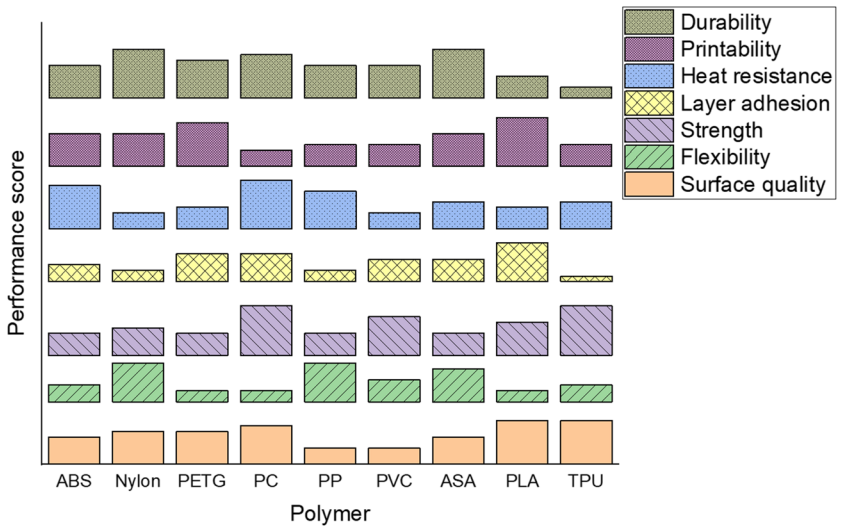

Fig. 9 Recommended polymers for the FFF process. Data extracted from references [43, 83]

Table 5 Typical FFF filament specifications. Data extracted from references [43, 83]

Material	Printing temperature* (°C)	Type	Remarks	Application consideration
PLA	180–235	Standard plastics	Easy to print Low-cost Midcore thermal and mechanical properties Available in various colors and specifications Severely limited by application temperature under 50 °C High surface roughness Biodegradable	Generally non-critical
ABS	200–260	Standard plastics	Difficult to print Low surface roughness Good thermal and mechanical properties	Generally non-critical
HiPS	230–250	Engineering plastics	Midcore mechanical properties Water soluble Biodegradable	Structural purposes
PolyVinyl Alcohol (PVA)	190–220	Engineering plastics	Water soluble Glossy but rough finish Limited mechanical and thermal properties Biodegradable	Structural purposes
Nylons (PA)	235–280	Engineering plastics	Generally difficult to print Good thermal and mechanical properties Low surface quality	Structural purposes
PET(G)	230–270	Engineering plastics	Easy to print Low dimensional accuracy due to shrinkage Good thermal and mechanical properties	Structural purposes
Polycarbonate (PC)	250–320	Engineering plastics	Excellent thermal and good mechanical properties	Structural purposes
Polycarbonate ABS (PC-ABS)	260–285	Advanced plastics	Average printability Good thermal and mechanical properties	Severe conditions
TPU	195–230	Engineering plastics	Generally difficult to print Flexible materials Excellent resistance to abrasion and wear	Structural purposes
PEEK	350–450	Advanced plastics	Generally difficult to print Excellent thermal and good mechanical properties	Severe conditions

*Data are compiled from various sources, including material datasheets and publications

enough to melt the outgoing feedstock before extrusion. However, if the temperature is too high, the filament will melt too rapidly, resulting in a porous and brittle object with poor surface quality [21]. Depending on the type of filament being used, the optimal printing temperature will vary. Typically, PLA is printed at 190–220 °C, while ABS is typically printed at 220–250 °C [35–37]. The ideal printing temperature should be referred to by the filament manufacturer to ensure the best results. A stable temperature at heaters is crucial in the fluidity of material, resulting in a smoother surface finish. Besides, the surface roughness can be decreased by increasing the model temperature because of the solidification delay. However, plastic adhesion with a base plate is problematic in very high or low printing temperatures [21]. As well as affecting the quality of the printed part, the temperature of the nozzle can also affect the speed of the printing process. In general, a higher temperature will lead to faster printing speeds, but it is crucial to find a balance between speed and quality.

4.1.3 Layer thickness

The height of each deposited stairstep is a notable parameter that can be controlled in the extrusion nozzle tip and/or shift in the *Z*-axis between consecutive slices accumulated on the bed. Adjusting the height of each stairstep can improve print quality and reduce the printing time. In general, a smaller stairstep height will produce a higher quality print, but the printing process will take longer [84, 85]. This parameter is the most significant challenge in obtaining a high surface finish in a cost-effective production time. The minimum feature size (smallest linewidth) is determined primarily by the nozzle diameter, which affects layer thickness nonlinearly, but geometry and build orientation also play an essential role [86]. Correctly setting up an optimum balance between layer thickness and printing time is highly influential in the pre-processing step. A smaller nozzle tip will generally result in lower layer thickness, better surface quality, and possibly decreased post-processing time. However, it increases the printing cost and time for the as-print parts, leading to more nozzle clocking and quality issues because of the pressure drop [21].

Since the quality of internal surfaces does not engage in the appearance of the part in most cases, consistent layer height has been seen as a waste of time [72]. Thus, it can be varied in different areas of the object according to the expected time-quality factor. For most FFF printers, the domain of layer thickness is variable in a certain range, i.e., there is a maximum and minimum value for changing the nozzle diameter. A few machines are limited to a single value, so it is required to set up other parameters to change the surface quality [21].

In several papers [84, 85], the layer thickness is reported as the most significant process parameter influencing surface roughness. However, this influence also depends on the other process parameters. Anitha et al. [87] established a set of experiments that showed that layer thickness significantly impacts the roughness of the FFF part compared to rod width and speed of deposition. Haque et al. [84] attempted to minimize the surface roughness of FFF build features using a numerical approach. After investigating various equations to control FFF parameters such as layer thickness, overlap distance, part orientation, and raster width, they reported that layer thickness has more influence on roughness than other parameters. They observed that increasing the overlap distance between two layers and part orientation leads to lower surface roughness. However, higher layer thickness and raster width increased surface roughness.

4.1.4 Infill density and air gap

The infill density defines the level of incorporated material inside the fabricated object. It might be varied from 0 to 100 percent according to the required balance between material consumption and mechanical properties [88]. Generally, a higher infill density leads to a heavier and stronger part, which increases the cost and the amount of material used in the printing process. Infill density and pattern are significant process parameters influencing surface quality [72]. Support structures must also be designed appropriately to support the geometry. Thus, they should be accurately chosen by considering the design and strength requirement, as well as the build time of the printed part. For instance, surface artifacts such as gaps and porosity have been observed even for 100% infill density under a scanning electron microscope (SEM) [89].

The distances or spaces between two adjacent rasters on the same layer are called the air gap or road gap [90]. Figure 10 depicts the air gap compared to other adjustable FFF process parameters. The default value taken for the air gap is zero, which means the end of the two nearest beads is in touch. There are two types of positive and negative gaps. The positive gap increases the gap to reduce the density and build time of structures, whereas the negative gap means overlapping two roads resulting in a long printing time and dense objects. While both positive and negative air gaps can enhance the surface finish, zero air-gap minimizes dimensional accuracy and part quality [21].

4.1.5 Raster width and angle

The raster width, also called road or contour width and (tool) path width, refers to the width of the melted bead path, which is added to fill interior regions of the FFF-printed samples [21]. According to the filament material, it is regularly 1.2 to 1.5 times the nozzle tip size [80]. As seen in Fig. 10, the

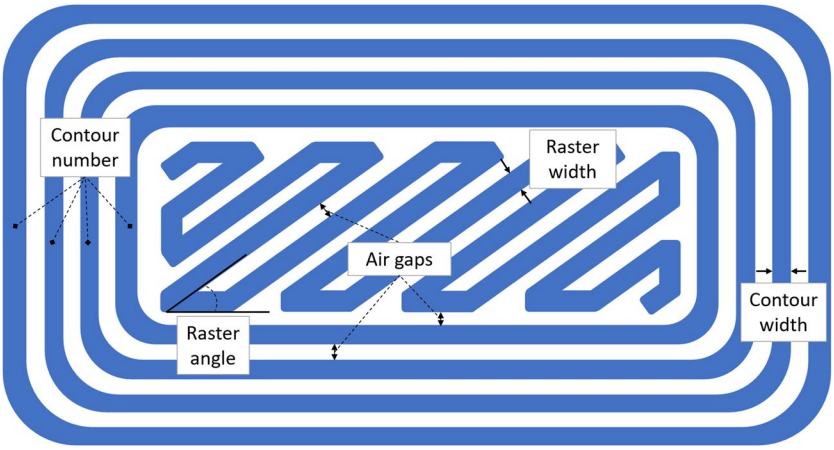

Fig. 10 Controllable parameters in FFF machine

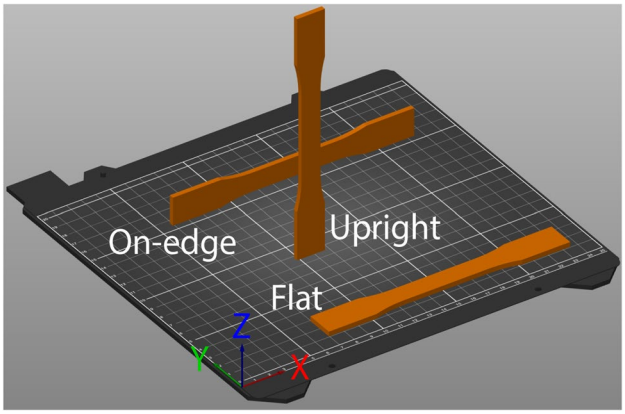

Fig. 11 Orientations commonly used for FFF parts

contour tool path width surrounding the object is defined as the contour width, slightly smaller than the nozzle diameter [21, 86]. The width of the most minor features in the *XY*-plane in FFF is about two times the path, much larger than the thickness of the layer in the *Z*-direction. To reach high mechanical performance, dimensional accuracy, and surface quality, the raster width should be minimized [86, 91]. It has been noticed that a wide contour width enhances geometrical precision and surface quality because heat evolved during extrusion can easily deform thin contours [92].

The raster direction compared to the *X*-axis of the build platform is known as the raster angle (Fig. 10). This parameter significantly affects the internal layer bonding and object appearance. The main approaches to raster angle are criss-cross (−45°/+45°), cross (0°/90°), and 30/°60°. Because of the variation of CAD models and printing parameters, there is a loose correlation among the studied strategies. Sood et al. [91] used a bacterial foraging algorithm to show that the 0° raster angle is the best option for dimensional accuracy, and 45° results in the best surface appearance. Kumar et al. [93] stated −45°/+45 as the best raster angle for the surface characteristics, including roughness.

4.1.6 Build orientation

The orientation (deposition) angle is a notable and highly flexible process parameter involving surface quality. It corresponds to the CAD model and coordinates machine system (Fig. 11). Wang et al. [94] considered the build orientation the most substantial PPP factor regarding dimensional accuracy. As a result of gravity and residual stresses, overhanging surfaces should be supported at less than 45° from the horizontal plane [19]. Several papers have studied the role of positioning the models in various *X*- and *Y*-directions on the surface finish and build times. For instance, Kattethota and Henderson [95] reported that the orientation angle of 0° yielded the best surface finish. Moreover, 0° and 90° were reported as the optimum build angles for balancing the build times, cost, and surface finish. By contrast, orientation angles between 40 and 60° were neither cost-effective nor quality-enhancing due to the maximum support material required for tilting the model [21].

Since different surface angles result in various surface roughness, the test part should comprise features considering different surface angles. In 1997, Reeves and Cobb [96] introduced a benchmark model called twisted pillar. It can consist of 18 or 31 square blocks, depending on the intervals (step), twisted 5° or 3° compared to the previous square (see Fig. 6a). Durgun and Ertan [97] also confirmed the close relationship between build direction and surface roughness.

Among the defects associated with different build orientations are warping, layer delamination, deformed overhangs, and poor surface quality [98, 99]. In terms of surface roughness, Buj-Corral et al. [99] reported both simulated and experimental amplitude roughness values to rise with build orientation angle, due to the stair-stepping effect. As reviewed by Jiang et al. [98], a change in print orientation also affects support generation, which ultimately affects the surface roughness after support removal. The choice of support structures can have a significant impact on the surface roughness of FFF prints, thereby influencing the

post-processing process. Furthermore, the orientation of the part impacts the support contact area, the build time, and the cost of the fabricated part.

4.1.7 Adaptive slicing

Adaptive slicing is termed as a protocol to slice various zones of the part into different thicknesses during building [78]. It contains balancing techniques needed to reach the optimum printing time versus surface finish. Generally, the CAD model is divided into polygons or closed curves by either the CAD software or a slicer before transferring the mesh model (STL file) to the printer. This process is called slicing, and the distance between two sequential horizontal planes is known as a slice [100]. The slicing process and the tessellation of the CAD file are expected to be the significant parameters involved in creating rough surfaces in the procedures of layer fabrication. The containment problem causes the original CAD model to deviate from the designed form when slicing a tessellated CAD model. Aside from the containment issue, the layer deposition causes a problem known as staircase effects [101].

Several researchers [17, 102] have studied several types of stepwise refinement, adaptive slicing, and identifying nonuniform fillet radius at different areas of printed objects. These methods consider automatically slicing algorithms, generating variable tool paths (.gcode), reducing build time, and minimizing surface roughness through varying heights depending on geometry [103]. These specific parameters rely entirely on the shape and dimensions of the designed part [21].

The major categories of slicing methods available for FFF printing are flat-layer, non-planar, and mixed-layer adaptive slicing, respectively. Zhao and Guo [104] listed the most important research studies on non-planar and mixed-layer adaptive slicing. They suggested method planning of mixed-layer adaptive slicing, which discusses the strategy for the process planning of more straightforward adaptive slicing approaches. Table 6 provides an overview of these slicing methods.

4.2 Surface roughness studies and discussion

The literature on process parameter optimization is classified according to the resulting properties. It can be based on the surface finish and smoothness, dimensional accuracy, build time, material behavior, dynamic and static (tribo-) mechanical/thermal behaviors, and manufacturing cost. Studies have centered on finding the best combinations of geometry and operation-specific characteristics. For instance, Durgun and Ertan [97] reported that surface roughness significantly impacts the flexural strength of ABS parts manufactured with infill 100% at different orientations and angles. Among the factors responsible for PLA and ABS surface roughness, the researchers identified layer thickness [105–107], build orientation [107], printing speed [105, 106], nozzle diameter [105, 106], and temperature [106] as the most critical parameters. Table 7 summarizes

Table 6 Adaptive slicing classification. Extracted from references [103, 104]

Method	Specification	Advantages	Disadvantages	Application
Planar slicing	Uniform layer thickness	Simple, effective, and robust	Lack of strength (poor performance) Stairstep effects (poor surface finish) Large numbers of layers (longer build time)	Widely used in slicing simple designs
Non-planar (curved layer) slicing	The nozzle is collinear with the normal direction of the curved surface Longer length filaments in curved inter-layer Fewer layers	Preserve randomly located, minute and critical surface features Reduced stairstep effects, at least in the tangential direction of the deposited filament High strength Enhanced surface quality Fewer build times	Complex method	For some specific shapes like thin, curved shell-type structures (skull bones, turbine blades, etc.)
Mixed-layer slicing	Multi-direction and variable layer thickness	Reduced stairstep effects Alleviated support structures Less building times Less anisotropy	No detailed automatic algorithms Complexity in decision-making logic	Complex parts Requiring more capable slicing methods

Table 7 Overview of studies on surface roughness in FFF (see text* below the table for abbreviations)

Materials | Machines	Methodology and studied parameters	Roughness range (μm)	Remarks	Ref
PLA | 3D Ultimaker 2 +	l.t. (0.06–0.18 mm), r.w. (0.2–0.25 mm), i.d. (20–40%), p.s. (20–100 mm/s), b.o. (0–45°), f.r. (99–101%) a.m. (DoE Taguchi L9), s.r.m.m. (contact profilometry)	R_a: 0.7–10.5 (T.), 4.7–12.8 (S.)	-l.t. was the most influential parameter on the s.r and d.a. -Shape and p.s. affected the T. R_a -S. R_a, influenced by l.t., and then by walls p.s. and b.o.	[108]
PLA | Tevo Tarantula Prusa i3	l.t. (0.10–0.38 mm), p.s. (19.46–76.54 mm/s), p.temp. (171.22–218.78 °C) a.m. (ANN and SOS), s.r.m.m. (contact profilometry)	R_a: 1.705–4.373	-Integrating ANN and SOS had a significant impact on performing the FFF process parameter for minimizing s.r., compared to the RSM method -Decreasing l.t., p.s., p. temp., and outer shell p.s for ANN-SOS resulted in minimum s.r. (2.011 μm), which was 12.36% smaller than the RSM method	[109]
PLA | FLSUN-QQ	l.t. (0.1–0.4 mm), r.w. (0.2–0.4 mm), p.temp. (190–210 °C), p.s. (60 mm/s), plat.temp. (60 °C), a.m. (ANN and SOS), s.r.m.m. (non-contact profilometry)	R_a: 5.40–33.65	-The effect of l.t. and p.temp. was more significant on the 3D s.r. compared to the other parameters -A theoretical model was developed based on the bonding neck-forming process	[110]
PLA & PLA-Graphene | BQ Witbox	i.d. (100%), m.c. (20–80 mm/s), l.t. (0.06–0.24 mm), and b.o. (H., on-edge, and V.) were studied to determine their influence on the geometric characteristics (d.a., f.e., s.t., and s.r.), a.m. (ANOVA, ANN, and RSM), s.r.m.m. (contact profilometry)	S_a H. orientation: 1.1–4.3 (PLA), 1.2–3.4 (PLA-Graphene)	-Compared to PLA filaments, PLA-Graphene improved functional properties with no loss in geometric quality -The best s.f. was obtained in the H. orientation -Variation of b.o. resulted in two different behaviors of s.r.: on-edge and V. orientations s.r. showed a quasi-linear growth with increasing l.t., but with no significant effect of m.c. H. orientation: filament crushing by the extruder in each layer produced lower values of s.r. -When texture was evaluated in the H. orientation, S_a depended on n.d. and l.t. -For the V. and on-edge orientation, S_a was affected only by l.t. -The effect of b.o. on S_a was primarily due to the deposition and cooling of the fused filament	[111]

Table 7 (continued)

Materials | Machines	Methodology and studied parameters	Roughness range (μm)	Remarks	Ref
Heat-resistant PEEK | Indmatec	p.temp nozzle (380–420 °C), p.temp platform (220–300 °C), p.s. (5–25 mm/s), l.t. (0.1–0.3 mm), r.w. (0.4 mm), overlap interval (0 mm), extrusion flow (100%), s.r.m.m. (non-contact profilometry)	R_z: 30–75	-s.r. model, considering diffusion, was introduced based on heat transfer -Diffusion affects surface morphology -The proposed design predicts s.r. by considering the printing parameters (r.w., l.t., p.s, and p.temp.) -The actual s.r. was affected by diffusion and tightening of the nozzle -s.r. decreases with the increase of p.temp. considering that nozzle temperature had a greater influence compared to platform temperature -Lower l.t. decreases the surface quality as the nozzle squeezing deteriorates the surface morphology. l.t. (0.15 mm) and p.s. (20 mm/s) were the optimal values -Application: Thermoplastic heat-resistant resins for aerospace, biomedical, mechanical, and electronic field	[112]
PLA | Tevo Tarantula Prusa i3	p.temp (185–205 °C), p.s. (36–60 mm/s), o.s.s. (29–40 mm/s), l.t. (0.18–0.30 mm), a.m. (ANOVA, RSM, PSO, and SOS, s.r.m.m. (contact profilometry)	R_a: 2.2 (SOS), 2.2 (PSO), 2.4 (RSM)	-All parameters with the order of p.s., l.t., o.s.s., and p.temp. affected s.r. -PSO and SOS improved by 8.5% and 8.8% of s.r., respectively, compared with the conventional RSM method -Lower l.t. and p.s., and higher p.temp. and o.s.s. resulted in a better s.f.	[44]
PLA | BQ Witbox	b.o. (V., on-edge, H.), l.t. (0.06–0.24 mm), p.s. (20–80 mm/s), p.temp. (190–220 °C), n.d. (0.4 mm), i.d. (100%), a.m. (ANOVA, RSM, and ANN), s.r.m.m. (contact profilometry)	S_a: 2.5–2.8 (T.), ~ 25 (H.)	-The effect of b.o. in the object's positioning on the build plate, l.t., and p.s. on the d.a., f.e., s.t., and s.r. were analyzed -s.r. exhibited two different behaviors depending on the build orientation at the optimum p.temp. (205 °C) -The V. and on-edge positions showed a linear increase in S_a and S_z at higher l.t., but p.s. had no significant effect. In the H. orientation, s.r. was conditioned by n.d., leading to a nearly 10 times increase in s.r.	[113]
ABS + TPU | Creality CR10	TPU contents (10 to 30 w.t.%) in ABS + TPU blends, p.temp. (230 °C), p.s. (30 mm/s, 8 mm/s for V.-printed specimens), travel speed (120 mm/s), o.s.s. (15 mm/s), r.a. (0°), i.d (100%), l.t. (0.2 mm), plat.temp. (90 °C), support-less printing, f.r. (100%), a.m. (ANOVA), s.r.m.m. (contact profilometry)	R_a: 2–7 (H.), 21–38 (V.); R_q: ~ 150–500 (H.), ~ 160–210 (V.)	-s.r. raised by increasing TPU content, resulting in higher adhesion of the ABS parts to the build platform -3D printability without heating the platform by adding TPU to the filament is achieved due to new intermolecular interactions -Application: Large-scale industrial applications as an alternative to pure ABS	[114]

Table 7 (continued)

Materials | Machines	Methodology and studied parameters	Roughness range (μm)	Remarks	Ref
PETG | Tevo Black Widow	l.t. (0.16–0.24 mm), p.temp. (240–250 °C), p.s. (40–60 mm/s), p.a. (500–1500 mm/s^2), f.r. (90–110%), a.m. (DoE Taguchi L27, ANOVA), s.r.m.m. (contact profilometry)	R_a: 0.91–10.64 (H.), 5.41–32.99 (V.)	-Influential parameters were studied to obtain lower values of R_a and S_a -f.r. and p.a. had the greatest influences on the s.r. -Application: Fabrication of traffic signs for the manufacture of LED spotlights	[115]
ABS & ABS + GF | Generous Twin	l.t. (0.4 mm), p.temp. (225–245 °C), p.s. (600 mm/min), i.d. (100% Rectilinear), r.a. (−45°, 0°, 45°, 90°), GF (0–15 wt.%), a.m. (DoE Taguchi L23, ANOVA), s.r.m.m. (contact profilometry)	R_a: 6.51–13.47	-s.r.became worse with increasing GF -p.temp. and coupling agent did not have any significant effects on s.r.	[116]
PEEK | Customized FFF	Printing parameters were set based on the FEA results. n.d. (0.4–0.8 mm), p.temp. (380–440 °C), p.s. (17–26 mm/s), l.t. (0.1–0.45 mm), s.r.m.m. (non-contact profilometry)	7.8–10.8 (H.), 10.1–19.3 (V.)	-Reduced s.r. for both H. and V. directions due to increased p.s. -Increased s.r. with higher n.d. -Thinner layers in a 0.4 mm nozzle caused sensitive s.r. to p.s. -Thicker l.t. resulted in higher s.r. -Gaps between layers were the leading cause of s.r. -Application: To replace traditional metal or ceramic parts for biomedical and aerospace applications	[117]

*Abbreviations: *a.m.* analysis methods, *b.o.* build orientation, *d.a.* dimensional accuracy, *f.e.* flatness error, *f.r.* flow rate, *i.d.* infill density, *l.t.* layer thickness (height), *m.c.* material consumption, *n.d.* nozzle diameter, *o.s.s.* outer shell speed, *p.a.* printing acceleration, *p.s.* printing speed, *p.temp.* printing (nozzle) temperature, *plat.temp.* platform temperature, *r.a.* raster angle, *r.w.* raster width, *s.f.* surface finish, *s.r.* surface roughness, *s.r.m.m.* surface roughness measurement method, *s.t.* surface texture, *S.* side, *T.* top, *H.* horizontal (XY), *V.* vertical (Z)

some of the significant literature on the essential parameters in the process optimization of FFF on the roughness range. Optimizing these parameters is one of the highly critical tasks for acquiring the desired surface quality and improving superior mechanical properties and material response.

Table 7 indicates that layer thickness can be considered the most significant FFF parameter that affects surface roughness and surface finish. Based on the results, surface roughness was reported primarily by R_a, S_a, R_z, and R_q. Furthermore, the range of roughness can be significantly different depending on the processing conditions from sub-micrometers to 33.65 µm for R_a in the studied works. Although the reported roughness varies tremendously, it is generally between 0.1 and 1 times the layer thickness, depending on the materials and measurement geometry. Also, build orientation is crucial in determining print quality, as horizontal and vertical surfaces differ. Slicing settings, object orientation, and considerations regarding the design for additive manufacturing (DfAM) guidelines could enhance roughness and resolution while decreasing the number of PPFTs required [118]. These results did not consider more complex features, such as ridges, holes, slots, and posts, coupled with motion and material flow dynamics.

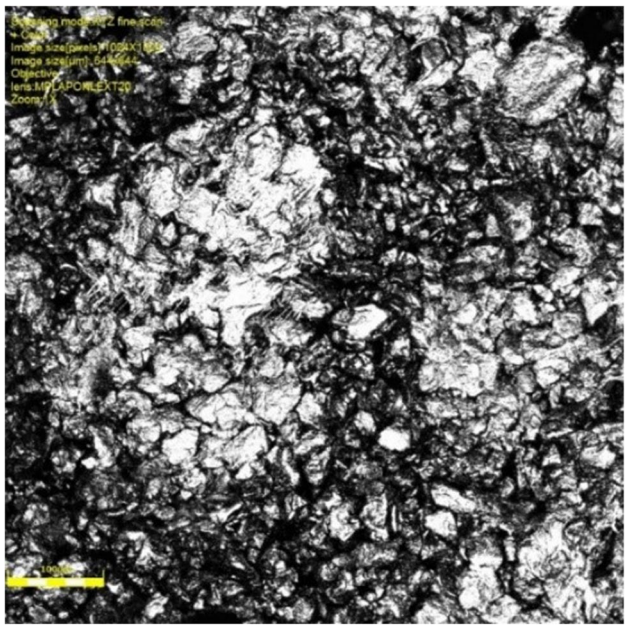

Fig. 12 2D laser scanning image of a part made of PA6, showing the typical surface texture of solid part samples printed with an EOS P500 FDR system

5 Selective laser sintering (SLS)

Parts produced by SLS are expected to have a high surface quality because of the precise nature of the laser, resulting in extensive usage in meeting functional needs. On the other hand, SLS-produced components have generally a greater surface roughness than other polymer AM techniques [119]. Several functional properties are affected by surface roughness, including frictional properties, heat transfer, and fatigue resistance in polymers, as well as the possibility of powder becoming loose, e.g., as a medical implant in the human body [120]. During SLS, the build platform is heated uniformly to exactly below the material melting point; this is a highly effective method to boost the build rate. However, it can cause unwanted "caking" of powder on the outer surface of the part. A preheating lamp to maintain the temperature under the melting temperature reduces thermal stresses, leading to part distortion, shrinkage, and lower dimensional accuracy at the surface. Due to entrapped air, many grainy features, voids, and porosities can be formed inside the packed powder (Fig. 12). Therefore, porosity is an inherent defect in SLS objects that can appear on the surface [3, 121].

SLS typically prints features as fine as 0.1–0.5 mm, making them an excellent choice for printing intricate latticework with thin walls and beams. While SLS parts do not need support due to a powder bed, temperature gradients during printing may deform the part and create very thin surface issues. In addition, because of thicker layers (90–150 µm) in SLS, the technique is more sensitive to the staircase effect. This effect in an SLS object is most prevalent on semi-horizontal surfaces [3]. In a similar method, SLM, since the melt pool is typically more extensive than the laser spot, the scan contour tracks are naturally shifted inwards to account for this issue and, consequently, rougher surfaces [122]. PPFTs usually improve the quality of large surfaces in these cases, but it would be more demanding for more complex and minor features.

There is a direct correlation between the amount of porosity in a part and material properties, such as the shape and size distribution of the powder and part processing conditions. Compared to semi-crystalline thermoplastics, amorphous thermoplastics produce more porous parts, which can either be an advantage or a disadvantage depending on the desired property of the piece. The fundamental problems with sintering are porosity and shrinkage in the parts. Still, they can be overcome with an optimal packing density (for porosity) and a careful choice of the sintering parameters [123, 124].

Low porosity is required if the appearance and mechanical properties are essential. The size distribution, reduced porosity, and enhanced surface finish affect powder flowability and packing density. Using infrared lamps or ambient heating helps prevent nonuniform shrinkage by keeping the polymer above the glass transition temperature, allowing the shrinkage process to be controlled. This requires slow cooling after the build is complete and must be considered when calculating the processing time for each part. On the

other hand, semi-crystalline thermoplastics experience a volume reduction during cooling due to crystallization, making amorphous thermoplastics the better choice [123, 124].

Poor surface quality is a common complaint when working with powdered raw materials. The conventional roughness range (referred to by R_a) of PBF is 5–25 µm. As well as the printing parameters, the quality of the surface can also be affected by the 3DP machine itself. Depending on the SLS machine, R_a can range from 10 to 20 µm with a peak-to-valley distance of up to 0.2 mm [3]. Sachdeva et al. reported a range of 8–12 µm for R_a [124]. Mechanical properties, particularly fatigue, can be affected by different surface roughness.

The AM powder-based procedure comprises semi-molten grains adhering to the outer surface, with occasional sharp grooves in between, prone to crack initiation [3]. Figure 13 depicts the three states influencing the surface quality in PBF.

The incomplete composition of powder materials may cause "orange peel" surfaces (Fig. 14). Incorrect powder reuse or non-homogeneous mixing is the main reason for this surface issue in the SLS technique [125, 126].

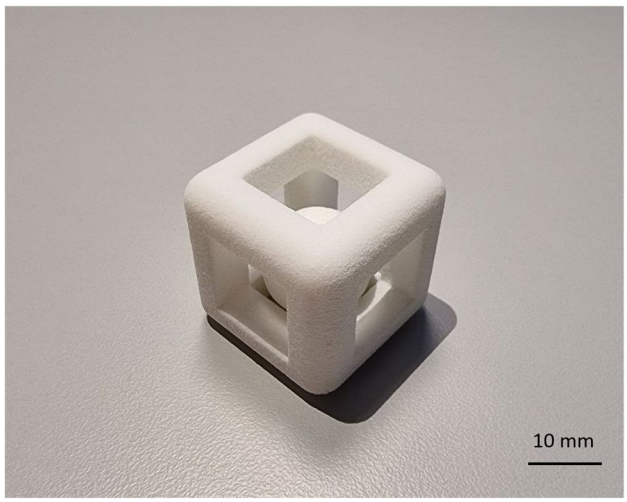

Fig. 14 Orange peel surface texture on PA12 (2200) SLS part

5.1 Process parameters

Several factors influence the performance of SLS systems. Precision and resolution are limited by the combination of powder particle size, layer thickness, and laser spot diameter. The selective melting of powder is done using two main tracks, including the contour and hatching tracks. In contour tracking, the outer layer of the required profile is melted, while the hatching track is used to melt the internal area bounded by the contour track [122].

The SLS as-printed surface roughness values differ considerably based on the preparation method, the equipment utilized, and the position of the sample surface concerning the layer accumulation [3]. The SLS parameters of the process (see Fig. 15) have been widely investigated in engineering fields [32, 127]. They can be classified into three major categories: laser, material, and chamber. The average powder size, layer thickness, and surface orientation all influence surface roughness. The physics of melting and solidification are also important. It is influenced by scan speed, laser power, hatch spacing (distance) or laser scan spacing, material viscosity, surface tension, and thermal boundary conditions like bed temperature. Research has shown that materials that have been degraded for enough time adversely affect the surface quality and increase the viscosity of melted powder [119]. Several factors determine the accuracy of the part and the minimum feature size, including powder sizes, laser spot sizes, feature orientation, aspect ratio, ability to control the melted region, and the resulting solidified geometry of the scanned areas. A thin layer of unfused powder adheres to the part surface due to heat dispersion into the surrounding powder, which must be eliminated during post-processing to achieve the best surface finish [32]. Overall, the main SLS printing factors influencing surface roughness can be classified as design, laser, material, and build chamber.

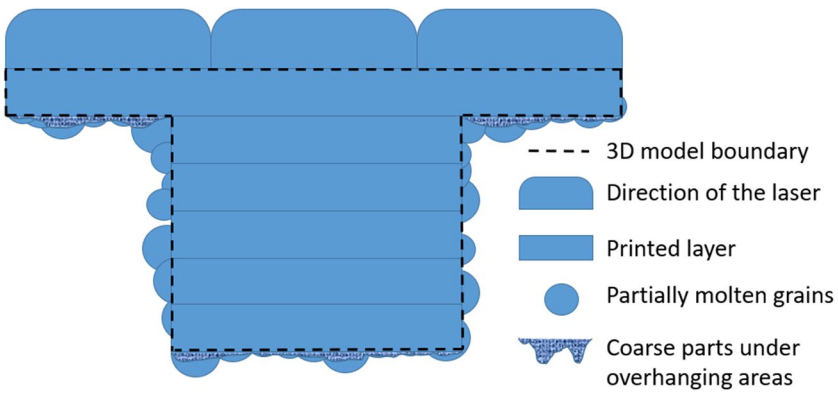

Fig. 13 Typical PBF surface configurations that impact surface quality

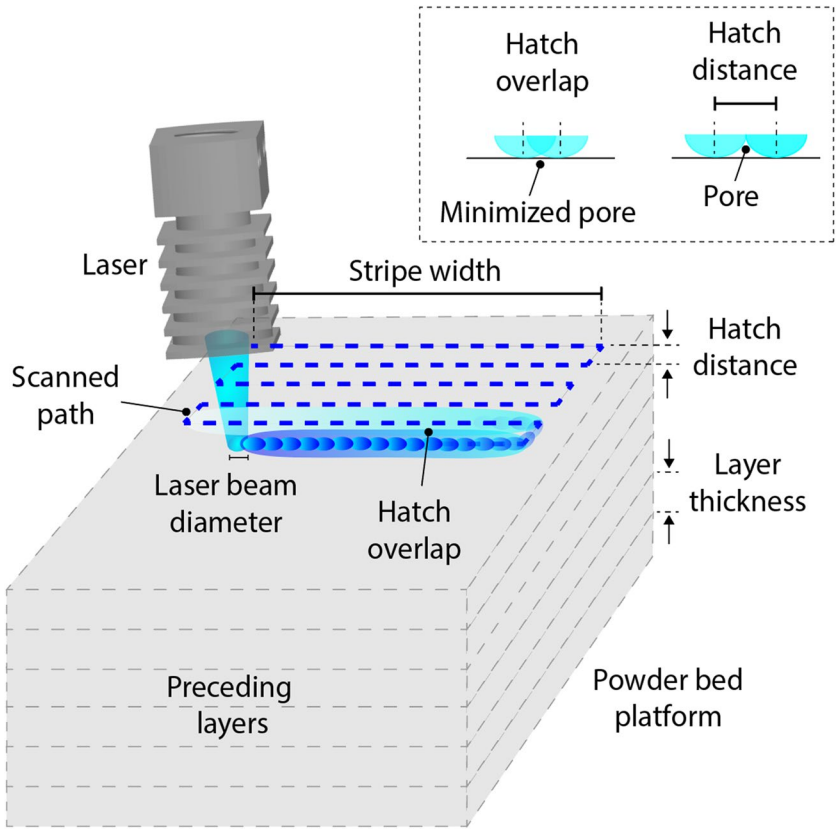

Fig. 15 A schematic of the SLS 3D printing process

Particle size distribution and particle shape can impact the quality and strength of the manufactured objects. These procedures are continued until the component has been produced entirely. SLS processes encounter many difficulties due to the complexity of the thermal interactions involved, which calls for technology-appropriate design and process planning. Relative stresses, microstructural formation, and surface quality are a few difficulties resulting in part deformation or failure [19]. To avoid thermal deformation, the component stays in the powder bed throughout the slow cooling phase [9, 128].

5.1.1 Design

The position and orientation of the SLS chamber are crucial when using 3D nesting during the design stage. As a result of the lower temperature of the platform, the bottom section of the construction volume is not as warm as the upper area. Due to the high temperature in the top half of the build volume, this area is more likely to experience powder adhesion. Process modeling for powder sintering might aid in predicting essential aspects that must be addressed during the early design phase [16].

The size of geometrical features has been discovered to be a significant determinant for the volume of partly sintered powders adhering to the component surface owing to heat intensities, severely impacting manufacturing precision. SLS design criteria should consider massive hot masses, a well-known phenomenon. For this purpose, Minetola et al. [16] suggested the SLS modulus, a metric developed to detect crucial heat concentrations in the chamber that can affect the dimensional accuracy of the produced part. Generally, an approximate part accuracy of ± 200 µm for small dimensions and ± 0.1–1% for large dimensions, as well as a minimum feature size of 0.5–1 mm, should be considered in the design of SLS parts [32, 121]. In Fig. 16, SLS shows sensitivity to feature size where there is a distinct area of separation using a gradient lattice-based design.

A cross-section of SLS parts shows how local and global features in the design influence part quality. The microscale portion comprises fused polymer powder particles ranging from 10 to 100 µm in diameter. The laser heats the particles, fusing them together before solidification. However, incomplete fusion can leave pores within the part, reducing strength, durability, and surface inhomogeneity. SLS parts feature a coarse surface texture at the mesoscale due to particle size polydispersity and unfused powder adhesion based on heat diffusion into the surrounding powder. Non-vertical features are stepped based on layer thickness and orientation [28, 129].

The laser spot size and heat dispersion into the powder limit the minimum feature size in the design step. Freeform

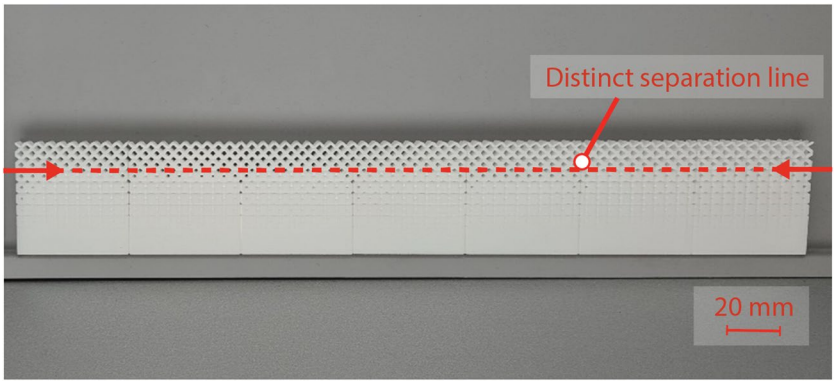

Fig. 16 Accuracy of gradient lattice-based structures in as-printed SLS samples

geometries, interior cavities (with holes for loose powders), and delicate lattice structures are all possible with SLS. Living hinges, latches, and interlocking parts can also be developed. Then, the interior features must be constructed so that loose powder may evacuate when the component is formed.

Because no support structures are required, and cooling warpage is minimal, unsupported walls and horizontal bridges are more flexible than the MEX system. Nevertheless, design and tolerancing must consider temperature gradients during printing shrinkage. Otherwise, very thin features can deform due to temperature variations in the print environment [130]. SLS cannot attain the same surface quality as other polymer AM, such as photopolymerization (SLA). In general, PBF AM processes, including SLS, slice in the *Z*-direction with constant or adaptive layer thickness, whereas the slicing method in filament-based AM is strictly a limiting factor due to lower dimensional precision because of the staircase effect, the required support structures for overhangs, and poor performance because of the anisotropic design caused by the slicing method [104].

5.1.2 Materials

SLS is versatile as it can process many types of polymers available in powder form, either thermoset or thermoplastic. The powder is vital for the packing density, which is influenced by other parameters, including particle size distribution, particle shape, and spreading system. Bimodal powder distribution can improve the packing density [131, 132], which is given by other parameters, such as particle shape, size width, distribution exponent, and packing mode [133]. Particle shape can affect the powder size distribution as the finer powder can facilitate reaching higher packing densities and improve flow and spreadability. The spreading system is also responsible for optimizing the packing density. A wrong method for the powder on the bed can cause flaws in the packing process and entail artifacts or holes in the part once sintered [134, 135]. The most common materials used in SLS are semi-crystalline polymers of PA12 and PA11 due to their well-defined melting temperature and melt-freeze thermal hysteresis [32]. Compared with amorphous thermoplastics, these polymers result in more favorable processing conditions and improved powder recyclability. Table 8 lists the common polymers used in SLS and their applications.

SLS can fabricate complex internal cavities with 3D lattice structures, but features for draining unfused powder must be included. Powder parameters, such as diameter, morphology, size distribution, crystallinity point, flowability, and melting point, also significantly affect the SLS method and the part quality. As a result, there is an increased demand for powders capable of performing SLS [137].

Powders were described as pre-processing parameters but can also be included as printing parameters. Since lasers and

Table 8 SLS AM polymer powders classified by structure and performance [32, 129, 136]

Application class	Structure		Main applications
	Amorphous	Semi-crystalline	
High-performance polymers	-	PEK, PEEK, PEKK	Motorsports, medical engineering, aerospace
Engineering polymers	PC*	PA6, PA11, PA12, TPE, POM*, PCL*, UHMWPE*, PLA*	Automotive industry, mechanical components, housings
Commodity polymers	PS, SAN*, PMMA*	PP, HDPE	Piping, chemical containers, tooling, medical devices, low-cost prototyping

*Commercially not available, only studied in the scientific literature

powder are connected, it is necessary to study and determine the power based on the powder that will be melted before picking up a laser. Polymers must be considered in terms of their heating properties to be suitable for SLS. Furthermore, the optical characteristics of powders determine the wavelength of light the materials absorb [138]. Semi-crystalline polymers are preferred because of their processability (e.g., PA12). There is a clear temperature range for these polymers, ranging from the glass transition temperature to the melting temperature, with a hysteresis window between melting and re-crystallization. The powder type, including recycled and virgin, can affect the surface quality. In general, recycled powders increase the instability of the feedstock properties, resulting in a higher surface roughness [119]. High flowability is a critical property of materials in the SLS technique. Powders must be highly flowable to minimize highly jagged and microscopic particles with strong inter-particle forces that lead to agglomeration and surface issues. Goodridge et al. [139] reported 45 and 90 μm as the most favorable range for powder size in SLS 3DP.

In PBF processes, loose powder is typically removed manually. However, it can be more aggressively removed by shockwave cleaning or dry-ice blasting [140], which alters the surface roughness significantly. Low-temperature heat treatment would be beneficial to improve surface quality. It would relieve imposed stress during laser sintering and improve mechanical properties.

Surface modification of powders can increase laser light absorption, flow, and spreadability. Feedstock enhancement could be used to investigate various powder blends with various or multi-modal particle size distributions (PSDs) and create particle-based models for forecasting the deposition parameters (e.g., spreading speed) and the powder bed packing (e.g., inter-particle friction) and [69]. The thermal history of the polymers is also essential as the molecular weight of the polymer can change when it goes through heat cycles, influencing its melting and solidification behavior. The working conditions significantly impact this powder, and the sintered cake cannot be recycled near the component. Fresh powder must be mixed with the remaining powder from the previous 3D printing procedure to closely match the specifications [3].

This technology works with a higher layer thickness (90–150 μm), making it more susceptible to the staircase effect. Because of the sintered grains on the surface, cleaning is difficult [3]. Powder bed systems are exposed to a frictional force with the bed and an inter-particle force that restrains their motion. For this reason, chemical additives can be added to the powder to have a higher spreadability [141, 142]. There is a variation in the laser beam over the whole build plate. The angle of incidence can significantly impact the outcome of the part [143]. Therefore, new machines with two laser beams are currently available. However, having two different power sources leads to a slightly different sintering process. Furthermore, portions of the stage where the two lasers work almost simultaneously cause a point or line of poor or no sintering.

5.1.3 Laser

The mechanical strength and density of SLS objects depend heavily on the laser beam energy density. As the laser rasterizes over the powder bed, its movement strategy and direction are essential. Generally, higher laser beam energy density results in higher densities and greater mechanical strength of the final part, up to a certain point. If the powder particles are over-melted beyond this threshold, the properties of the part may begin to deteriorate [144]. The most often used SLS printers use diode lasers. The laser power (P), the laser scan speed (v), the focus diameter, and the hatch distance (scan line distance) all affect energy density (ED) [145]. The hatch distance includes two parameters: layer thickness (t) and scan space (s). Depending on the laser power (P) and beam movement on the materials, the powder bed obtains the proper heat for fusion. Accordingly, ED is the laser beam input energy per unit area (J/mm^2), and it can be calculated using Eq. (17) [146]:

$$ED = \mathrm{P}/(v \times t \times s) \tag{17}$$

In this equation, if the hatch distance (in mm) is more than the effective laser diameter (in mm), the effective laser spot size would be considered [147].

Sintering requires a certain amount of laser power due to laser-powder interaction, which depends on the material and layer thickness. Because the laser beam diameter and material formulation affect absorption, they can raise or lower the sintering/melting temperature. It affects the laser wavelength required for sintering. In addition, pulse durations (for pulsed lasers), geometries, and frequencies can impact surface quality. Shorter pulse durations can lead to more precise melting and less heat buildup, resulting in smoother surfaces with less porosity. There is usually an offset between the laser and the design border because of the light spot that must be considered. During the sintering process, a low-power laser is used to smear the particles that can remain attached along the contour [134, 148].

The dimensional accuracy of the printed product causes excellent process accuracy in SLS. Shrinkage is one of the critical factors influencing accuracy, and the quantity of shrinkage seen hugely depends on materials and laser sources. Laser power and scan length have a substantial impact on X-direction shrinkage, whereas beam speed and laser power have a significant effect on Y-direction shrinkage. In contrast, bed temperature, beam speed, and hatch spacing considerably affect shrinkage in the Z-direction [130].

5.1.4 Build chamber

A typical mainstream SLS system has a medium build size of 340 × 340 × 600 (mm). When a product exceeds the build platform volume, it must be split into multiple pieces, designing separation planes, and considering subsequent assembly procedures affecting the surface quality [149]. The part size is constrained on the upper end, restricted by the build volume of the printer and the ability of the optics system to scan the entire area. This volume typically ranges between 10 and 1000 L (0.01–1 m^3). However, it is possible to reach a smaller size in some designs as 0.005 m^3. Due to the minimal residual stresses, the entire build volume may be utilized by stacking pieces on top of one another without the requirement for support to connect the parts to the build platform. The size of small parts is constrained by the minimal feature size, the related precision and resolution, and the assembly of the components [149]. The powder particle and laser spot size restrict the precision of less prominent features. All these variables, coupled with the powder material and thermal boundary conditions, affect solidification kinetics and, hence, dimensional accuracy. In terms of depth and length, the larger-the-better rule applies to the part size to obtain the desired object, whereas roughness and geometric precision are determined by the nominal-the-better rule [127].

Several build chamber parameters, such as layer thickness, roller speed, heating–cooling rates, build size, and powder and feed bed temperatures, impact the SLS process. There are several gradients of temperature in the build chamber to be considered [150]. Besides the *Z*-axis, where the part suffers a decrease in temperature for the higher layers while the stage moves downward, the platform has some increased temperature along the diagonals, and the center can be caused by the presence of heaters or mechanical components underneath. The blade shape used for powder application also affects the surface quality. Beitz et al. [69] demonstrated that a flat bottom form was more advantageous than sharp or slightly rounded edges. Due to the larger horizontal contact zone between the powder bed and blade, the powder material is compressed evenly, resulting in a more dense and consistent powder layer.

5.2 Surface roughness studies and discussion

SLS allows the production of components with high levels of complexity, almost no geometrical constraints, and no need for a tool or a mold. The resulting parts have an enhanced surface roughness due to optimizing the processing settings, the build orientation, and the powder characteristics [66]. Although roughness cannot be removed entirely, several researchers have attempted to decrease the deficiency by modifying the printing process parameters and operating at different parameter levels.

In many cases, PPFTs primarily affect the surface roughness obtained through SLS. Nevertheless, several studies have attempted to optimize the parameters of the process. Sachdeva et al. [124] investigated and used response surface methodology (RSM) to optimize the SLS process parameters for roughness (R_a, R_z, and R_q). Beitz et al. [66] reported that the CLSM measurement yielded roughness ranges of R_a: ~ 24–31 µm and R_z: ~ 157–181 µm, while the XMT method produced R_a: ~ 22–27 µm and R_z: ~ 128–148 µm for PA12 powder. Most research has focused on PA12 as the feedstock material to determine optimal parameters for processing based on roughness conditions. However, limited research [151, 152] has been conducted on other materials. As listed in Table 9, different process parameters were considered in the method.

In agreement with the reviewed papers in Table 9, the average particle size, layer thickness, and surface orientation can substantially influence surface roughness among a wide range of variables. Material viscosity, surface tension, and thermal boundary conditions such as bed temperature play a role in melting and solidification. Heat dispersion into the surrounding powder generates a thin layer of unfused powder to cling to the component surface to achieve the most delicate surface quality. The powder size and the laser spot restrict the part accuracy of less prominent features. These parameters, coupled with the powder material and temperature boundary conditions in the system, influence solidification dynamics, which can also affect dimensional accuracy. Shrinkage during cooling can cause additional losses in part accuracy for bigger features. Concerning laser power, a low energy density can result in loose powder particles that are unable to melt and fuse together sufficiently, resulting in parts that are weak and porous. In contrast, if the energy density is too high, the powder may melt and fuse excessively, resulting in rough surfaces, distortions, and even cracks in the finished parts [119, 127].

While the SLS parts generally show higher surface roughness (10 µm < R_a < 20 µm) compared to FFF (1 µm < R_a < 10 µm), SLS offers many benefits compared to other polymer-based AM techniques [158]. To begin with, no support structures or foundations are needed during the SLS process, since the unused powders support the components. Therefore, there is no roughness caused by support removal. Even though SLS uses unused powders to support the components being printed, this is usually insufficient to prevent all types of deformations. As a result, post-processing steps such as stress relieving and annealing may be required to reduce residual stresses and deformations [119, 157].

Additives such as initiators, binders, and catalysts are not required, which implies that the components are more likely to be utilized in the medical field since additives may cause toxicity. Moreover, although SLS resolution is not as excellent as other AM methods, such as SLA, the mechanical

Table 9 Overview of studies on surface roughness in SLS (see text* below the table for abbreviations)

Materials | Machines	Methodology and studied parameters	Roughness range (μm)	Remarks	Ref
PA12 (2221) | EOS Formiga P110	p.temp. (167 °C), l.p. (25 W), h.d. (0.25 mm), p.s. (2500 mm/s), l.t. (0.1 mm), p-p. (glass-bead), s.r.m.m. (contact + non-contact profilometry)	Tactile A: R_z: 95–120; R_a: 13–17 Tactile B: R_z: 100–124; R_a: 13–17 FV: S_z: 180–240; S_a: 14–18 FPT: S_z: 270–400; S_a: 15–22 CLSM: S_z: 350–450; S_a: 23–27	-Optical and tactile methods showed increased values for R_z, which was typical for SLS parts -R_z and S_z were easily influenced by outliers, so they are not ideal for describing s.r. -R_a and S_a allow a narrower distribution, but peaks and valleys can cancel out -The tip in the tactile method changed the surface -The tip pulls loose particles from the surface or cannot detect valleys. The measured values are quickly reproducible, but the actual topography was uncharacterizable -Optical measuring methods allowed 3D visualization of surface topography, but results vary. FV results closely resembled tactile measurements	[66]
PA12 | DTM 2500plus	l.p. (12.5–17.5 W), plat.temp. (128–138 °C), l.t. (0.12–0.18 mm), a.m. (DoE Taguchi L9, ANOVA), s.r.m.m. (contact profilometry)	R_a: 1.45–1.79	-Optimal values of PPP for s.r. were l.p. (15 W), plat.temp. (133 °C), and l.t. (0.15 mm) -The portion of key parameters influencing s.r. were plat.temp. (55.6%), l.t. (23.11%), and l.p. (16.07%)	[127]
PA12 | DTM 2500 & Sinterit Lisa desktop SLS	DTM 2500: l.p. (10 and 13 W), r.s. (7.62 and 12.7 cm/s), h.d. (0.152 and 0.127 mm), plat.temp. (175 °C), l.t. (0.1 mm), e.d. (0.15 J/mm^2) Sinterit Lisa: p.r. (0.84 and 1.08), e.d. (400–700 J/mm^2), a.m. (ANOVA), s.r.m.m. (non-contact profilometry (FV))	DTM: S_a: 12.431–23.847; a.r.: 1.620–2.454 Lisa: S_a: 13.757–14.328; a.r.: 1.620–2.454	-Lower r.s. and recycled powder (compared to virgin) contributed to a higher s.r. -The greatest average s.r. was recorded when l.p. (13 W), r.s. (7.62 cm/s), h.d. (127 μm), and recycled powder was used -The smallest average s.r. was recorded when l.p. (13 W), r.s. (12.7 cm/s), h.d. (127 μm), and virgin powder was used -The same settings were used to maximize and minimize the area ratio, which helped investigate the tribological properties of SLS parts -s.r. was not significantly affected by powder type or p.r. -Based on ANOVA for s.r., the main effects were powder type, h.d., and r.s.	[119]

Table 9 (continued)

Materials | Machines	Methodology and studied parameters	Roughness range (μm)	Remarks	Ref
PA12 | Sintratec Kit	3 different combinations of blade and roller (counter-rotating roller, forward-rotating roller, and a combination of blade and roller), l.p. (Diode Laser: 2.3 W, 445 nm), plat.temp. (bed: 171 °C, chamber: 147 °C), h.d. (550 mm/s), l.t. (0.120 mm), f.d. (0.25 mm), h.d. (0.3 mm), s.r.m.m. (non-contact profilometry (CLSM and XMT))	CLSM: R_a: ~ 24–31; R_z: ~ 157–181 XMT: R_a: ~ 22–27; R_z: ~ 128–148	-Forward-rotating roller caused defects in the powder bed -The lowest R_a was achieved with a flat bottom geometry of the blade -A round or sharp blade reduced the effective V. compression force, leading to increased R_a -The obtained s.r. was affected mainly by the measuring method -There was no significant difference between the three fractions of PA12 surface quality, confirmed by s.r. measurements in powder deposition direction and perpendicular to it -A flat bottom shape was found to be more advantageous than sharp or slightly rounded edges for the surface quality of a powder bed, resulting in lower s.r. -There was no significant difference between the direction of application of the powder and that perpendicular to it -As with the arithmetic s.r., powder composition and blade geometry had a similar influence on the average s.r. -The fine and coarse powders and the powder deposition direction had no significant influence on s.r.	[69]
PA12 (2200) | EOS Formiga P110	The cross-sections were hatched alternately, p.size (d50, 3: 58 μm) l.p. (25 W), p.s. (2500 mm/s), plat.temp. (167 °C), l.t. (0.1 mm), e.d (0.4 (J/mm^2), b.o. (0°, 45°, 90°), s.r.m.m. (non-contact profilometry	S_a: ~ 25 (H.), 30 (45°), ~ 25 (V.); S_z: ~ 285 (H.), 315 (45°), 235 (V.); R_z: 3 (H.), 0.5 (45°), 1.5 (V.)	-Highest s.r. measured at a layer orientation of 45° -Tribological applications: 90° orientation partially led to a longer running-in-phase as higher wear	[153]

Table 9 (continued)

Materials | Machines	Methodology and studied parameters	Roughness range (μm)	Remarks	Ref
PS & PS + CB | DTM 2000	CO_2 laser at a chamber filled with the nitrogen atmosphere with a maximal 5.5% O_2 PS at preheating conditions: plat.temp. (90 and 100 °C), l.p. (6–21 W), p.s. (1000 mm/s), h.d. (0.15 mm: about one-third of f.d.), plat.temp. (167 °C), l.t. (0.1 mm), e.d. (0.1–0.12 J/mm^2) PS with 0.3 wt-% CB at plat.temp. (100 °C), l.t. (0.1 mm), preheated at 65 °C by infrared radiation heating s.r.m.m. (contact profilometry)	PS at plat.temp. (90 °C): R_a: ~ 14–42; R_z: ~ 100–270 PS at plat.temp. (100 °C): R_a: ~ 3-13; R_z: ~ 10–100 PS + CB at plat.temp. (100 °C): R_a: ~ 18–34; R_z: ~ 125–240	-Evaluation of the processability of PS and the use of CB as a coloring additive was conducted, focusing on the bed temperatures and laser parameters -s.r. of the monolayer parts indicated the coalescence between the consecutive laser tracks -Higher plat.temp., different laser scan strategies, or more l.p. optimization can improve surface quality -Higher R_a and R_z at plat.temp. (90 °C) when used higher l.p., especially in the transversal direction due to lousy coalescence between consecutive laser scan tracks at this bed temperature -Optimal processing parameters being at plat.temp. (100 °C) and l.p. (18 W) -Application: Investment casting	[151]
PA12 (2200) | EOS P395	The DeVIDE software was used to predict R_a values for various implants using CT scan data, the material, and the standard build parameters: laser type CO_2, l.p. (50 W), p.s. (8000 mm/s), plat.temp. (176 °C), l.t. (0.12 mm)	Predicted R_a: 14.4-34.67	-A simulation-based s.r. evaluation was performed to assess various implant prototypes -Application: Medical purpose, bone implants	[154]
PA12 (650) & PCL | OpenSLS	p.size (55 μm for PA12 and 600 μm for PCL), s.r.m.m. (SEM)	Unsmoothed: R_a: ~ 34.0 (PA12), ~ 115.6 (PCL) Smoothed: R_a: ~ 3.9	-R_a was proportional to particle size for both nylon and unsmoothed PCL -Large powder grain (~ 500 μm) led to part surfaces with high s.r. -Unsmoothed PCL had R_a that reflected the visible rough texture of sintered PCL -Smoothed PCL exhibited significantly improved mechanical properties, making it a superior material for bone medical purposes -Application: Tissue engineering	[155]
PA11 | -	b.o. (H. and V.), s.r.m.m. (contact profilometry)	As-printed R_a: ~ 25-50 (T.), ~ 7-35 (B.) After p-p. R_a: ~ 15-25 (T.), ~ 3-15 (B.)	-An increase in the *XY* and *ZY*-orientations was shown to increase s.r. -p-p. significantly reduced s.r. due to a more consistent density	[156]

Table 9 (continued)

Materials | Machines	Methodology and studied parameters	Roughness range (μm)	Remarks	Ref
SLS: PA12 | EOS Formiga P110 MJF: PA12 | HP MultiJet Fusion 3D 4200	SLS: l.p. (16 W), plat.temp. (167 °C), l.t. (0.1 mm), p.s. (1500 mm/s), and h.d. (0.25 mm), CO_2 laser (λ: 10.6 μm) MJF: l.t. (0.08 mm), p.s. (10 s/layer) s.r.m.m. (contact profilometry)	SLS: R_a: ~ 14.62 (T.), ~ 14.40 (B.) MJF: R_a: ~ 15.58 (T.), ~ 6.31 (B.)	-The set of parameters for SLS could be optimized for the best s.f. -T. and B. s.r. of the SLS were very similar -T. s.r. of SLS and MJF were extremely close, but B. s.r. of MJF was significantly better than SLS, likely due to detailing agent application -In SLS, the un-melted core was distinctly smaller than in MJF due to the powerful instant heating capability of the laser -A higher crystallinity was observed in SLS parts compared to MJF, which resulted in higher impact properties and better d.a.	[157]
SLS: PA12 | DTM 2500plus MJF: PA12 | HP MultiJet Fusion 3D 4200	l.p. (38 W), p.s. (10 mm/s), h.d. (0.25 mm), plat.temp. (175 °C), l.t. (0.1 mm), e.d. (0.15 J/mm^3), a.m. (ANOVA), s.r.m.m. (contact profilometry)	SLS: S_q: ~ 17.5 (B.), ~ 24 (S.), ~ 19 (T.); S_{sk}: ~ -0.3 (B.), ~ -0.15 (S.), ~ -0.1 (T.); S_{ku}: ~ 3.2 (B.), ~ 3.5 (S.), ~ 3.3 (T.) MJF: S_q: ~ 16-17.5 (B.), ~ 17-19 (S.), ~ 17.5-24 (T.); S_{sk}: ~ -0.4-0 (B.), ~ -0.45 to -0.1 (S.), ~ 0.1-0.5 (T.); S_{ku}: ~ 3.0-4.5 (B.), ~ 3.2-4.3 (S.), ~ 3.1-4.2 (T.)	-There was a significant impact of the orientation within the build chamber on the bottom surface of the cubes -The influence of orientation was reflected in a similar value of S_q for all the cubes, but a distinct height distribution was indicated by S_{sk} and S_{ku} -Because of thermal bleeding, T. s.r. of SLS varied depending on the selected build region -SLS and MJF exhibited this inhomogeneity issue, and the cube closest to the platform's center (usually the most isothermal region) revealed a skewed and spiked height distribution -Homogeneous surface topography across parts requires thermal bleeding control	[28]

*Abbreviations: *a.m.* analysis methods, *a.r.* area ratio, *b.o.* build orientation, *d.a.* dimensional accuracy, *e.d.* energy density, *f.d.* focus diameter, *h.d.* hatch distance, *l.t.* layer height, *l.p.* laser power, *p.r.* power ratio, *p.s.* printing speed (laser scanning speed), *p.size* powder size, *p.temp.* printing temperature, *plat.temp.* platform temperature, *p-p.* post-processing, *r.s.* roller speed, *s.f.* surface finish, *s.r.* surface roughness, *s.r.m.m.* surface roughness measurement method, *B.* bottom, *S.* side, *T.* top, *H.* horizontal, *V.* vertical

properties of SLS components are usually superior, making the surface of these components more stable over time. The resolution issue may be addressed by improving the laser system. In theory, SLS technology is not material-restricted, and most powders may be utilized in SLS, provided that the laser wavelength and power meet the sintering material requirements. However, this kind of laser/point-based technology (e.g., SLA or SLS) has a common drawback of low processing speed because of the methodology of "point → line → face (slice) → body" [157].

6 Vat photopolymerization (VPP)

Vat photopolymerization produces parts with a resolution close to 100 nm [159], leading to superior surface quality. While the design choice can bring some advantages and some disadvantages in terms of texture, the process selection is still critical. In a top-down VPP setup, the build plate dips in the resin to create a new layer, and generally, a recoating system makes the printed surface smoother. Despite this mechanism and a consequent reduction of the necessary supports, the recoating procedure may cause some convex undulations on the resin surface and on the printed layer afterward. It is due to tensions, especially with highly viscous resins or really thin layers. Thus, surface bubbles can remain trapped inside the part but also can groove the surface [160, 161]. Using scraper blades can attenuate these issues by adjusting the layer thickness of the new resin on top of the part [162].

Alternatively, the bottom-up approach, where the light source is placed below the vat, and the build platform move stepwise upwards, resulting in accurate details but a more corrugated surface [163]. Moreover, confined layers due to the space in between the transparent window at the bottom of the vat and the build plate allow the system to achieve better Z resolution. However, the layer, once cured, attaches to the glass window, and the detachment step might cause it to lose material and have defects. To reduce detachment forces during this phase, the vat is usually coated with a polydimethylsiloxane (PDMS) layer or an anti-adhesive membrane made of PTFE [161, 164] with an additional protective layer of fluorinated ethylene propylene (FEP) to have good anti-sticking effect and durability [165]. The latter seems more resistant to degradation and all the problems this may cause to the quality of microfeatures [166] but has a more complex tightening method that can lead to deformed features and light refraction when applied incorrectly [161]. These approaches constitute a layer-wise method and generate staircases along vertical surfaces.

VPP defects generally occur due to non-optimized print parameters, insufficient supports, improper model generation, and contamination in the build platform and resin material. For each layer to be cured entirely through its thickness and uniformly recoated, the print parameters, such as scan speed, power source, and recoating process, must be optimized [167]. Another common problem with VPP resins is their tendency to turn yellow quickly. This is mainly because of overexposure to ultraviolet light, which also causes clear prints to appear matte yellow (Fig. 17).

6.1 Process parameters

6.1.1 Design

The design role in PPP regards creating the model system on a CAD system and handling the photosensitive resin independently of the technology used. CAD format is tessellated into the STL data, and this is the phase where decisions about surface modeling are made. For instance, essentially flat and/or thick sections are prone to warp because of shrinkage. The STL file approximates three-dimensional surfaces with triangular facets, which may result in errors in dimension, form, and surface [168]. Incorrect conversion of a solid model into an STL file can cause missing or distorted features. In stereolithographic technology, the STL file is sliced into several horizontal layers and then commonly saved in CLI file format [169]. Similar to the FFF method, many parameters such as print direction, layer thickness, the inclination of the part, hatch spacing, fill spacing, hatch over-cure, border over-cure, and fill cure depth are essential to improve surface quality without resorting to a large number of facets and a long build time [168, 170]. Considering the presence of supports is crucial because if the support density is insufficient, the part can also shift or detach entirely from inadequate supports

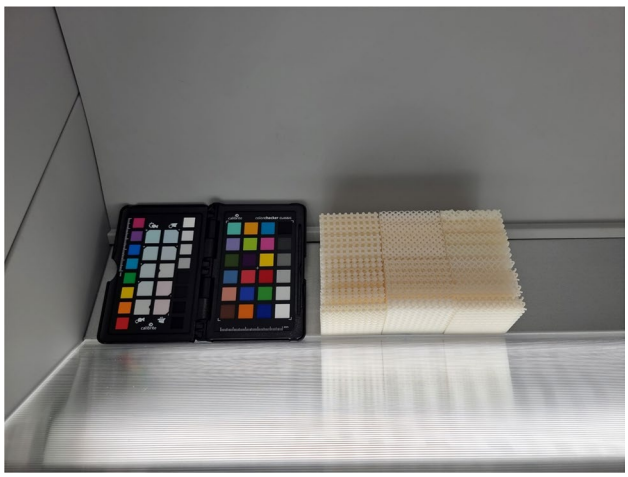

Fig. 17 Appearance and accuracy of gradient lattice-based structures in as-printed SLA samples using PrimaCreator Value resin. After 12 h, a yellowish color began to appear

[171]. The supports cause unavoidable staircase effects on bent or sloped surfaces, but they can be reduced by adjusting the printing parameters mentioned above [172]. In this case, the adaptive slicing method, as a typical practice in FFF, is acquiring more attention to improve the surface quality and surface roughness in VPP methods [96, 173].

6.1.2 Materials

The most popular materials for VPP are photosensitive resins, usually containing acrylates, methacrylates, vinyl, and epoxies monomers/oligomers. Acrylates and methacrylates monomers/oligomers are a subcategory of the vinyl group, and the presence of the carboxylic group (-COOH) in the vinyl position confers them high photo speed as they react quickly when exposed to UV radiation. Moreover, they behave differently in terms of radical formation. Acrylates tend to form secondary radical ends, whereas methacrylates tend to form tertiary radical ends. This difference in radical end formation makes methacrylates more stable and less reactive than acrylates. However, both of them undergo significant shrinkage with associated stress that might result in warping or curling [174, 175]. Moreover, they suffer from the inhibiting influence of oxygen, and this facilitates the formation of a sticky surface appearance due to oligomer formation [176]. They also have low viscosity and critical energy, increased light sensitivity, relatively high dependence on humidity and temperature fluctuations, and controllable mechanical properties [177].

Vinyl monomers appear in both radical and cationic polymerizations, and a mix with acrylates or epoxies enhances their respective characteristics. They provide relatively low thermal resistance and low glass transition temperature, and they tend to exhibit brittleness, low elongation, toughness, and impact resistance [178]. Epoxy monomers instead have an oxirane functional group, which is a three-member ring formed between oxygen and two carbon atoms, and when they react, these rings open, resulting in vacancies for other chemical bonds. This opening is known to have an influence on the volume change because the bonds remain the same and, as a result, epoxy resins typically present much smaller shrinkage and much less tendency to warp and curl. Furthermore, the products have high structural stability, higher mechanical performance, insensitivity to oxygen, and lower shrinkage stresses compared to radical polymerization of (meth)acrylates and vinyl monomers [175, 179]. All these monomers can be also added as additives with the function of chain transfer agents, specifically addition-fragmentation chain transfer (AFCT) agents, in a poly-functional way, with the intent of having, for instance, lower shrinkage stress, higher cross-linking density, or tougher polymers [180, 181]. Besides monomers/oligomers and additives, the photocurable resin generally presents reactive diluents, UV stabilizers/blockers, and photoinitiators.

Also, adding particles as reinforcement in a resin can result in reduced or absent curing or in an accumulation of the particles, leading to a nonuniformity or degradation of the support. Studies about the size of the particles [182] and their interaction [183] were found essential to obtain the best outcome. Therefore, in VPP, the cure kinetics of the polymerization process related to the resin viscosity, light intensity, chemical functionality, illumination time, and the additives in the formulations play a crucial role in determining the final surface finishing and appearance of the prints [179]. In fact, the choice of light absorbers, the photoinitiator, and the monomers and oligomers can reduce the staircase effects, improve the resolution of printed objects, and produce optically more transparent layers and surfaces. Kowsari et al. [184] evaluated the influences of polymer formulation on the printing resolution and surface quality. In particular, by trying different formulations of (meth)acrylates-based monomers and oligomers with some of the most common photoinitiators, they found that dimethacrylate-based resins can improve the surface finishing by reducing the staircase effects and removing jagged edges. Moreover, enhancing the expected reflectance at the same wavelength is possible with different photopolymer formulations [177]. The selection of photocurable resins is usually according to the properties needed, such as quality of finish [185], durability [186], flexibility [187], transparency [188], bio-compatibility [185, 187], and cost [189]. They need to be stored in dark rooms to avoid the photopolymerization process initiates.

Moreover, when the resin is poured into the vat, it may contain air bubbles that reduce the achievable resolution and cause surface artifacts in the final object. Therefore, removing all the impurities and air from the photopolymer is necessary. It is possible to do so by shaking the resin manually or with the help of some machines, such as roller grills or shaking machines [161]. When the resin is not fully polymeric but with a mole percentage of other compounds, another step that is part of the pre-processing is the mixing process, which is requested to be as uniform as possible.

Polymers are not the only materials that can be used in photopolymerization processes. Diptanshu et al. [182] assessed how introducing fine ceramic powder can improve the density and reduce the porosity of the prints. The interaction between photopolymer and photons greatly influences the surface quality of the part. As well as laser power and uncontrolled photon flux, a nonuniform surface relief during the material solidification generates features much larger than the voxel size. Ambient factors, such as vibrations and jittering of the laser and its scattering while impinging the surface, may cause voxel displacements and fluctuations of printed voxels, inducing a weaker photon flux and defects in

the layer so formed [184, 190]. During the printing process, contaminants, such as partially cured regions or external particles, can cause voids and deficiencies in the build since the resin cannot be recoated evenly. A damaged resin tank or dirty optics may also result in improperly cured regions, resulting in internal voids or inclusions. Last, voids within the resin caused by trapped air or not uniformly recoating the next layer will result in voids in the printed part [177]. Photopolymerization can also be affected by oxygen inhibition due to a different air in the room (with an inert gas), high-intensity irradiance lamps, or physical barriers [191, 192].

6.1.3 Printer setup

The setup of the printer and the influence of polymer mass and viscosity can also affect the surface finish, which is divided into two major categories:

- The *bottom-up* approach: the material is cured through a window, and a membrane of PTFE is placed in the bottom of the vat with a light source. In this setup, the build plate is raised every time to let the new resin occupy the volume underneath, and a "peel" step is necessary to detach the cured resin from the bottom of the vat. The "peel" step is time-consuming because the resin needs extra time to recover the initial state before starting the new layer [193].
- The *top-down* approach: a light source above the vat cures the material, and the build plate is submerged. Instead of "peel" steps, this setup employs continuous light exposure to cure the resin. It enables the achievement of high resolutions and printing speeds for this approach. The surface is traversed with a scraper to recoat and minimize eventual surface tensions [162] or can provide a dynamic characterization of the shape of the surface of the resin and adjust the light intensity accordingly [194].

Regarding the exposure strategies, in the bottom-up approach, there are no micro-fluctuations or contamination of the resin during the process since the bottom of the vat flattens each layer, but the detaching step might cause a corrugated surface with accurate details in the surface of the products [163]. However, in the top-down approach, there is not as much stress on the printed part during the printing process as in the bottom-up approach since the subsequent layer is not being sheared off after each layer is cured. Nonetheless, the overall distortions of the surface due to the motion of the stage normally require a recoating procedure that still can cause undulations on the printed layer. Moreover, longer printing times and slightly better resolution and quality of the printing drive the choice for the bottom-up approach. Other setups are related to different components that make the technology unique and solve some of the drawbacks. For instance, an oxygen-permeable window in CLIP technology solves the peeling step issue by preventing the resin from attaching to the window. At the same time, it controls the curing of the resin letting it have sufficient time to flow underneath the build plate and completely homogeneously the curing of the subsequent layer. In this way, the platform can move almost continuously upward [191, 192].

DPP technology uses an LCD unit to project the sliced 2D images, which has great potential resolution/cost-wise but has overall limited optical efficiency and lower resolution. In addition, working with an electric field that blocks the passage of light has a low switching speed (within 20 ms), and this may cause a few liquid crystals to remain trapped, resulting in weak light leakage and lower resolution [169, 179]. Hot lithography has the advantage of having a heating element able to control the viscosity of the resin and the temperature of the process. A higher temperature increases the reactivity of the monomers and the polymerization rate and the efficiency of the process [195].

Two-photon photopolymerization employs a femtosecond compact laser beam as a light source that absorbs two photons simultaneously. The photons are absorbed by the photoinitiators at the same frequency (degenerate process) in the near-infrared range (NIR). To trigger the third-order nonlinear two-photon absorption process, light sources with very high photon density are required. Since the light intensity in the laser beam respects a Gaussian distribution, in TPP, the square value is considered, and the region where polymerization occurs is lower than in normal conditions. In this way, a pulsed femtosecond laser with an acoustic-optical modulator (AOM) to disperse the beam into zero- and first-order diffractions or two light beams (stimulated emission depletion or STED) are the most preferred setups, because they can modulate the intensity and better control over the cross-linking process. Therefore, the resolution of the process and the connected feature size of the voxel improve until reaching details of 100 nm [32]. The concept is described in more detail in a study by Malinauskas et al. [258].

6.1.4 Curing system

In most cases of VPP, the substance is sensitive to light (but not necessarily), i.e., it will absorb the energy of the photons [177]. This energy induces either phase transitions (evaporation, melting, plasma) or chemical reaction in the material. As many materials can absorb light energy, VPP is a very versatile method for selection. However, there are significant variations in the specifications of the main VPP branches, such as the light source (UV or laser), feature size (nm to m), applicable materials, sensitivity to processing parameters, and the possibility of multi-material printing and commercialization capability.

In most VPP technologies, the object is created by irradiation of the photosensitive resin with a UV or laser beam source that enables the cross-linking of the polymer chains. It is scattered and absorbed when UV radiation or a laser beam hits the surface. This creates a threshold for the penetration of the light in the resin and, therefore, a cure depth for the photopolymerization process. The cure depth is given by Eq. (18) [169]

$$C_d = D_p \ln\left[E_{max}/E_c\right] \tag{18}$$

where the maximum exposure energy is represented by E_{max}, the critical energy required from the resin to begin the reaction is denoted by E_c, and D_p is the depth of penetration defined by

$$D_p = 1/(2.3\varepsilon[I]) \tag{19}$$

where $[I]$ is the concentration of the photoinitiator and ε is the molar extinction coefficient.

The energy dose considerably affects surface roughness and dimensional accuracy through the curing process [196]. In SLA, the projection system is the key factor that can sensibly modify the appearance of the part. A galvanometer scanning technology provides the steered beam through a movable mirror system to the resin surface and determines the precision grade. The exposure energy at the surface is determined by the steered beam as follows:

$$E = \sqrt{2/\pi}(P/W_o V_s) \tag{20}$$

where P denotes the laser power, W_0 is the beam radius, and V_s represents the scan speed [169]. In line with the equations above, it is possible to see how much the entire process can undergo the projection system.

The power, velocity, and hatching of the laser spot determine the depth and size of the feature. Independently from the build orientation, there is a low anisotropy set by the cure depth according to the layer thickness. In fact, the layer thickness is lower than the cure depth, which means that an additional beam dose passes through to the previous layer to facilitate the adhesion and the bonds between subsequent layers [161, 197]. Furthermore, the width of cured resin (L_w), as determined by the center of the laser beam, influences the resolution and dimensional accuracy. When the laser beam passes over the same points while hatching the layer, some points might be over-cure or under-cure. For a successful solidification, it is essential to define a hatch spacing related to the width of the cured resin [169]. Nonuniform laser power density is another important parameter that can be caused by either acceleration or deceleration of the galvanometer at the end of the hatching and along the boundaries. This can be overcome by either modulating the laser power as a function of scanning speed during acceleration or deceleration or keeping the same scanning speed while switching on and off throughout the job [198].

6.2 Surface roughness studies and discussion

The parameters affecting the surface quality can be identified by further examination of the most critical technologies in VPP. Nowadays, the research in surface quality for the Vat photopolymerization technique is extensive, mainly because it combines an affordable price with high performance in terms of printing precision and time. There has been considerable research on SLA and DLP, the oldest and most commercialized technologies. Still, new trends are emerging due to their faster print speeds, such as CLIP [32, 191], and higher and higher resolution, like TPP [194]. Instead of surface roughness, recent significant research results are presented, focusing on SLA and DLP in Table 10.

According to Table 10, the quality of VPP printing is primarily determined by the photopolymerization process, exposure strategies, and projection systems. Generally, the projection system plays a prominent role in the resolution and printing quality outcome. The microstructure heavily depends on the technology used, and even if all the parameters are optimized, there will always be an error that is impossible to entirely remove. For instance, the light permanently distorts how it impinges on the resins. However, the sum of errors can also outperform other optimizations.

In the same VPP technique, the most predominant parameters influencing the roughness are the build orientation and the layer thickness. Indeed, they are directly connected with the staircase effects. In the top-down approach, once immersed in the resin, the part goes down with a depth based on the layer thickness [183]. Reeves and Cobb [207] found a mathematical model for the approximation of the surface roughness considering the layer thickness and the plane orientation (Fig. 18). It consists in

$$R_a = \left(L_t(\tan\varphi\sin\theta + \cos\theta)/4\right) + K \tag{21}$$

where R_a is the roughness average, L_t is the layer thickness, φ is the layer profile angle, θ the surface angle, and K is the composition roughness (up-facing or down-facing roughness).

As discussed above, different systems can offer various methods to get very high resolution, but many other parameters must be considered. Regarding the resin material, the interplay with different photoinitiators, monomers, or oligomers [184], the addition of additives such as stabilizers or light absorbers [32], the addition of ceramic powder [182], and the resulting viscosity [183] in the resin can influence the cross-linking process on the resultant resolution and

Table 10 Overview of studies on surface roughness in VPP (SLA and DLP) (see text* below the table for abbreviations)

Materials | Machines	Methodology and studied parameters	Roughness range (μm)	Remarks	Ref
Proprietary Resin | SLA XJRP-SPS600	f.d. (0.1 mm), l.t. (0.1 mm), p.s. (8 m/s), b.o. ([10–90°], 10° step), s.r.m.m. (contact profilometry)	R_a: ~ 3–17	-b.o. 10° and 90° resulted in the highest (17 μm) and lowest (3 μm) s.r. -Increasing b.o. continuously decreased s.r. -The s.r. was remarkably reduced after coating with the polyethylene wax emulsion	[199]
UTR9000 resin | SLA Shanghai Lite-450	l.t. (0.09, 0.12, 0.15, 0.18 mm), over-cure (0.19, 0.21, 0.23, 0.25 mm), l.p. (270, 290, 310 and 330 mW), h.d. (0.07, 0.08, 0.09 and 0.10 mm), p.t. (5 min), r.h. (34%), a.m. (DoE Taguchi L16), s.r.m.m. (contact profilometry)	R_a: ~ 3.76–3.99 (for different l.t.), ~ 9.87–20.05 (for different width), ~ 6–30 (V.), ~ 1.49–2.6 (H.)	-The process parameters that affect the s.r. in the direction parallel to the scanning direction were based on the following order: l.t. > l.p. > p.t. > h.d. -High random errors in the direction parallel to the scanning direction at various positions for the same part, whereas s.r. differed according to b.o. due to l.p., temperature, and r.h. inside the machine	[200]
PR48 CPS resin |Ember DLP	l.t. (0.010, 0.025, and 0.050 mm), e.t. (1.2–2 s), s.r.m.m. (non-contact profilometry)	R_a: 1.5–6.4 (V.), ~ 2.2–2.4 (H.); R_z: 9.7–21.9 (V.), ~ 7.1–8.6 (H.); R_q: 15.9–49.4 (V.), ~ 67.5–74 (H.); R_{sk}: 0.1–0.4 (V.), 0.1–0.2 (H.)	-The surface profile angle was predicted with a maximum error of 2°, and the average s.r. was predicted with an error of 2.7 μm -The l.t. was found to influence the light-induced s.r compared to the exposure time	[201]
Accura ClearVue | SLA ProJet 6000 HD	b.o. ([0–90°], 30° step for each of F., S., and T. direction), a.m. (DoE Taguchi L20, ANOVA), s.r.m.m. (non-contact profilometry)	R_a: ~ 1.2–3.4, 2.102 (F.), 2.181 (S.), 2.177 (T.), 1.733 (H.), 2.686 (30°), 2.546 (60°), 1.649 (V.)	-Very low s.r. values were observed for SLA parts -The surface where layers are parallel to the b.o. showed higher s.r. compared to the surface with perpendicular layers due to the staircase effect	[202]
Synthetic Grey Resin V3 | SLA Formlabs Form 2	l.t. (0.025, 0.050, and 0.100 mm), b.o. (0° and 15°), Model structure (solid vs. hollow), was printed at different positions and configurations, a.m. (ANOVA, post-hoc tests, and Student's t-test), s.r.m.m. (contact profilometry)	R_a: ~ 0.025–2.18 (H.), ~ 0.025–2.86 (15°)	-The model structure did not affect s.r., but b.o. did -Higher printing precision was reached by aligning the models across the front of the build platform, reducing overhangs, using support structures, and selecting a high-printing resolution -The staircase effect on the bent or sloped surfaces was caused by the support structure and b.o. It can be reduced by adjusting other PPP	[172]

Table 10 (continued)

Materials | Machines	Methodology and studied parameters	Roughness range (μm)	Remarks	Ref
Watershed 1120 | SLA Viper SI2	b.o. ([0–180°], 2° step), h.d. (50, 75, 100, 125 μm), l.p. (100 mW for border and 58 mW for h.d.), p.s. (20.5 mW for border and 124.1 mW for h.d.), l.t. (0.1 mm), resolution (7.6 μm (*XY*) and 2.5 μm (Z), continuous-wave laser (Nd:YVO4 solid-state, λ: 354.7 nm) f.d. (250 μm), a.m. (ANOVA), s.r.m.m. (contact + non-contact profilometry)	Contact profilometry: R_a: 1.2, R_q: 1.6, R_z: 6.2 Non-contact profilometry: R_a: 1.0, R_q: 1.3, R_z: 6.0	-Increasing b.o. from 0 to 90° resulted in higher s.r. followed by a slow drop -In the range of 90 to180°, s.r. was increased gradually, followed by a quick drop -Higher h.d. resulted in higher s.r. and less p.s. -The effect of p.t. on s.r. was negligible	[173]
- | SLA apparatus	b.o. (0–90°), l.t. (0.08, 0.1, and 0.12 mm), a.m. (DoE full factorial design, blocking technique), s.r.m.m. (contact + non-contact profilometry)	R_a: ~ 3.2	-b.o. and l.t. affected s.r. -Post-curing played a negative role in s.r.	[203]
Dental LT Clear Resin | Customized DLP: projector (OPTOMA EX330e) SLA Formlabs Form 2	b.o. (0° and 45°), e.t. (18 s), Measurements of s.r. along and perpendicular to the b.o. were carried out, s.r.m.m. (contact profilometry)	DLP R_a: 0.57 (H., T.), 1.37 (H., S.), 0.675 (45°, T.), 1.67 (45°, S.) SLA R_a: 0.995 (H., T.), 1.225 (H., S.), 1.24 (45°, T.), 1.815 (45°, S.)	-Characterizing the projector light spectrum and using photosensitive resins with detailed curing specifications were significant in terms of material curing to get a higher control on material processing and have lower s.r., good optical properties, and d.a.	[165]
NovaFab casting resin | DLP	a.m. (PSO)	Before optimization R_a: 21–38 After optimization R_a: 13–31	-p.s. increase by volume decomposition technique and eliminating supports -Segmentation design improves p.s. (by 45.2%), reduces material consumption (by 15.8%), and s.r. (by 19%) through decreasing the support structures and lowering the height of the segment	[204]
HDDA, Irgacure 819, SUDAN | Customized DLP: DMD projection system + UV LED (365 nm)	l.t. (0.050, 0.080, and 0.100 mm), c.t. (2, 3, and 4 s), b.o. (60 to 90°), Gaussian radius (12 μm), Concentrations: Monomer (4460 mol/m^3), Photoinitiator (48.27 mol/m^3), Stabilizer (4.06 mol/m^3), Environmental oxygen (8.69 mol/m^3) plat.temp. (300 K), incident light intensity (24.5 mW/cm^2), Projection micro-stereolithography (PμSL) for modeling photopolymerization is implemented by Comsol Multiphysics software, a.m. (DoE Taguchi L27, Multi-Objective PSO)	*RMSE*: 1.45 (V.) 2.13–22.48 (60°)	-All parameters with the order of photoabsorber, c.t., l.t., and oxygen concentrations affected s.r. -Based on PSO, the framework increases p.s. for 50% at the same surface quality for b.o. 90° -Optimized samples showed 18% increases in the surface quality for b.o. 60° at the fastest printing speed -Increasing p.s. resulted in rougher surfaces -V. s.r. (90°) was generally lower than s.r. for tilted surfaces (60°)	[205]

Table 10 (continued)

Materials | Machines	Methodology and studied parameters	Roughness range (μm)	Remarks	Ref
5 different Zortrax resins | DLP Inkspire 3D	5 specimens of each resin type were printed with l.t. (0.05 mm), b.o. (0°), i.d. (100%), h.d. (5 mm), and e.t. (10 s) Theoretical s.r. was calculated using analytical pixel analysis measured at 2.4 mm distance, s.r.m.m. (contact profilometry)	R_a: 0.410–1.027; R_z: 2.370–5.844	-More rigid materials (black, basic gray) showed better flatness because of better bonding during the solidification process -s.r. values were similar for 4 resins. Transparent Yellow resin showed almost 2 times higher s.r. (Maximum R_a and R_z) compared other resins -In transparent resins, overcuring might happen as projected UV light while curing the next layer in order might have reached already cured layers. It partially increased e.t in comparison to non-transparent resins	[206]

* Abbreviations: *a.m.* analysis methods, *b.o.* build orientation (direction), *c.t.* curing time, *d.a.* dimensional accuracy, *e.t.* (layer) exposure time, *f.d.* focus diameter, *h.d.* hatch distance, *i.d.* infill density, *l.p.* laser power, *l.t.* layer height (thickness along Z-direction), *p.s.* printing speed, *p.t.* post-cure time, *plat.temp.* platform temperature, *r.h.* relative humidity, *s.f.* surface finish, *s.r.* surface roughness, *s.r.m.m.* surface roughness measurement method, *F.* front, *S.* side, *T.* top, *H.* horizontal, *V.* vertical

quality of the features fabricated. On the other side, volumetric shrinkage throughout the curing course is the primary source of errors and the primary parameter of geometrical error [169]. Local temperature variations [208], UV intensity, and exposure time are critical factors that can affect surface roughness and cause under-cured or over-cured parts leading to geometrical errors.

Although various researchers have examined the level of mechanical anisotropy for SLA-printed parts [197, 209], Shanmugasundaram et al. [202] and Hague et al. [210] reported that SLA-printed components can be considered isotropic. The capability to produce isotropic components with SLA is a significant advantage over other AM techniques, such as FFF.

7 Material jetting (MJT)

PolyJet technology typically produces high-quality parts with a smooth surface. However, dimensional accuracy for large pieces is usually not similar to other processes, such as VPP, since it uses large droplets, and the accuracy decreases. The accuracy for medium-small size parts is comparable to the other AM technologies [134].

The amount of surface roughness depends on several geometrical and process parameters. MJT produces full-density parts by overlapping adjacent droplets and curing or solidifying them on the spot [8, 211]. A defect can be caused by a clogged nozzle or, in rare instances, by errors in the jetting toolpath. Most AM jetting systems used by professional AM companies are well calibrated and deposit uniform layers without accumulating errors and porosities. However, local variations in topography and layer thickness must be considered when mixing multiple materials and at the interface between the part and the support (Fig. 19). This is caused by the formation of a mini pool and droplets similar to that seen in welding [212, 213].

A variety of methods are available to address and mitigate porosity during the material jetting process, such as using appropriate printing parameters [8, 211], optimizing material properties [214], increasing the number of printed layers to fill in any gaps or voids, as well as modifying the printing pattern [215]. The use of appropriate printing parameters such as droplet size, spacing, and temperature; optimization of material properties such as viscosity, surface tension, and curing time; and modification of the printing pattern such as zigzag instead of straight lines [216] can reduce void formation by ensuring that the material is deposited uniformly and consistently.

While polymer jetting improves the quality and tailor ability of mechanical properties, in general, the properties (particularly toughness and elongation) do not match those of photopolymer parts made by SLA. Jetting compatibility requires resin formulations, compromising the selection of optimal photocuring chemistries [134].

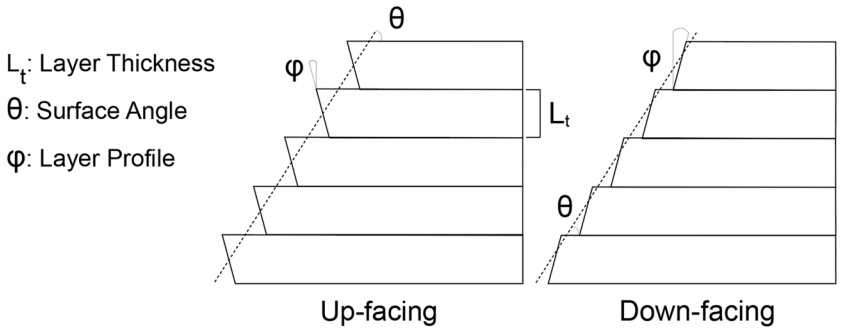

Fig. 18 Surface roughness for a stepped plane. Adapted from Reeves and Cobb [96]

7.1 Process parameters

MJT performance is determined by the fundamentals of the process, such as placement and fusion of consecutive droplets, as well as droplet impact, spreading, and curing. Since the MJT system contains many functions, as described, the printing QAs undergo a higher range of parameters that need to be considered. For instance, part quality in MJT depends on the substrate, material velocity, dynamic viscosity, nozzle distance, total pressure, surface tension, density, the diameter of the nozzle, position accuracy of the *XYZ* motion stages, platform movements, etc. [134]. This section discusses these parameters in four main categories: materials, designs, surface finish settings, and printheads and rollers.

7.1.1 Design

Design plays a crucial role in achieving greater accuracy and preventing printing errors. Due to the layer-by-layer setup of the technology, most of the aspects related to the design of the model described in the section for FFF also have an impact here. However, the layer thickness, orientation, hatch spacing, and speed are more relevant for this technology. Droplet size, spacing, and how they impact the build platform affect the line surface finishing. The less space between droplets results in defects in the reduction of line edges and improvement of the resolution [217]. Accordingly, layer thickness is the most crucial parameter, as seen for most other AM technologies. Generally, a lower layer thickness improves the QAs of the prints. At the same time, a lower space between lines causes a decrease in the eventual ripple along the top and bottom of a layer, resulting in different surface roughness based on the design orientations [24, 70, 217].

Design orientation, including the building location on the build plate, also affects the surface roughness. According to the study by Yang et al. [218], orientation induces different roughness values in the parts. *XZ* build orientation seems to give the highest surface roughness value, while *XY* has the lowest, with the top and the bottom surface reaching high smoothness [218, 219]. Similar to FFF, leveling the build platform prevents distortions and failures and reduces surface defects. An infill density of less than 100% is not regularly achievable for AM parts made from

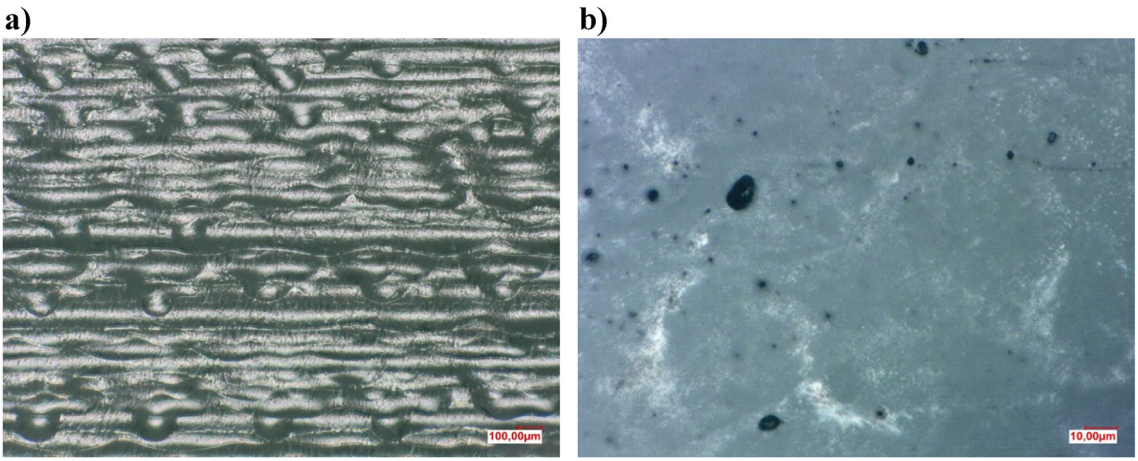

Fig. 19 **a** Deposited droplets in a layer-by-layer structure and **b** porosities in the structure of parts printed by Stratasys PolyJet J55 printer

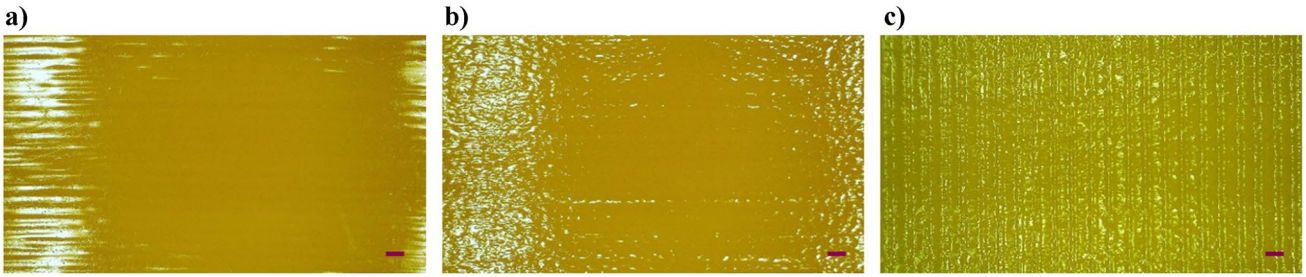

Fig. 20 MJT-printed samples at different wedge angles: **a** 0°, **b** 45°, and **c** 90° (scale bar represents 1 mm)

photo resins since support is needed for overhanging features during the printing process to avoid collapse [64]. Figure 20 illustrates how build orientation (wedge angle) can affect the surface texture of samples printed under similar conditions.

7.1.2 Materials

In most cases, the MJT process uses polymers and plastics, such as Tango and Vero commercial resin. Each of these series has different ingredients. For instance, the FullCure 870 VeroBlack digital material comprises acrylic monomers, epoxy acrylate, urethane acrylate oligomers, and photoinitiators. As an example of support material, FullCure 705 contains acrylic monomers, polyethylene glycol, propane, glycerol, and a photoinitiator [24]. Due to the small and expensive range of materials that can be printed, MJT is limited in its material availability. In particular, waxes and photopolymers are the only commercially available polymers.

MJT "inks" are photo resistors mixed (blended) with waxes and some photopolymers. In modern systems, six liquids (CMYK-W + Support) can be handled simultaneously in separate containers. The printhead can combine multiple materials in a single part and blend pairs and trios of selected base resins to create hybrid properties and colors. They are also called digital materials, defined as composite materials developed for AM (mainly PolyJet 3D printing) with predetermined mechanical and visual properties [220]. Additionally, jetting of multiple materials facilitates support removal and allows high-detail visual representations and functional prototypes to be generated in full color.

Materials are divided into two main categories of base resins and support materials. The term "resin" refers to solids and highly viscous materials, but more commonly to liquids that harden in response to an agent (e.g., heat, setting agents, or light). Base resins carry the main functional characteristics and colors, each with unique characteristics. Thus, a machine can use them as a palette to receive hybrid materials. They are the basis for inks and can be used without mixing or combined to reveal new properties. Resins are a wide variety of different natural and synthetic materials. They consist of long monomer chains, forming cross-link bonds during the curing process. According to their chemical compounds, resins can be silicones, epoxies, acrylics, alkyds, etc. They can be divided into several categories: strong engineering, rigid general-purpose material, biocompatible, transparent rigid, castable, strong and tough, flexible, simulated (digital) polypropylene, simulated (digital) ABS, and composite resins [221, 222].

Material jetting requires supporting structures, and some resins are optimized for easy removal. They come in various types with different solubility parameters, which affect the range of the chemicals needed to fully dissolve them. Besides, support materials used on the surface will determine whether the surface is glossy or matte, which affects the surface roughness. The supporting resins can become soft during the printing process, which allows them to be removed manually, and the final touches are applied using a water jet. Wax-like support material is generally more rigid than gel-like material and, therefore, cannot be easily removed, resulting in a reduction in surface quality [223].

One of the most challenging aspects of this type of technology is the ejecting of the photocurable resin. For this reason, the materials in play assume a crucial role in the process.

In order to be jetted, resins need to have the correct viscosity according to their composition. For instance, Cheng et al. [224] heated the resin to 70 °C, while Jabari et al. [225] mixed and sonicated the resin with a graphene dispersion to obtain an appropriate flowability. There are many methods to gain the correct viscosity for various resins. Still, a resin generally needs to be as liquid as possible to avoid suspending particles that might cause artifacts or reduced accuracy [134]. Particles in the resin lead to imbalances during the drop creation, with sizes that may differ from each other. In fact, this occurs because there are disturbances during the ejection that may change the extrusion setup with an earlier breakup of the drop. Moreover, the droplet spreading and roller performance at each layer deposition can assume different physiognomy [226].

As with binder jetting, another critical parameter to consider is the impact of the droplet on the surface. According

to Zhou et al. [227], three forces describe the droplet impact dynamics: inertia, surface tension, and viscous force. At the build plate level, the inertia force is converted into surface energy, and it needs to overcome the surface tension to obtain a flat shape. It means that the inertial force needs to be greater than the surface tension, which is helped by the viscous force. Moreover, the potential difference imparted by the piezoelectric system strengthens the surface tension and increases the impact angle or the height of the ejection [227, 228]. On the other hand, if the height is excessive, head and rear vortexes on the droplet can be formed because the ejection and the drop may impact the surface with different angles and energies [228].

7.1.3 Printhead and roller

Material jetting can print very tiny liquid droplets that reach resolutions around 1600 dpi and 16 µm [229]. The resolution depends on the ejection system but is also related to the droplet size. However, decreasing the specimen thickness increases the magnitude of distortions in the photopolymerization process [219].

Two printing modes are available in PolyJet technology: high speed and high quality with a low layer thickness. If the ejected droplet size is not big enough to cover the spacing between two subsequent ones, the printhead must pass over the same point one more time. According to the offset to fulfill, up to four rounds of jetting may be needed [230]. It is common for MJT printers to jet photocurable resin from different nozzles simultaneously; however, the build platform function may differ (Fig. 21). A roller module leveling mechanism is required to remove the excess resin and flatten the surface to reach the desired layer thickness. After this step, the droplet is immediately cured [223].

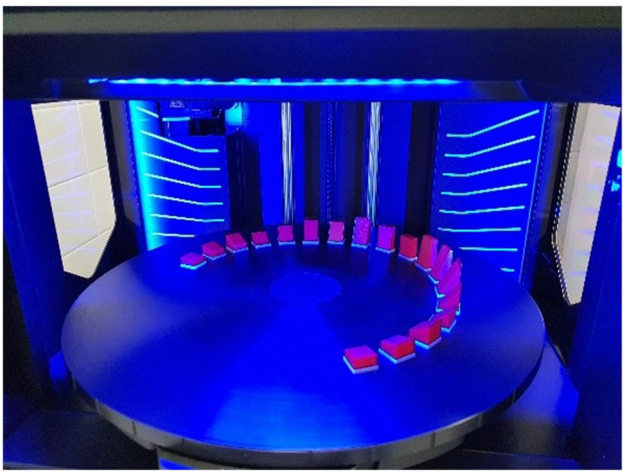

Fig. 21 An illustrative photo of the rotary build tray of the PolyJet J55 printer

The hatch spacing in MJT, like other AM techniques such as SLS and BJT, contributes to the texture and morphology of the surface [134, 231]. It comprehends the pulse width and the frequency with which droplets are ejected, and the ejection system series of rounds passes over the same point to create an entire surface. Printing speed is connected with the hatch spacing because it is also based on the sweep speed at which the hatch arises [134].

The quality of the droplet is another aspect to consider. Bussmann et al. [232] showed that impact velocity and angle are essential in terms of quality printing and surface roughness. The effect of rough cured drops may avoid the impact of fingering (perturbed leading edges) and splash (refer to Fig. 20).

Droplet impact, spreading, and curing limit the accuracy of parts and the motion system, which is often a gantry operated by a motor. Droplet spreading and curing restrict the wall thickness, also known as the minimum in-plane feature size (X, Y). As a result of droplet spreading, the wall thickness is much thicker than the layer thickness (Z) [233]. The minimum feature size increases with the aspect ratio because of the precision of layer-layer registration. Regarding the maximum feature size, it is generally constrained by the build volume of the printer. The foundations of MJT do not restrict feature width; however, few printhead components contain blocking features.

Droplets size and printing speed are the key points for a correct saturation rate and quality printing. Droplets of smaller size can give a better resolution of the printing, but if they are too small, they do not spread effectively. High printing speed can cause a loss of accuracy and resolution because the droplet does not have time to spread effectively [217]. Therefore, adjusting the printing speed makes it possible to favor better material spreading. Accordingly, every droplet indeed has a spreading radius time-dependent, $r(t)$, given by

$$r(t) = (a + bt)^n \tag{22}$$

where t is time and a, b, and n are constants that determine the growth rate, initial size, and shape of the droplet. These constants can also be related to other factors, such as the viscosity of the liquid, the surface tension between the liquid and the surface, and the contact angle between the liquid and the surface as in other hydrodynamic theories [234].

Imperfections in finishing are a common problem on the surface of MJT parts, which frequently have a rough or ribbed surface finish caused by overlapping material layers [235]. Miyanaji et al. [236] reported that the three most common jetting techniques for polymeric droplets are single, overlapping, and overlaying droplets. Overlapping droplets give better control for fine sizes.

7.1.4 Surface finish setting

Surface roughness values vary depending on the surface finish settings, and a correlation between surface roughness and finish settings can be complicated to establish [8]. In the case of a glossy finish, surfaces will not be covered by support materials except overhanging structures and the bottom of the part. Support materials will be covered when a matte finish is selected [223]. A glossy surface finish produces a lower surface roughness level, resulting in longer fatigue life. Generally, printing parts with a glossy finish setting is recommended to achieve higher surface quality [237].

Many current studies are trying to reach full-color printing by improving resolution and surface finish related to multi-color materials. Some studies have been carried out by Udroiu et al. [24] on matte and glossy surfaces by setting different process parameters. In particular, they found a correlation with the surface roughness R_a given by

$$R_a = t/4(|\cot\varphi\sin\theta + \cos\theta| \bullet K_1), K_1 < 1 \quad (23)$$

where t is the layer thickness, φ is the droplet contact angle, θ is the plan orientation, and K_1 is the correction coefficient based on the PPFTs used. Some other studies instead have been focused on trying to improve the tuning of colors without jagged shifts between adjacent layers [238].

7.2 Surface roughness studies and discussion

Compared to other AM techniques, research concerning the surface roughness of MJT technology has been very limited. This contrasts with the fact that MJT appears more relevant to aesthetic applications and artistic purposes. Most of the research in MJT has focused on the relationship between a few pre-processing parameters and the surface finish. However, several publications [70, 239] have used mathematical models to estimate the roughness characteristics of parts printed with PolyJet technologies. Table 11 summarizes significant research related to surface roughness in MJT.

In agreement with Table 11, positioning the part along the build tray substantially impacts the surface roughness in MJT parts. There was generally less roughness on horizontal surfaces than on vertical planes. On horizontal surfaces, roughness is determined by the droplet spreading and interaction of successive droplets for line and plane formation. In contrast, on vertical surfaces, it is controlled by the interaction of consecutive layers, resulting in stair-stepping equal to the layer thickness of the printed part. The spreading of droplets leads to extremely thin layers, resulting in smooth horizontal and vertical surfaces at the mesoscale [233]. As Udroiu et al. [243] demonstrated, the build type (matte or glossy) substantially affected surface roughness. Although MJT with R_a generally less than 10 μm can be considered to be between FFF (~ 1 μm < R_a < ~ 35 μm) and VPP (R_a < ~ 5 μm) in terms of surface roughness, the machines show much less variability compared to FFF and more variation compared to VPP methods. Again, and similar to FFF, SLS, and VPP methods, R_a and S_a were the most commonly reported roughness parameters.

8 Comparative studies and discussion

Table 12 summarizes recent comparative studies on the significant polymer additive manufacturing processes.

Most benchmarks developed for AM were intended to measure the implementation of a single technology and a limited number of parameters, as discussed in the previous section. The comparison of various AM methods has been the focus of several studies. For instance, Mou and Koc [118] compared three AM technologies, FFF, SLA, and MJT, on four machines in terms of their surface roughness, edge sharpness, and dimensional accuracy. According to their results, FFF produced a rough surface and irregular dimensional accuracy, SLA manufactured smoother surfaces but resulted in the distortion of thin features (< 1 mm), and MJT fabricates surfaces with comparable surface roughness and dimensional accuracy. Sillani et al. [28] reported the trend of surface roughness on the bottom and top surfaces of MJT and SLS seems to be about identical. Minetola et al. [16] evaluated three polymer-based 3DP machines by analyzing their dimensional accuracy using ISO IT grades. They reported a thinner layer gives a greater definition of the features geometry and higher dimensional accuracy. Li et al. [64] compared FFF, SLA, and MJT based on cost, sustainability, and surface roughness quality factors. They reported MJT and SLA as the best and moderate AM methods in tactile and visual assessments, respectively. However, unique SLA materials were considerably more valued in the hedonic sensation category. Results indicated the lowest overall ranking for FFF but with the capability of manufacturing with the lowest environmental problems and costs, confirming its sustainability.

In terms of dimensional accuracy, for instance, Minetola et al. [16] reported that despite the increased layer thickness (0.21 mm against 0.10 mm), the Arburg Freeformer machine outperformed the Prusa i3 for more comprehensive ISO ranges of the primary size. However, layer thickness was the most essential element for improved dimensional accuracy for smaller feature sizes. Roach et al. [2] used inkjet printing for PEGDA/PI material over the PEI substrate manufactured by the FFF method. They reported that direct-ink-writing (DIW) surface modification process for FFF substrate reduces the surface roughness, resulting in improved conductivity for electronics and radio frequency

Table 11 Overview of studies on surface roughness in MJT (see text* below the table for abbreviations)

Materials | Machines	Methodology and studied parameters	Roughness range (μm)	Remarks	Ref
RGD720 (SUP706B) | PolyJet Objet Connex1	b.o. (H. and V.), s.f. (matte or glossy), high-quality printing mode, l.t. (0.016 mm), s.r.m.m. (contact profilometry)	R_a: 0.03–13.59	-Geometries printed along *X*-direction (H.) had lower s.r. than *Y*-direction (V.) -s.r. caused by printing strategies considerably affected the aerodynamic performance of the fixed-wing UAVs -The lift coefficient was more sensitive to s.r. than the drag coefficient -To reduce distortion and improve surface quality, airfoil geometries should be printed horizontally -g.f. produces better surface quality than matte, but it depends on the tray location -Application: UAVs	[237]
FullCure830 | PolyJet Objet 350	Focused on the relationship between the b.o. (0°, 45°, and 90°), the geometry and s.f. based on the draft angle, roundness, waviness, and s.r.. l.t. (0.016 mm), s.r.m.m. (non-contact profilometry)	S_q:1.16–2.86 S_a: 0.95–2.33 S_{sk}: − 0.12–0.22 S_{ku}: 2.55–4.7	-The geometry and surface quality of castings were greatly affected by the d.a. and s.f. of foundry patterns -The lowest values for S_q and the highest surface quality were reported for V. samples (90°), due to the lack of support material -Application: Foundry industry	[240]
RGD836 & Agilus 30 FLX 935 (SUP706) | PolyJet J750	T. s.r. was examined, s.f. (matte or glossy), s.h. (30, 50, 85, and 100), l.t. (27 μm, 900 dpi), *XY* resolution (0.042 mm, 600 dpi), n.d. (10 μm), 96 nozzles for each head and 4 heads in total, a.m. (ANOVA), s.r.m.m. (contact profilometry)	g.f.: R_a: 1.641 (V.), 1.381 (H.) m.f.: R_a: 2.606 (V.), 2.280 (H.)	-g.f. showed lower s.r. than matte samples -s.r. was lower with a higher Shore hardness -There was no interaction between these two factors, and the lowest s.r. achieved by combining a g.f. with a Shore hardness rating of 100	[223]
Fullcure 720 (Fullcure 705) | PolyJet Objet 350 V	l.t. (0.016 and 0.030 mm), s.f. (matte v glossy), b.o. ([0–90°], 30° step), a.m. (ANOVA), s.r.m.m. (contact profilometry)	R_a: 2.77–17.63	-The s.r. prediction model was proposed based on the droplet contact angle -s.f. and b.o. were the significant factors affecting s.r. -Detailed theoretical and experimental analyses of droplet impact and capillary spread were presented to determine droplet contact angles -s.r. increased at higher b.o. up to 90°, then decreased until 180° for m.f. -Higher l.t. caused a marginal increase in s.r. -The proposed model accounted for the surface profile created by samples and support droplet geometry and was thus relevant only for m.f. or downward-facing g.f.	[70]

Table 11 (continued)

Materials	Machines	Methodology and studied parameters	Roughness range (μm)	Remarks	Ref
FullCure 720, VeroBlue 840 FullCure 870 (FullCure 705)	PolyJet Objet 350 V	l.t. (0.016 mm), s.f. (matte or glossy), b.o. ([0¯90°], 15° step), p.temp (72 °C), pre.temp (68 °C), printhead vacuum (6.2 atm.), r.h. (30%), a.m. (ANOVA and GLM), s.r.m.m. (contact profilometry)	R_a: ~ 0.5–15	-b.o. an s.f., and their interaction significantly affected R_a -Min R_a resulted for g.f., oriented perpendicular to the scanning direction -Maximum R_a resulted for b.o. 75–85° -There were some issues with g.f., including step marks between 75° and 85° and a boundary transition between matte and glossy areas -g.f. had a similar s.r. regardless of b.o. compared to m.f.	[24]
Fullcure 720 (Fullcure 705)	PolyJet Objet 250	l.t. (0.016 and 0.030 mm), s.f. (matte or glossy), s.c. (50 and 90%), a.m. (DoE Taguchi L4, ANOVA, and ANOM), s.r.m.m. (contact profilometry)	R_a: 0.8–12 R_q:1.01–16 R_z:4.95–80	-s.f. significantly affected s.r. compared to l.t. and s.c. -The optimized process parameter values were the same, and the best results were achieved using the 16 μm layer thickness and glossy style. While the scale factor could not be considered a dominant factor	[241]
FullCure 720 (Fullcure 705)	PolyJet Objet 330	b.o. (6 axis: *XY*, *XZ*, *YZ*, *YX*, *ZX*, and *ZY*), l.t. (0.016 mm), XY resolution (42 and 84 μm) s.f. (matte or glossy), p.p. (water pressure or caustic soda), a.m. (DoE full factorial design, ANOVA), s.r.m.m. (contact profilometry)	R_a: 0.78–5.08 (X), 1.04–15.01 (Y), 1.19–21.41 (Z)	-b.o. and s.f. significantly affected s.r. -g.f. resulted in the best s.r. results in all three axes, but it led to geometry limitations (thin walls) -The critical surfaces should be placed close to the *XY*-plane for the best s.r.	[242]
FullCure 720 (Fullcure 705)	PolyJet Objet 330	H. s.r. and texture were investigated l.t. (0.016 mm), s.f. (matte or glossy), s.r.m.m. (contact profilometry)	g.f.: R_a: 0.84, R_z: 3.8 m.f.: R_a: 1.04, R_z: 5.6	-s.r. of g.f. was lower than that of m.f. but with significant variations in the results	[243]
FullCure 720 (Fullcure 705)	PolyJet Objet 260	l.t. (0.016 mm), *XY* resolution (42 μm, 600 dpi), s.r.m.m. (contact profilometry)	R_a: 0.40 (H.), 4.55 (V.) R_z: 4.02 (H.), 30.28 (V.)	-s.r. was heavily influenced by its position relative to the printing axis, affecting mechanical and geometric properties -s.r. (2–8 μm), like osteoblast size, increases cell growth and attachment to scaffolds, promoting proliferation -R_a (4.55 μm) in surfaces parallel to the printing axis (*Z*) was like the s.r. of scaffold surfaces with other polymers, which could facilitate cell adhesion and differentiation into osteoblasts -Application: Porous structures and scaffold design for bone tissue engineering	[244]
Fullcure 720 (Fullcure 705)	PolyJet Objet 260	l.t. (0.016 mm), s.f (glossy), b.o. ([0–90°], 5° step), a.m. (regression analysis), s.r.m.m. (contact profilometry)	R_a: 0.818–4.024	-The existing s.r. prediction models were only applicable for m.f. parts, showed high error, while it was checked for the estimation of s.r. of the parts printed with g.f.	[239]

Table 11 (continued)

Materials | Machines	Methodology and studied parameters	Roughness range (μm)	Remarks	Ref
VisiJet M2R-WT (VisiJet M2-SUP) | Project MJP2500 modeled	*XYZ* resolution (800 × 900 × 790 dpi) l.t. (0.032 mm), s.r.m.m. (contact profilometry)	R_a: 0.338–8.532	-MJT parts should be placed along the maximum area in contact with the base plate due to better heat dissipation from the hot layers to the base plate, leading to a uniform fusion between the layers and causing less dimensional deviation and better surface properties	[245]

*Abbreviations: *a.m.* analysis methods, *b.o.* build orientation (direction), *d.a.* dimensional accuracy, *g.f.* glossy finish, *l.t.* layer height (thickness along Z-direction), *m.f.* matte finish, *n.d.* nozzle diameter, *p.temp.* printing temperature, *pre.temp.* preheating temperature, *r.h.* relative humidity, *s.f.* surface finish, *s.c.* scale of the model, *s.r.* surface roughness, *s.r.m.m.* surface roughness measurement method, *H.* horizontal, *V.* vertical

(RF) applications. Nazir and Jeng [252] introduced high-speed additive manufacturing by merging PBF, MJT, and sintering technology without coupling 3DP with subtractive methods. They showed that while the MJF process was substantially quicker than the SLS method, the SLS PA12 parts showed 15% lower R_a when compared to the high-speed MJF.

9 Summary

The 3D-layered nature of AM processes and partially melted particles influence the definition of the component surface. Accordingly, controlling PPPs can dramatically affect the 3D features on a rough surface for AM components. The deliberate surface modification based on surface texture metrics in 3DP products is more demanding than ever with 3D measurement and characterization development, which can comprehensively reflect the surface topography.

Fabricating a part using layer-by-layer deposition in which the produced part exhibits a staircase effect causes the surface to become rougher. It is possible to reduce this problem by being aware of the regular surface roughness of the parts in advance or predicting the roughness values during pre-processing. Accordingly, the PPPs based on process parameter optimization have been discussed to list the parameters that have the most critical influence on the roughness of as-printed polymers. This comparative review emphasized the growing interest in understanding AM system restrictions and discrepancies so that a better selection of 3DP technology can be made based on project constraints. This study summarized the significant advances in additive manufacturing, including the incorporation of AM design decisions to assist in identifying candidate solutions, as well as information regarding roughness considerations for the selected processes.

As mentioned in the previous section, the best possible surface and optimum roughness according to an application can be obtained by adjusting the fabrication parameter. The other choice is to investigate the optimum mix of PPFTs that can be applied to any AM objects. However, it increases the cost, time, and complexity of the process. Production settings may be tweaked to favor speed above surface quality if this combination proves effective.

A variety of strategies have been employed by various groups to achieve this objective. Most studies have focused on the top surface of the parts because many factors contribute to the surface roughness distribution of a 3DP object, such as layer height. It is revealed from the literature review that the workflow of surface modification in the pre-processing step heavily depends on the complexity of the design and the desired quality-time–cost balance. Surface modification techniques are currently not standardized and depend on factors such as geometry and intended application. As a result, the following AM

Table 12 Overview of comparative studies on surface roughness in FFF, SLS, VPP (SLA and DLP), and MJT (see text* below the table for abbreviations)

Materials | Machines	Methodology and studied parameters	Roughness range (μm)	Remarks	Ref
FFF: PPSF | Titan Stratasys SLS: PA12 (2210) FR | EOS P390	FFF: r.w. (0.5080 mm); l.t. (0.254 mm), solid-normal filling strategy SLS: the sorted strategy (contour, filling, contour), l.t. (0.15 mm), l.p. (30 W), p.s. (1000 mm/s), h.d. (0.3 mm), s.r.m.m. (contact profilometer)	FFF: R_a: 0.40–28.11; R_z: 1.44–126.06; R_t: 3.35–144.64 SLS: R_a: 11.84–29.27; R_z: 82.99–187.93; R_t: 90.46–227.17	-SLS/PA produced a much smoother surface, but FFF/PPSF presented slightly better d.a. -FFF produced parts with periodic surface profiles, whereas SLS produced those with irregular surfaces -Application: Flame-retardant plastics were used in critical applications, such as aircraft interior parts	[152]
SLS: PA12 | EOS P390 & P1000 Prodways MJT: VeroBlack resin | Connex 500 Stratasys	SLS P390: p.size (45–70 μm) and l.t. (120 μm) SLS P1000: p.size (45–60 μm) and l.t. (100 μm) MJT: l.t. (16 and 32 μm), b.o. (0°, 45°, 90°) s.r.m.m. (contact profilometer)	SLS P390: R_a: 16 (H.), 23 (V.), 22 (45°); R_z: 108 (H.), 148 (V.), 149 (45°) SLS P1000: R_a: 16.5 (V.); R_z: 118 (V.) MJT (16 μm): R_a: 12 (V.); R_z: 79 (V.) MJT (32 μm): R_a: 20 (V.); R_z: 125 (V.)	-Higher l.t. resulted in higher p.s., and had a greater influence on s.r. than partly molten grains adhering to the surface -The 45° surfaces were rough and had a stair-like appearance, which was exacerbated by the heaviest layers. This kind of s.r. was difficult to evaluate -s.r. of the 1-year-old SLS P1000 was better than that of the 10-year-old SLS P390 -Surfaces for SLS parts tend to trap impurities more than MJ's smooth and shiny surface	[3]
SLS: PA12 (2200) | EOS P396 MJF: PA12 | HP MultiJet Fusion 3D 4200 HL: Cubicure Resin | Hot Lithography Caligma 200	Standard parameter setting "Balance" was used for MJF (20% new + 80% aged powder) and SLS s.r.m.m. (contact profilometry)	MJF: R_a: 11.9 SLS: R_a: 13.4 HL: R_a: 6.1	-Semi-crystalline MJF-PA and LS-PA possessed similar R_a -If parts contain pressurized fluid without any further s.f., HL-MA has the potential for rapid crack propagation due to its surface texture -Application: Automotive industry, motorcycle design, and low-pressure parts such as fuel tanks and lightweight fairings or high-pressure parts such as valves	[246]

Table 12 (continued)

Materials | Machines	Methodology and studied parameters	Roughness range (μm)	Remarks	Ref
FFF: PLA | Ultimaker 3 Extended SLA: Proprietary Resin | Nobel 1.0 A MJT: RGD840 (SUP705) | PolyJet Objet 260 VisiJet M3-X (VisiJet S300) | ProJet MJP 3600	FFF: l.t. (200 μm), *XY* resolution (12.5, 12.5 μm) SLA: l.t. (25 μm), *XY* resolution (130, 130 μm) MJT: PolyJet: l.t. (12 μm), *XY* resolution (42, 42 μm, 600 dpi) ProJet: l.t. (32 μm), *XY* resolution (375, 450 dpi) a.m. (ANOVA), s.r.m.m. (contact profilometry)	FFF: R_a: 4.93 SLA: R_a: 0.34 MJT: R_a: 2.12 (PolyJet), 3.84 (ProJet)	-PolyJet produced acceptable s.r. and round edges but a superior s.f. when the model was printed in the glossy mode -s.r. and e.d. of ProJet printers were significant weaknesses on a microscopic level -Despite acceptable d.a., FFF printed rough surfaces with poor e.d. on the as-printed raw object. The final product of FFF prints needed to be post-processed -SLA printer produced a significantly smooth surface, but the distortion of thin features (< 1 mm) -R_q and R_z for all samples followed the same pattern as R_a with similar significance -Application: Prototyping, physical visualization, and end-product manufacturing	[118]
SLS: PA 3200 GF | - MJT: Digital ABS | -	SLS and MJT were used to manufacture molding for conventionally fabricated aluminum milled tools a.m. (ANOVA), s.r.m.m. (non-contact profilometry)	MJT: R_a: 0.77; R_q: 1.35; R_z: 8.90 SLS: R_a: 11.59; R_q: 14.71; R_z: 64.01	-SLS molds had significantly rougher surfaces than MJT molds, causing more notch effect -The tool surface of the polymer mold inserts should be treated to improve the design modifications of the mold inserts -Application: Rapid tooling, injection molding	[14]
FFF: PLA & ABS | Makerbot replicator & Makerbot replicator 2X SLA: Proprietary Resin | Formlabs Form 1 + MJT: VeroClear & DM Gray 60 | PolyJet Objet 260	FFF: l.t. (100 μm), i.d. (15% for PLA and 10% for ABS) SLA: l.t. (50 μm), i.d. (100%) MJT: l.t. (16 μm for DM and 32 μm for Vero), i.d. (100%) a.m. (Kendall's coefficient of concordance, sensorial analysis), s.r.m.m. (contact profilometry)	FFF: R_a: ~ 8 (PLA), ~ 9 (ABS); R_z: ~ 33 (PLA); ~ 37 (ABS); R_{ku}: ~ 2.3 (PLA) and ~ 2.5 (ABS) SLA: R_a: ~ 20; R_z: ~ 19; R_{ku}: ~ 2.8 MJT: R_a: ~ 4 (Vero), ~ 3 (DM); R_z: ~ 18 (Vero), ~ 16 (DM); R_{ku}: ~ 2.7 (Vero), ~ 2.6 (DM)	-Focused on three critical aspects of personal 3D printing processes, including manufacturing cost, sustainability, and visuotactile perception of s.r. -MJT samples had the best subjective quality (all hedonic, tactile, and visual assessments), but the highest costs and environmental impact -The SLA sample scored middle in tactile and visual assessments, but its hedonic sensation score was significantly higher than the FFF sample -R_z was superior to R_a and R_q in sensory judgments of s.f. -Besides R_z, surface texture and color affected sensory judgments -A significant correlation was found between R_z and the tactile and visual assessment -R_{ku} correlated best with the hedonic rank -Application: Prototyping and personal 3D printers	[64]

Table 12 (continued)

Materials | Machines	Methodology and studied parameters	Roughness range (μm)	Remarks	Ref
FFF: PLA +| Pratham desktop SLS: PA12 (2200) | EOS P396 DLP: ABS TRU Resin | EKA DLP MJT: VisiJet M2R-WT (VisiJet M2-SUP) | Projet MJP 2500	d.a, s.r., and p.s. were considered in the decision criteria. a.m. (Hybrid MCDM and sensitivity analysis), s.r.m.m. (contact profilometry)	FFF: R_a: 6.11 SLS: R_a: 11.79 DLP: R_a: 3.06 MJT: R_a: 19.96	- The ranking obtained to achieve the desired d.a., and surface quality is MJT > SLS > FFF > DLP - MJT provided the highest d.a. and lower s.r.	[247]
FFF: PLA | BQ Witbox II SLS: PA12 | EOS P760 SLA: Digital Wax | DWS 020X Systems MJT:—| Polyjet Objet30 Pro	SLA, FFF, SLS, Polyjet are compared in terms of d.a. and s.r. FFF: l.t. (300 μm) MJT: l.t. (16 μm) s.r.m.m. (contact profilometry)	FFF: R_a: 39.3; R_z: 238.1 SLS: R_a: 15.4; R_z: 133.8 SLA: R_a: 0.2; R_z: 2.8 Polyjet: R_a: 2.5; R_z: 22.3	-The following ranking in terms of s.r. values were reported FFF > SLS > MJT > SLA -Application: RF/Microwave Components	[248]
FFF: ABS | Fortus 450mc SLA: Gray Pro resin | Formlabs MJF: PA12 | HP MultiJet Fusion 3D 4200	FFF: l.t. (254 μm), i.d. (100%), r.a. (45°) SLA: l.t. (100 μm) MJF: ratio of pristine to recycled powder (30:70), l.t. (80 μm) T. s.r. was measured at 3 separate locations, s.r.m.m. (non-contact profilometry)	FFF: S_a: 5.277–7.111; S_q: 6.845–8.782 SLA: S_a: 1.830–2.137; S_q: 2.452–2.856 MJF: S_a: 8.740–11.980; S_q:10.054–16.293	-SLA resulted in the lowest deviation and values of s.r. -T. S_a and S_q of MJF sample were lower than FFF -Filling patterns in FFF as a trajectory process resulted in rougher H. surfaces compared to nontrajectory MJF -Application: Permeability test rig	[249]
SLA: Gray RS-F2-GPGR-04 | Form 2 SLA DLP: Freeprint model 385 grau (DETAX) | SolflexW170 MJT: VisiJet Wax VisiJet M3 Hi-Cast (VisiJet S300) | ProJet MJP 3600	b.o. (45°) SLA: l.t. (25 μm) DLP: l.t. (25 μm) MJT: l.t. (16 μm) a.m. (Shapiro–Wilk test, Tukey post hoc test, and the Kruskal–Wallis test), s.r.m.m. (non-contact profilometry)	R_z: 0.012–0.032 (SLA), 0.015–0.043 (DLP), 0.010–0.018 (MJT)	-Skin structure replication was more dependent on the AM method chosen than on other stages of production -MJT showed superior accuracy compared with SLA or DLP -Application: Facial prosthesis fabrication	[250]
FFF: PLA, ABS, PVA, PEVA and HIPS | Wanhao duplicator 6 DLP: 405 nm Resin | Wanhao D7 DLP LCD	FFF: l.t. (200 μm), r.a. (Crossed 45°/135°), b.o. (0°, 45°, 90°) DLP: l.t. (100 μm) s.r.m.m. (contact profilometry)	DLP: R_a: ~ 4 (H., S.), ~ 4.4 (H., T.), ~ 13.2 (45° S.), ~ 12.2 (45° T.), ~ 10.4 (V., S.), ~ 0.8 (V., T.) FFF: R_a: ~ 1.6 (H., S.), ~ 10.8 (H., T.), ~ 10.2 (45° S.), ~ 17.0 (45° T.), ~ 9.6 (V., S.), ~ 3.6 (V., T.)	-Choosing the 3DP method and changing b.o. can significantly affect s.r. and tribological performance -Parts made with DLP are prone to stick–slip phenomena, particularly at b.o. (45° and 90°) -Application: Tribological purposes	[251]

*Abbreviations: *a.m.* analysis methods, *b.o.* build orientation (direction), *d.a.* dimensional accuracy, *e.d.* energy density, *h.d.* hatch distance, *i.d.* infill density, *l.t.* layer height, *l.p.* laser power, *p.s.* printing speed (laser scanning speed), *p.size* powder size, *r.a.* raster angle, *r.w.* raster width, *s.f.* surface finish, *s.r.* surface roughness, *s.r.m.m.* surface roughness measurement method, *S.* side, *T.* top, *H.* horizontal, *V.* vertical

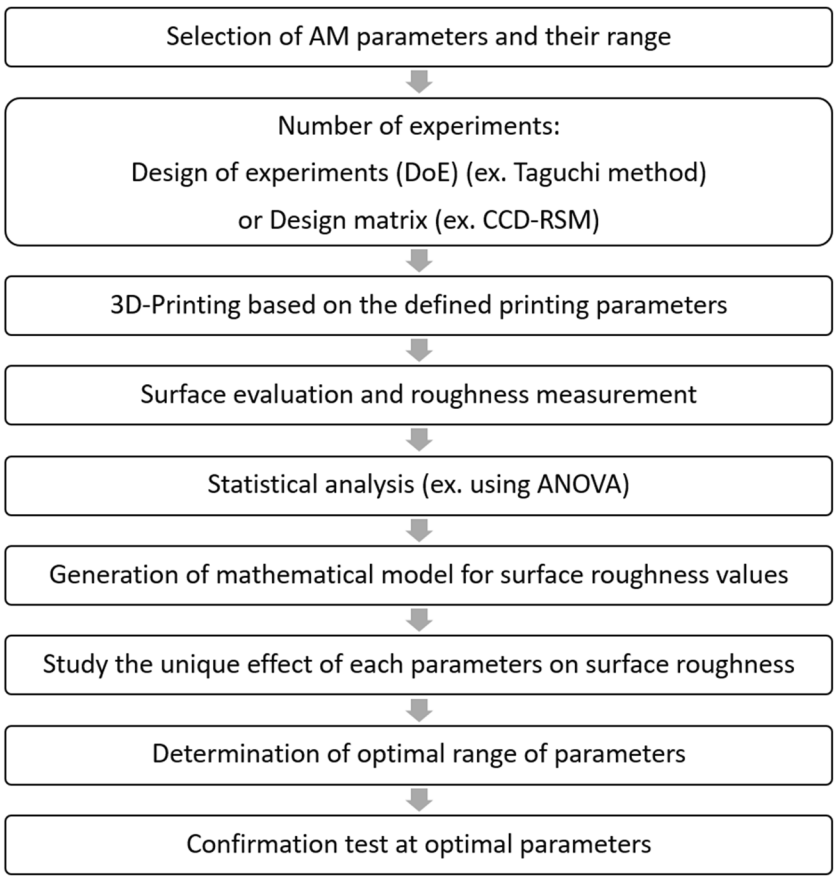

Fig. 22 Suggested 3DP workflow to enhance as-printed surfaces

workflow in Fig. 22 can lead to optimum surface modification by altering roughness before and during processing.

Along with the literature review, the Taguchi method, full factorial method, response surface method (RSM), and analysis of variance (ANOVA) were the most used methods for optimizing the surface roughness of 3D printers. In the case of RSM, it is generally a time-consuming method depending on the orthogonal matrix used [44]. Thus, it has been less widely used than the Taguchi method to date. The combination of specific optimization parameters may result in parts with no known surface roughness, which would have to undergo fundamental design changes. Current capabilities are limited without developing a new surface modification workflow that considers the PPFTs requirements during the pre-processing phase. Frequently, DfAM necessitates the redesign of parts initially planned for conventional methods such as machining. Post-processing must be integrated into the design process at an earlier stage, and the role of each component must be considered. Specifically, post-processing using ultraprecision technology is gaining increasing attention as it provides high-quality parts with improved surface finish and dimensional accuracy [253]. The importance of having precise geometries and smooth surfaces is particularly important for polymer optics and devices, where optimal performance depends on precise geometries and smooth surfaces.

According to the studied literature, the appropriate AM technique selection determines manufacturing efficiency, accuracy, and model size. Thus, it determines whether the actual and nominal roughness is conforming and will allow AM to be better integrated with roughness requirements. For instance, while FFF technology has the advantage of being efficient and cost-effective for small-scale production, accuracy may be limited when the production of large and complex parts is required. The recorded R_a results were generally less than 5 and 10 µm for the studied VPP and MJT methods, respectively, 10 to 20 µm for SLS, and between 1 and over 30 µm for FFF. Accordingly, SLA and DLP technologies, offer high accuracy and resolution for larger and more complex parts with more stable roughness results at various printing processes, considering SLS is at the opposite end of the roughness spectrum. While MJT can fabricate ultimately smooth parts in the sub-micrometer ranges similar to VPP, their 3D-printed surface can be as rough as FFF, depending on the selected processing method. However, both VPP and MJT AM categories can be time-consuming and expensive, limiting their suitability for competing with mass production in the present form.

Selection of the proper AM technique will also require an in-depth examination of the surface measurement techniques. The measuring method results in significant uncertainty in

roughness evaluation due to PPP. It is reported that the stylus in contact-based profile measurement scratches and physically smooths the surface, leading to slight compliance with the actual topography. However, it is time efficient, more reproducible, and provides comparable results even when the tip radius varies [3]. Accordingly, tactile roughness measurement and R_a were frequently reported as the main method and roughness metrics in the reviewed articles. However, R_z performed better than R_a since it accurately represents both tactile and visual roughness. Nevertheless, observers are influenced by appearance attributes such as color, texture, glossiness, and translucency when evaluating roughness and surface finish [254]. In particular, polymeric parts represent most of these appearance attributes.

Considering the results, mainstream 3DP technologies differ significantly in terms of surface roughness. The FFF method makes extending applications across various applications challenging due to its poor surface quality. However, FFF objects seem more appropriate for analyzing application-based purposes. SLA is considered a low-cost desktop device that directly competes with FFF because of its higher print resolution and reduced surface roughness. The SLS technique is still being developed for this purpose, and MJF is emerging as a promising technique. In general, the surface roughness of the SLA and MJT was reported to be better than the SLS components. Compared to other polymer AM techniques, their inherent smooth surface finish and great dimensional accuracy imply that painting and coating are rarely required.

Combining these data confirms that the reviewed 3DP methods cannot produce ready-to-use end products and that PPFT is necessary. As a significant finding, it is revealed that there is a demand for further investigation on the appearance of 3D-printed structures, dealing explicitly with their QAs issues. Optimization of AM should not be conducted to achieve complete control over roughness. It is primarily due to the lack of reproducibility in AM technology and the role mainly played by post-processing. Further research is required to establish the links between different PPPs and the quality of the surfaces of AM-made components, as discussed in the next section.

10 Future trends and capabilities

The importance of surface roughness in the final product is recognized by both conventional and advanced manufacturing methods, especially for critical and small products. To increase the applicability of AM processes, it is necessary to assess the surface finish of as-printed polymers and to provide guidance on AM process windows and limitations [8]. 3D and 2.5D printing with multi-materials and multi-colors will be key to the future development of AM technology [255]. The techniques mentioned in this study can also provide insight into other advanced materials, such as nanoparticle and their suspensions with functional properties [256–258], surface treatment [259, 260], and liquid metals to use in AM technology. Furthermore, fiber reinforcement and composition can be incorporated into almost all AM methods [261]. The development of eco-friendly materials, the use of polymers, durability, and sustainability are also major concerns [262]. As an emerging trend in advanced manufacturing, the combination of several AM technologies presents new challenges in terms of surface finish.

There is a growing interest in 4D additive manufacturing, which is a relatively new research area. Smart materials can be developed more quickly by developing multi-material 4D printing [263, 264]. A 4D-printed part can thus be carefully controlled in terms of surface texture and topography as a microstructure to achieve more complex geometrical transformations. Therefore, monitoring the surface roughness of smart materials is an essential step. As with 3D multi-material printing, it can present similar challenges, such as limited material choice, printing resolution, slow mechanical performance, and dimensional accuracy [263]. It will be necessary to implement multi-material additive manufacturing in a variety of applications as part of multidisciplinary research and development [262].

The lack of aesthetically appropriate materials for AM necessitates further investigation. An understanding of the induced anisotropic arrangements and their impact on the build platform (chamber) and product properties may be improved by using sophisticated algorithms and numerical techniques [211]. The fundamental material application procedure, as well as the actual applied stresses, heat, and weathering agents, requires further investigation. Aside from the roughness value, the roughness distribution is also of critical importance to the use of AM components in the future. Therefore, there are various capabilities available to examine how printing factors impact other mechanical performance factors, such as compressive strength and tensile strength. As a result of these findings, AM products are likely to be applied to parts for automotive, aerospace, and jewelry applications that require high-dimensional accuracy and proper surface characteristics.

Author contribution Ali Payami Golhin: Conceptualization, methodology, investigation, data curation, formal analysis, visualization, writing—original draft, writing—review and editing. Riccardo Tonello: Conceptualization, writing—original draft, writing—review and editing. Jeppe Revall Frisvad: Writing—review and editing, supervision. Sotirios Grammatikos: Writing—review and editing, supervision. Are Strandlie: Writing—review and editing, supervision, project administration, funding acquisition.

Funding Open access funding provided by NTNU Norwegian University of Science and Technology (incl St. Olavs Hospital - Trondheim University Hospital) The authors acknowledge the funding received on this project from the ApPEARS-ITN project funded by the European Union's H2020 research and innovation program under the Marie Skłodowska-Curie grant agreement No. 814158.

Data availability The data supporting the findings of this study are available within the manuscript.

Code availability Not applicable.

Declarations

Ethics approval Not applicable.

Consent to participate Not applicable.

Consent for publication Consent to publication has been received from all co-authors before the work is submitted.

Conflict of interest The authors declare no competing interests.

References

1. Li S, Li JY, Jiang ZW et al (2022) Controlling the columnar-to-equiaxed transition during Directed Energy Deposition of Inconel 625. Additive Manufacturing 57:102958. https://doi.org/10.1016/j.addma.2022.102958
2. Roach DJ, Roberts C, Wong J, et al. (2020) Surface modification of fused filament fabrication (FFF) 3D printed substrates by inkjet printing polyimide for printed electronics. 36:https://doi.org/10.1016/j.addma.2020.101544
3. Magnien J, Cosemans P, Nutal N et al (2020) Current surface issues in additive manufacturing. Wiley Online Library. https://doi.org/10.1002/ppap.201900154
4. Stiles A, Kobler W, Yeole P, et al. (2022) Photopolymer formulation towards large scale additive manufacturing of autoclave capable tooling. 50:https://doi.org/10.1016/j.addma.2021.102571
5. Bertacchini F, Bilotta E, Demarco F, et al. (2021) Multi-objective optimization and rapid prototyping for jewelry industry: methodologies and case studies. 112:2943-2959https://doi.org/10.1007/s00170-020-06469-2
6. Poyanco J-M, Pizarro F, Rajo-Iglesias E (2022) Cost-effective wideband dielectric planar lens antenna for millimeter wave applications. Sci Rep 12:1–10. https://doi.org/10.1038/s41598-022-07911-z
7. Quinlan HE, Hasan T, Jaddou J et al (2017) Industrial and consumer uses of additive manufacturing: a discussion of capabilities, trajectories, and challenges. J Ind Ecol 21:S15–S20. https://doi.org/10.1111/jiec.12609
8. Payami Golhin A, Sole AS, Strandlie A (2023) Color appearance in rotational material jetting. Int J Adv Manuf Technol 124:1183–1198. https://doi.org/10.1007/s00170-022-10536-1
9. Nath SD, Nilufar S (2020) An overview of additive manufacturing of polymers and associated composites. 12:2719https://doi.org/10.3390/polym12112719
10. Wohlers T (2021) Technical, market, and strategic advice on additive manufacturing, 3D printing, and rapid product development, in Wohlers Report 2021. Wohlers Associates.
11. Carlota V (2020) Polymer 3D printing market to generate $11.7 billion in 2020. 2020 March 4, 2020. Accessed 10 January; Available from: https://www.3dnatives.com/en/polymer-3d-printing-market-2020-040320204.
12. Panin SV, Buslovich DG, Kornienko LA et al (2019) Structure, as well as the tribological and mechanical properties, of extrudable polymer-polymeric UHMWPE composites for 3D printing. J Frict Wear 40:107–115. https://doi.org/10.3103/S1068366619020090
13. Goldin N, Dodiuk H, Lewitus D (2017) Enhanced thermal conductivity of photopolymerizable composites using surface modified hexagonal boron nitride fillers. Compos Sci Technol 152:36–45. https://doi.org/10.1016/j.compscitech.2017.09.001
14. Kampker A, Triebs J, Kawollek S et al (2019) Direct polymer additive tooling – effect of additive manufactured polymer tools on part material properties for injection moulding. Rapid Prototyping J 25:1575–1584. https://doi.org/10.1108/RPJ-07-2018-0161
15. Aslani KE, Vakouftsi F, Kechagias JD, et al. (2019) Surface roughness optimization of Poly-Jet 3D printing using grey taguchi method. in Proceedings - 2019 3rd International Conference on Control, Artificial Intelligence, Robotics and Optimization, ICCAIRO 2019. https://doi.org/10.1109/ICCAIRO47923.2019.00041
16. Minetola P, Calignano F, Galati M (2020) Comparing geometric tolerance capabilities of additive manufacturing systems for polymers. Addit. Manuf. 32:https://doi.org/10.1016/j.addma.2020.101103
17. Vyavahare S, Teraiya S, Panghal D et al (2020) Fused deposition modelling: a review. Rapid Prototyping J 26:176–201. https://doi.org/10.1108/RPJ-04-2019-0106
18. Turner BN, Gold SA (2015) A review of melt extrusion additive manufacturing processes: II. Materials, dimensional accuracy, and surface roughness. Rapid Prototyping J 21:250–261. https://doi.org/10.1108/RPJ-01-2013-0012
19. Gordon ER, Shokrani A, Flynn JM, et al. (2016) A surface modification decision tree to influence design in additive manufacturing, R. Setchi, et al., Editors., Springer Science and Business Media Deutschland GmbH. 423–434. https://doi.org/10.1007/978-3-319-32098-4_36
20. Parandoush P, Lin D (2017) A review on additive manufacturing of polymer-fiber composites. Compos Struct 182:36–53. https://doi.org/10.1016/j.compstruct.2017.08.088

21. Chohan JS, Singh R (2017) Pre and post processing techniques to improve surface characteristics of FDM parts: a state of art review and future applications. Rapid Prototyping J 23:495–513. https://doi.org/10.1108/RPJ-05-2015-0059
22. Panda B, Noor Mohamed NA, Tay YWD, et al. (2018) Effects of slag addition on bond strength of 3D printed geopolymer mortar: an experimental investigation. in Proceedings of the International Conference on Progress in Additive Manufacturing. https://doi.org/10.25341/D4QG6D
23. Piedra-Cascón W, Krishnamurthy VR, Att W, et al. (2021) 3D printing parameters, supporting structures, slicing, and post-processing procedures of vat-polymerization additive manufacturing technologies: a narrative review. https://doi.org/10.1016/j.jdent.2021.103630
24. Udroiu R, Braga IC, Nedelcu A (2019) Evaluating the quality surface performance of additive manufacturing systems: methodology and a material jetting case study. Mater. 12:https://doi.org/10.3390/ma12060995
25. Gülcan O, Günaydın K, Tamer A (2021) The state of the art of material jetting—a critical review. 13:https://doi.org/10.3390/polym13162829
26. Sinha A, Swain B, Behera A, et al. (2022) A review on the processing of aero-turbine blade using 3D print techniques. 6:https://doi.org/10.3390/jmmp6010016
27. Marques A, Miranda G, Silva F, et al. (2021) Review on current limits and potentialities of technologies for biomedical ceramic scaffolds production. 109:377-393https://doi.org/10.1002/jbm.b.34706
28. Sillani F, Kleijnen RG, Vetterli M et al (2019) Selective laser sintering and multi jet fusion: process-induced modification of the raw materials and analyses of parts performance. Addit Manuf 27:32–41. https://doi.org/10.1016/j.addma.2019.02.004
29. (2021) Additive manufacturing - General principles - Fundamentals and vocabulary, in ISO/ASTM 52900:2021. International Organization for Standardization: Geneva, Switzerland. 1–36.
30. Jonušauskas L, Juodkazis S, Malinauskas M (2018) Optical 3D printing: bridging the gaps in the mesoscale. J Opt 20:https://doi.org/10.1088/2040-8986/aab3fe
31. Elkholy A, Kempers R (2020) Enhancement of pool boiling heat transfer using 3D-printed polymer fixtures. Exp. Therm. Fluid Sci. 114:https://doi.org/10.1016/j.expthermflusci.2020.110056
32. Ligon SC, Liska R, Stampfl J et al (2017) Polymers for 3D printing and customized additive manufacturing. Chem Rev 117:10212–10290. https://doi.org/10.1021/acs.chemrev.7b00074
33. Alex Xu BL, Martin Erharter, Vatche Kourkejian (2021) Polymer additive manufacturing market today and in the future. 2021. Accessed 1 July; Available from: https://www.rolandberger.com/en/Insights/Publications/Polymer-additive-manufacturing-Market-today-and-in-the-future.html.
34. Gorjan L, Tonello R, Sebastian T et al (2019) Fused deposition modeling of mullite structures from a preceramic polymer and γ-alumina. J Eur Ceram Soc 39:2463–2471. https://doi.org/10.1016/j.jeurceramsoc.2019.02.032
35. Ojansivu M, Johansson L, Vanhatupa S, et al. (2018) Knitted 3D scaffolds of polybutylene succinate support human mesenchymal stem cell growth and osteogenesis. Stem cells international 2018:https://doi.org/10.1155/2018/5928935
36. Ou-Yang Q, Guo B, Xu J (2018) Preparation and characterization of poly(butylene succinate)/polylactide blends for fused deposition modeling 3D printing. ACS Omega 3:14309–14317. https://doi.org/10.1021/acsomega.8b02549
37. Zhakeyev A, Wang P, Zhang L, et al. (2017) Additive manufacturing: unlocking the evolution of energy materials. Adv Sci 4:https://doi.org/10.1002/advs.201700187
38. De Matos Costa AR, Crocitti A, Hecker De Carvalho LHD, et al. (2020) Properties of biodegradable films based on poly(butylene succinate) (PBS) and poly(butylene adipate-co-terephthalate) (PBAT) blends. 12:2317. https://doi.org/10.3390/polym12102317
39. Williams JM, Adewunmi A, Schek RM, et al. (2005) Bone tissue engineering using polycaprolactone scaffolds fabricated via selective laser sintering. 26:4817-4827https://doi.org/10.1016/j.biomaterials.2004.11.057
40. Eshraghi S, Das S (2010) Mechanical and microstructural properties of polycaprolactone scaffolds with 1-D, 2-D, and 3-D orthogonally oriented porous architectures produced by selective laser sintering. Acta Biomater 6:2467. https://doi.org/10.1016/j.actbio.2010.02.002
41. Salmoria GV, Fancello EA, Roesler CR et al (2013) Functional graded scaffold of HDPE/HA prepared by selective laser sintering: microstructure and mechanical properties. J Adv Manuf Technol 65:1529–1534. https://doi.org/10.1007/s00170-012-4277-y
42. Han X, Yang D, Yang C, et al. (2019) Carbon fiber reinforced PEEK composites based on 3D-printing technology for orthopedic and dental applications. 8:https://doi.org/10.3390/jcm8020240
43. Wu H, Fahy WP, Kim S, et al. (2020) Recent developments in polymers/polymer nanocomposites for additive manufacturing. Prog Mater Sci 111:https://doi.org/10.1016/j.pmatsci.2020.100638
44. Saad MS, Nor AM, Baharudin ME et al (2019) Optimization of surface roughness in FDM 3D printer using response surface methodology, particle swarm optimization, and symbiotic organism search algorithms. Int J Adv Manuf Technol 105:5121–5137. https://doi.org/10.1007/s00170-019-04568-3
45. Mikhalchan A, Tay TE, Banas AM et al (2020) Development of continuous CNT fibre-reinforced PMMA filaments for additive manufacturing: a case study by AFM-IR nanoscale imaging. Mater Lett 262:127182. https://doi.org/10.1016/j.matlet.2019.127182
46. Stewart ML (2020) 3D-printed polypropylene transtibial sockets: mechanical behavior. Proc Inst Mech Eng. https://doi.org/10.1177/0954406220943922
47. Mckeen LW (2018) The effect of sterilization on plastics and elastomers. William Andrew Publishing.
48. Chen N, Wan C, Zhang Y et al (2004) Effect of nano-CaCO3 on mechanical properties of PVC and PVC/Blendex blend. Polym Test 23:169–174. https://doi.org/10.1016/S0142-9418(03)00076-X
49. Rostam S, Ali AK, Abdalmuhammad FH (2016) Experimental investigation of mechanical properties of PVC polymer under different heating and cooling conditions. J Eng. 2016:https://doi.org/10.1155/2016/3791417
50. Sobha A, Sreekala P, Narayanankutty SK (2017) Electrical, thermal, mechanical and electromagnetic interference shielding properties of PANI/FMWCNT/TPU composites. Prog Org Coat 113:168–174. https://doi.org/10.1016/j.porgcoat.2017.09.001
51. Eom R-I, Lee H, Lee Y (2019) Evaluation of thermal properties of 3D spacer technical materials in cold environments using 3D printing technology. Ann Int Med 11:1438
52. Tricco AC, Lillie E, Zarin W et al (2018) PRISMA extension for scoping reviews (PRISMA-ScR): checklist and explanation. Ann Intern Med 169:467–473. https://doi.org/10.7326/M18-0850
53 Burck C (2005) Comparing qualitative research methodologies for systemic research: the use of grounded theory, discourse analysis and narrative analysis. J Fam Ther 27:237–262. https://doi.org/10.1111/j.1467-6427.2005.00314.x
54. Wohlers T (2020) 3D printing and additive manufacturing: global state of the industry, in Wohlers Report 2020. Wohlers Associates
55. Du S, Liu C, Huang D (2015) A shearlet-based separation method of 3D engineering surface using high definition metrology. Precis Eng 40:55–73. https://doi.org/10.1016/j.precisioneng.2014.10.004
56. Geng H, Li J, Xiong J et al (2018) Formation and improvement of surface waviness for additive manufacturing 5A06 aluminium

alloy component with GTAW system. Rapid Prototyping J 24:342–350. https://doi.org/10.1108/RPJ-04-2016-0064
57. Scheers J, Vermeulen M, De Maré C et al (1998) Assessment of steel surface roughness and waviness in relation with paint appearance. Int J Mach Tools Manuf 38:647–656. https://doi.org/10.1016/S0890-6955(97)00113-2
58. Wi K, Suresh V, Wang K, et al. (2020) Quantifying quality of 3D printed clay objects using a 3D structured light scanning system. Addit. Manuf. 32:https://doi.org/10.1016/j.addma.2019.100987
59. Triantaphyllou A, Giusca CL, Macaulay GD et al (2015) Surface texture measurement for additive manufacturing. Surf Topogr-Metrol Prop 3:8. https://doi.org/10.1088/2051-672x/3/2/024002
60. Iso (2021) Geometrical product specifications (GPS) — surface texture: profile — Part 2: Terms, definitions and surface texture parameters, in ISO 21920–2:2021. International Organization for Standardization: Geneva, Switzerland. 1–86
61. Iso (2021) Geometrical product specifications (GPS) — surface texture: areal — Part 2: Terms, definitions and surface texture parameters, in ISO 25178–2:2021. International Organization for Standardization: Geneva, Switzerland. 1–64
62. Gadelmawla ES, Koura MM, Maksoud TMA, et al. (2002) Roughness parameters. 123:133-145https://doi.org/10.1016/S0924-0136(02)00060-2
63. Bruce RW (2012) Handbook of lubrication and tribology, volume II: Theory and design. Vol 2 CRC press
64. Li Y, Linke BS, Voet H et al (2017) Cost, sustainability and surface roughness quality – a comprehensive analysis of products made with personal 3D printers. CIRP J Manuf Sci Technol 16:1–11. https://doi.org/10.1016/j.cirpj.2016.10.001
65. Townsend A, Senin N, Blunt L et al (2016) Surface texture metrology for metal additive manufacturing: a review. Precis Eng 46:34–47. https://doi.org/10.1016/j.precisioneng.2016.06.001
66. Launhardt M, Worz A, Loderer A et al (2016) Detecting surface roughness on SLS parts with various measuring techniques. Polym Test 53:217–226. https://doi.org/10.1016/j.polymertesting.2016.05.022
67. Krolczyk G, Raos P, Legutko S (2014) Experimental analysis of surface roughness and surface texture of machined and fused deposition modelled parts. 21:217-221
68. Leach R (2011) Optical measurement of surface topography. Vol. 8. Springer
69. Beitz S, Uerlich R, Bokelmann T, et al. (2019) Influence of powder deposition on powder bed and specimen properties. Mater. 12:https://doi.org/10.3390/ma12020297
70. Kumar K, Kumar GS (2015) An experimental and theoretical investigation of surface roughness of poly-jet printed parts: this paper explains how local surface orientation affects surface roughness in a poly-jet process. Virtual Phys Prototyping 10:23–34. https://doi.org/10.1080/17452759.2014.999218
71. Kim GD, Oh YT (2008) A benchmark study on rapid prototyping processes and machines: quantitative comparisons of mechanical properties, accuracy, roughness, speed, and material cost. 222:201–215. https://doi.org/10.1243/09544054jem724
72. Payami Golhin A, Strandlie A, John Green P (2021) The influence of wedge angle, feedstock color, and infill density on the color difference of FDM objects. J Imaging Sci Technol 65:1–15. https://doi.org/10.2352/J.ImagingSci.Technol.2021.65.5.050408
73. Grimm T, Wiora G, Witt G (2015) Characterization of typical surface effects in additive manufacturing with confocal microscopy. 3:014001
74. Sood AK, Ohdar RK, Mahapatra SS (2009) Improving dimensional accuracy of fused deposition modelling processed part using grey Taguchi method. Mater Des 30:4243–4252. https://doi.org/10.1016/j.matdes.2009.04.030
75. Livesu M, Ellero S, Martínez J, et al. (2017) From 3D models to 3D prints: an overview of the processing pipeline. in Computer Graphics Forum. Wiley Online Library.2. https://doi.org/10.1111/cgf.13147
76. Taufik M, Jain PK (2020) Part surface quality improvement studies in fused deposition modelling process: a review. Aust J Mech Eng. https://doi.org/10.1080/14484846.2020.1723342
77. Turner BN, Strong R, Gold SA (2014) A review of melt extrusion additive manufacturing processes: I. Process design and modeling. Rapid Prototyp J 20:192–204. https://doi.org/10.1108/RPJ-01-2013-0012
78. Singh D, Singh R, Boparai KS (2018) Development and surface improvement of FDM pattern based investment casting of biomedical implants: a state of art review. J Manuf Process 31:80–95. https://doi.org/10.1016/j.jmapro.2017.10.026
79. Popescu D, Zapciu A, Amza C et al (2018) FDM process parameters influence over the mechanical properties of polymer specimens: a review. Polym Test 69:157–166. https://doi.org/10.1016/j.polymertesting.2018.05.020
80. Agarwala MK, Jamalabad VR, Langrana NA, et al. (1996) Structural quality of parts processed by fused deposition. Rapid Prototyp. J. https://doi.org/10.1108/13552549610732034
81. Abdulhadi HS, Mian A (2019) Effect of strut length and orientation on elastic mechanical response of modified body-centered cubic lattice structures. Proc. Inst. Mech. Eng Part L J Mat Des Appl 233:2219–2233. https://doi.org/10.1177/1464420719841084
82. Hafsa MN, Kassim N, Ismail S et al (2018) Study on surface roughness quality of FDM and MJM additive manufacturing model for implementation as investment casting sacrificial pattern. J Mech Eng 5:25–34
83. Guessasma S, Belhabib S, Nouri H (2019) Microstructure, thermal and mechanical behavior of 3D printed acrylonitrile styrene acrylate. Macromol Mater Eng. 304:https://doi.org/10.1002/mame.201800793
84. Haque ME, Banerjee D, Mishra SB et al (2019) A numerical approach to measure the surface roughness of FDM build part. Elsevier Ltd. https://doi.org/10.1016/j.matpr.2019.07.659
85. Reddy V, Flys O, Chaparala A, et al. (2018) Study on surface texture of fused deposition modeling. Elsevier B.V.https://doi.org/10.1016/j.promfg.2018.06.108
86. Czyżewski P, Marciniak D, Nowinka B, et al. (2022) Influence of extruder's nozzle diameter on the improvement of functional properties of 3D-printed PLA products. 14:https://doi.org/10.3390/polym14020356
87. Anitha R, Arunachalam S, Radhakrishnan P (2001) Critical parameters influencing the quality of prototypes in fused deposition modelling. J Mater Process Technol 118:385–388. https://doi.org/10.1016/S0924-0136(01)00980-3
88. Srinivasan R, Ruban W, Deepanraj A, et al. (2020) Effect on infill density on mechanical properties of PETG part fabricated by fused deposition modelling. Materials Today: Proceedings https://doi.org/10.1016/j.matpr.2020.03.797
89. Xia H, Lu J, Dabiri S et al (2018) Fully resolved numerical simulations of fused deposition modeling. Part I: fluid flow Rapid Prototyp J. https://doi.org/10.1108/RPJ-12-2016-0217
90. Gebisa AW, Lemu HG (2018) Investigating effects of fused-deposition modeling (FDM) processing parameters on flexural properties of ULTEM 9085 using designed experiment. Mater. 11:https://doi.org/10.3390/ma11040500
91. Sood AK, Mahapatra S, Ohdar R (2011) Weighted principal component approach for improving surface finish of ABS plastic parts built through fused deposition modelling process. Int J Rapid Manuf 2:4–27. https://doi.org/10.1504/IJRapidM.2011.040687

92. Peng AH (2012) Methods of improving part accuracy during rapid prototyping. Adv Mater Res 430:760–763. https://doi.org/10.4028/www.scientific.net/AMR.430-432.760
93. Sugavaneswaran M, Nayak U, Saha S, et al. (2018) Additive manufacturing of fractal antenna for electronics applications. Pro-AM10.25341/D49W29
94. Wang T-M, Xi J-T, Jin Y (2007) A model research for prototype warp deformation in the FDM process. Int J Adv Manuf Technol 33:1087–1096. https://doi.org/10.1007/s00170-006-0556-9
95. Kattethota G, Henderson M (1998) A visual tool to improve layered manufacturing part quality. in 1998 International Solid Freeform Fabrication Symposium. https://doi.org/10.26153/tsw/616
96. Reeves PE, Cobb RC (1997) Reducing the surface deviation of stereolithography using in-process techniques. Rapid Prototyp. J. https://doi.org/10.1108/13552549710169255
97. Durgun I, Ertan R (2014) Experimental investigation of FDM process for improvement of mechanical properties and production cost. Rapid Prototyp. J. https://doi.org/10.1108/RPJ-10-2012-0091
98. Jiang J, Xu X, Stringer J (2018) Support structures for additive manufacturing: a review. J manuf mater process 2:64. https://doi.org/10.3390/jmmp2040064
99. Buj-Corral I, Domínguez-Fernández A, Durán-Llucià R (2019) Influence of print orientation on surface roughness in fused deposition modeling (FDM) processes. Materials 12:3834. https://doi.org/10.3390/ma12233834
100. Pandey PM, Reddy NV, Dhande SG (2003) Slicing procedures in layered manufacturing: a review. Rapid Prototyp J. https://doi.org/10.1108/13552540310502185
101. Rahmati S, Vahabli E (2015) Evaluation of analytical modeling for improvement of surface roughness of FDM test part using measurement results. Int J Adv Manuf Technol 79:823–829. https://doi.org/10.1007/s00170-015-6879-7
102. Böning G, Jahnke P, Feldhaus F et al (2020) Stepwise analysis of potential accuracy-influencing factors of iodine quantification on a fast kVp-switching second-generation dual-energy CT: from 3D-printed phantom to a simple solution in clinical routine use. Acta Radiol 61:424–431. https://doi.org/10.1177/0284185119861312
103. Pandey PM, Reddy NV, Dhande SG (2003) Real time adaptive slicing for fused deposition modelling. 43:61-71https://doi.org/10.1016/S0890-6955(02)00164-5
104. Zhao D, Guo W (2020) Mixed-layer adaptive slicing for robotic additive manufacturing (AM) based on decomposing and regrouping. J Intell Manuf 31:985–1002. https://doi.org/10.1007/s10845-019-01490-z
105. Yang L, Li S, Li Y et al (2019) Experimental investigations for optimizing the extrusion parameters on FDM PLA printed parts. J Mater Eng Perform 28:169–182. https://doi.org/10.1007/s11665-018-3784-x
106. Shirmohammadi M, Goushchi SJ, Keshtiban PM (2021) Optimization of 3D printing process parameters to minimize surface roughness with hybrid artificial neural network model and particle swarm algorithm. Progress Additive Manuf 6:199–215
107. Hooshmand MJ, Mansour S, Dehghanian A (2021) Optimization of build orientation in FFF using response surface methodology and posterior-based method. 27:967-994https://doi.org/10.1108/RPJ-07-2020-0162
108. Mendricky R, Fris D (2020) Analysis of the accuracy and the surface roughness of FDM/FFF technology and optimisation of process parameters. 27:1166–1173. https://doi.org/10.17559/TV-20190320142210
109. Saad MS, Mohd Nor A, Abd Rahim I, et al. (2022) Optimization of FDM process parameters to minimize surface roughness with integrated artificial neural network model and symbiotic organism searchhttps://doi.org/10.1007/s00521-022-07370-7
110. Jiang S, Hu K, Zhan Y, et al. (2022) Theoretical and experimental investigation on the 3D surface roughness of material extrusion additive manufacturing products. 14:https://doi.org/10.3390/polym14020293
111. García E, Núñez PJ, Chacón JM, et al. (2020) Comparative study of geometric properties of unreinforced PLA and PLA-Graphene composite materials applied to additive manufacturing using FFF technology. Polym. Test. 91:https://doi.org/10.1016/j.polymertesting.2020.106860
112. Wang P, Zou B, Ding S (2019) Modeling of surface roughness based on heat transfer considering diffusion among deposition filaments for FDM 3D printing heat-resistant resin. Appl Therm Eng 161:https://doi.org/10.1016/j.applthermaleng.2019.114064
113. García Plaza E, Núñez López PJ, Caminero Torija MÁ, et al. (2019) Analysis of PLA geometric properties processed by FFF additive manufacturing: effects of process parameters and plate-extruder precision motion. Polym. 11:https://doi.org/10.3390/polym11101581
114. De Leon AS, Dominguez-Calvo A, Molina SI (2019) Materials with enhanced adhesive properties based on acrylonitrile-butadiene-styrene (ABS)/thermoplastic polyurethane (TPU) blends for fused filament fabrication (FFF). Mater Des 182:11. https://doi.org/10.1016/j.matdes.2019.108044
115. Barrios JM, Romero PE (2019) Improvement of surface roughness and hydrophobicity in PETG parts manufactured via fused deposition modeling (FDM): an application in 3D printed self-cleaning parts. 12:https://doi.org/10.3390/ma12152499
116. Amiri A, Zolfaghari A, Shakeri M (2022) 3D printing of glass fiber reinforced acrylonitrile butadiene styrene and investigation of tensile, flexural, warpage and roughness properties. Polym Compos. https://doi.org/10.1002/pc.26937
117. Wang P, Zou B, Xiao H et al (2019) Effects of printing parameters of fused deposition modeling on mechanical properties, surface quality, and microstructure of PEEK. J Mater Process Technol 271:62–74. https://doi.org/10.1016/j.jmatprotec.2019.03.016
118. Mou YA, Koc M (2019) Dimensional capability of selected 3DP technologies. Rapid Prototyp J 25:915–924. https://doi.org/10.1108/RPJ-03-2019-0061
119. Petzold S, Klett J, Schauer A, et al. (2019) Surface roughness of polyamide 12 parts manufactured using selective laser sintering. Polym Test 80:https://doi.org/10.1016/j.polymertesting.2019.106094
120. Kim TB, Yue S, Zhang Z et al (2014) Additive manufactured porous titanium structures: through-process quantification of pore and strut networks. J Mater Process Technol 214:2706–2715. https://doi.org/10.1016/j.jmatprotec.2014.05.006
121. Kruth J-P, Levy G, Klocke F et al (2007) Consolidation phenomena in laser and powder-bed based layered manufacturing. CIRP Ann 56:730–759. https://doi.org/10.1016/j.cirp.2007.10.004
122. Van Bael S, Kerckhofs G, Moesen M et al (2011) Micro-CT-based improvement of geometrical and mechanical controllability of selective laser melted Ti6Al4V porous structures. Mater Sci Eng A 528:7423–7431. https://doi.org/10.1016/j.msea.2011.06.045
123. Allison J, Sharpe C, Seepersad CC (2017) A test part for evaluating the accuracy and resolution of a polymer powder bed fusion process. J Mech Des, Trans ASME 139:https://doi.org/10.1115/1.4037303
124. Sachdeva A, Singh S, Sharma VS (2013) Investigating surface roughness of parts produced by SLS process. Int J Adv Manuf Technol 64:1505–1516. https://doi.org/10.1007/s00170-012-4118-z

125 Yang F, Schnuerch A, Chen X (2021) Quantitative influences of successive reuse on thermal decomposition, molecular evolution, and elemental composition of polyamide 12 residues in selective laser sintering. Int J Adv Manuf Technol 115:3121–3138. https://doi.org/10.1007/s00170-021-07368-w

126. Uddin M, Williams D, Blencowe A (2021) Recycling of selective laser sintering waste Nylon powders into fused filament fabrication parts reinforced with Mg particles. 13:https://doi.org/10.3390/polym13132046

127. Akilesh M, Elango PR, Devanand AA, et al. (2018) Optimization of selective laser sintering process parameters on surface quality. in 3D Printing and Additive Manufacturing Technologies. 141–157

128 Wang X, Jiang M, Zhou Z et al (2017) 3D printing of polymer matrix composites: a review and prospective. Composites Part B: Eng 110:442–458. https://doi.org/10.1016/j.compositesb.2016.11.034

129. Yuan S, Shen F, Chua CK et al (2019) Polymeric composites for powder-based additive manufacturing: materials and applications. Prog Polym Sci 91:141–168. https://doi.org/10.1016/j.progpolymsci.2018.11.001

130. Raghunath N, Pandey PM (2007) Improving accuracy through shrinkage modelling by using Taguchi method in selective laser sintering. Int J Mach Tools Manuf 47:985–995. https://doi.org/10.1016/j.ijmachtools.2006.07.001

131. Xiong Y, Pei H, Lv Q et al (2022) A facile fabrication of PA12/CNTs nanocomposites with enhanced three-dimensional segregated conductive networks and electromagnetic interference shielding property through selective laser sintering. ACS Omega 7:4293–4304. https://doi.org/10.1021/acsomega.1c06021

132. Sofia D, Chirone R, Lettieri P et al (2018) Selective laser sintering of ceramic powders with bimodal particle size distribution. Chem Eng Res Des 136:536–547. https://doi.org/10.1016/j.cherd.2018.06.008

133. Brouwers H (2006) Particle-size distribution and packing fraction of geometric random packings. Phys Rev E 74:031309. https://doi.org/10.1103/PhysRevE.74.031309

134. Gibson I, Rosen D, Stucker B, et al. (2014) Additive manufacturing technologies. Vol. 17. Springer.

135. Chatham CA, Long TE, Williams CB (2019) A review of the process physics and material screening methods for polymer powder bed fusion additive manufacturing. Prog Polym Sci 93:68–95. https://doi.org/10.1016/j.progpolymsci.2019.03.003

136. Xia M, Nematollahi B, Sanjayan J (2019) Printability, accuracy and strength of geopolymer made using powder-based 3D printing for construction applications. Automation in Construction 101:179–189. https://doi.org/10.1016/j.autcon.2019.01.013

137. Zhu X, Yang Q (2020) Sintering the feasibility improvement and mechanical property of UHMWPE via selective laser sintering. Plast Rubber Compos. https://doi.org/10.1080/14658011.2020.1718321

138. Charoo NA, Barakh Ali SF, Mohamed EM et al (2020) Selective laser sintering 3D printing–an overview of the technology and pharmaceutical applications. Drug Dev Industr Pharmacy 46:869–877. https://doi.org/10.1080/03639045.2020.1764027

139. Goodridge RD, Dalgarno KW, Wood DJ (2006) Indirect selective laser sintering of an apatite-mullite glass-ceramic for potential use in bone replacement applications. 220:57-68https://doi.org/10.1243/095441105X69051

140. Uhlmann E, Rethmeier M, Graf B, et al. (2015) Flexible manufacturing with an additive process chain design, production and surface finish. in ASPE Spring topical meeting - achieving precision tolerances in additive manufacturing (Proceedings). Raleigh, NC, USA

141. Gao X, Abreu Faria G, Zhang W, et al. (2020) Numerical analysis of non-spherical particle effect on molten pool dynamics in laser-powder bed fusion additive manufacturing. Comput Mater Sci 179:https://doi.org/10.1016/j.commatsci.2020.109648

142. Puttonen T, Salmi M, Partanen J (2021) Mechanical properties and fracture characterization of additive manufacturing polyamide 12 after accelerated weathering. Polym Test. 104:https://doi.org/10.1016/j.polymertesting.2021.107376

143. Bibas C (2022) Lens-free optical scanners for metal additive manufacturing 74:1176–1187. https://doi.org/10.1007/s11837-021-05044-8

144. Zhan S, Guo AXY, Cao SC, et al. (2022) 3D printing soft matters and applications: a review. Int J Mol Sci. 23:https://doi.org/10.3390/ijms23073790

145. Caulfield B, Mchugh PE, Lohfeld S (2007) Dependence of mechanical properties of polyamide components on build parameters in the SLS process. J Mater Process Technol 182:477–488. https://doi.org/10.1016/j.jmatprotec.2006.09.007

146. Gibson I, Shi D (1997) Material properties and fabrication parameters in selective laser sintering process. Rapid Prototyping J. https://doi.org/10.1108/13552549710191836

147. Zhang H, Leblanc S (2018) Processing parameters for selective laser sintering or melting of oxide ceramics. In Additive Manufacturing of High-performance Metals and Alloys-Modeling and Optimization, I. Shishkovsky, Editor., IntechOpen. 1–44

148. Lupone F, Padovano E, Casamento F, et al. (2022) Process phenomena and material properties in selective laser sintering of polymers: a review. 15:https://doi.org/10.3390/ma15010183

149. Liu W, Zhu ZC, Ye SH et al (2019) Investigation of professional design practice: a framework for designing plastic consumer products for additive manufacturing. Int J Mater Prod Technol 58:104–128. https://doi.org/10.1504/ijmpt.2019.097663

150. Yaagoubi H, Abouchadi H, Taha Janan M (2021) Numerical simulation of heat transfer in the selective laser sintering process of Polyamide. Energy Reports 12(7):189–199. https://doi.org/10.1016/j.egyr.2021.08.089

151. Strobbe D, Dadbakhsh S, Verbelen L et al (2018) Selective laser sintering of polystyrene: a single-layer approach. Plast Rubber Compos 47:2–8. https://doi.org/10.1080/14658011.2017.1399532

152. Borille AV, De Oliveira GJ, Lopes D (2017) Geometrical analysis and tensile behaviour of parts manufactured with flame retardant polymers by additive manufacturing. Rapid Prototyping J 23:169–180. https://doi.org/10.1108/RPJ-09-2015-0130

153. Wörz A, Drummer D (2018) Tribological anisotropy of selective laser sintered PA12 parts. Polym Test 70:117–126. https://doi.org/10.1016/j.polymertesting.2018.06.028

154. Modi YK, Sanadhya S (2018) Design and additive manufacturing of patient-specific cranial and pelvic bone implants from computed tomography data. J Braz Soc Mech Sci Eng 40:https://doi.org/10.1007/s40430-018-1425-9

155. Kinstlinger IS, Bastian A, Paulsen SJ, et al. (2016) Open-Source Selective Laser Sintering (OpenSLS) of nylon and biocompatible polycaprolactone. PLoS ONE 11:https://doi.org/10.1371/journal.pone.0147399

156. Ellis A, Brown R, Hopkinson N (2015) The effect of build orientation and surface modification on mechanical properties of high speed sintered parts. Surf Topogr Metrol Prop. 3:https://doi.org/10.1088/2051-672X/3/3/034005

157. Xu Z, Wang Y, Wu D et al (2019) The process and performance comparison of polyamide 12 manufactured by multi jet fusion and selective laser sintering. J Manuf Processes 47:419–426. https://doi.org/10.1016/j.jmapro.2019.07.014

158. Goodridge RD, Tuck CJ, Hague RJM (2012) Laser sintering of polyamides and other polymers. Prog Mater Sci 57:229–267. https://doi.org/10.1016/j.pmatsci.2011.04.001

159. Glückstad J, Palima D (2017) Light robotics: structure-mediated nanobiophotonics. Elsevier
160. Bártolo PJ (2011) Stereolithography: materials, processes and applications. Springer Science & Business Media.
161. Ribo MM (2020) Vat photopolymerization process chain. Technical University of Denmark, Kgs. Lyngby
162. Renap K, Kruth J-P (1995) Recoating issues in stereolithography. Rapid Prototyp. J. https://doi.org/10.1108/13552549510094223
163. Santoliquido O, Colombo P, Ortona A (2019) Additive manufacturing of ceramic components by digital light processing: a comparison between the "bottom-up" and the "top-down" approaches. J Eur Ceram Soc 39:2140–2148. https://doi.org/10.1016/j.jeurceramsoc.2019.01.044
164. Pedersen DB, Zhang Y, Nielsen JS, et al. (2016) A self-peeling vat for improved release capabilities during DLP materials processing. in 2nd International Conference on Progress in Additive Manufacturing. Research Publishing Services
165. Barone S, Neri P, Paoli A, et al. (2019) Development of a DLP 3D printer for orthodontic applications. in Procedia Manufacturing. https://doi.org/10.1016/j.promfg.2020.01.187
166. Ribó MM, Islam A (2017) 3D printing of bio-inspired surfaces. in Wilhelm und Else Heraeus Seminar: Bio-inspired, Nano-and Microstructured Surfaces: New Functionality by Material and Structure.
167. Thompson MK, Mischkot M (2015) Design of test parts to characterize micro additive manufacturing processes. Elsevier. https://doi.org/10.1016/j.procir.2015.07.065
168. Zhou JG, Herscovici D, Chen CC (2000) Parametric process optimization to improve the accuracy of rapid prototyped stereolithography parts. Int J Mach Tools Manuf 40:363–379. https://doi.org/10.1016/S0890-6955(99)00068-1
169. Salonitis K (2014) Stereolithography. in Comprehensive materials processing, S. Hashmi, Editor., Elsevier Ltd. 19–67
170. Khorasani ER, Baseri H (2013) Determination of optimum SLA process parameters of H-shaped parts. J Mech Sci Technol 27:857–863. https://doi.org/10.1007/s12206-013-0111-1
171. Pagac M, Hajnys J, Ma Q-P, et al. (2021) A review of vat photopolymerization technology: materials, applications, challenges, and future trends of 3D printing. 13:598. https://doi.org/10.3390/polym13040598
172. Arnold C, Monsees D, Hey J, et al. (2019) Surface quality of 3D-printed models as a function of various printing parameters. 12:https://doi.org/10.3390/ma12121970
173. Khodaii J, Rahimi A (2020) Improving the surface roughness in stereolithography by controlling surface angle, hatch spaces, and postcuring time. 2:e12193. https://doi.org/10.1002/eng2.12193
174. Bagheri A, Jin J (2019) Photopolymerization in 3D printing. ACS Appl Polym Mater 1:593–611. https://doi.org/10.1021/acsapm.8b00165
175. Rosen DW (2008) Stereolithography and rapid prototyping. in BioNanoFluidic MEMS. p. 175–196
176. Hanemann T, Honnef K (2018) Optical and thermomechanical properties of doped polyfunctional acrylate copolymers. 10:337https://doi.org/10.3390/polym10030337
177. Corbel S, Dufaud O, Roques-Carmes T (2011) Materials for stereolithography. in Stereolithography: Materials, Processes and Applications, P.J. Bártolo, Editor., Springer US: Boston, MA. 141–159
178. Crivello JV, Reichmanis E (2014) Photopolymer materials and processes for advanced technologies. Chem Mater 26:533–548. https://doi.org/10.1021/cm402262g
179. Shaukat U, Rossegger E, Schlögl S (2022) A review of multimaterial 3D printing of functional materials via vat photopolymerization. 14:2449. https://doi.org/10.3390/polym14122449
180. Manapat JZ, Chen Q, Ye P, et al. (2017) 3D printing of polymer nanocomposites via stereolithography. Macromol Mater Eng 302:https://doi.org/10.1002/mame.201600553
181. Peer G, Eibel A, Gorsche C, et al. (2019) Ester-activated vinyl ethers as chain transfer agents in radical photopolymerization of methacrylates. 52:2691-2700https://doi.org/10.1021/acs.macromol.9b00085
182. Diptanshu MG, Ma C (2019) Vat photopolymerization 3D printing of ceramics: effects of fine powder. Manuf Let 21:20–23. https://doi.org/10.1016/j.mfglet.2019.07.001
183. Medellin A, Du W, Miao G, et al. (2019) Vat photopolymerization 3D printing of nanocomposites: a literature review. J. Micro Nano-Manuf. 7:https://doi.org/10.1115/1.4044288
184. Kowsari K, Zhang B, Panjwani S, et al. (2018) Photopolymer formulation to minimize feature size, surface roughness, and stair-stepping in digital light processing-based three-dimensional printing. 24:627–638. https://doi.org/10.1016/j.addma.2018.10.037
185. Srinivasan M, Kalberer N, Kamnoedboon P et al (2021) CAD-CAM complete denture resins: an evaluation of biocompatibility, mechanical properties, and surface characteristics. J Dent 114:103785. https://doi.org/10.1016/j.jdent.2021.103785
186. Miedzińska D, Gieleta R, Popławski A (2020) Experimental study on influence of curing time on strength behavior of sla-printed samples loaded with different strain rates. 13:5825https://doi.org/10.3390/ma13245825
187. Zips S, Hiendlmeier L, Weiß LJK et al (2020) Biocompatible, flexible, and oxygen-permeable silicone-hydrogel material for stereolithographic printing of microfluidic lab-on-a-chip and cell-culture devices. ACS Appl Polym Mater 3:243–258. https://doi.org/10.1021/acsapm.0c01071
188. Park HK, Shin M, Kim B et al (2018) A visible light-curable yet visible wavelength-transparent resin for stereolithography 3D printing. NPG Asia Mater 10:82–89. https://doi.org/10.1038/s41427-018-0021-x
189. Zuchowicz NC, Belgodere JA, Liu Y, et al. (2022) Low-cost resin 3-D printing for rapid prototyping of microdevices: Opportunities for supporting aquatic germplasm repositories. 7:49. https://doi.org/10.3390/fishes7010049
190. Takada K, Sun H-B, Kawata S (2005) Improved spatial resolution and surface roughness in photopolymerization-based laser nanowriting. Appl Phys Lett 86:071122. https://doi.org/10.1063/1.1864249
191. Janusziewicz R, Tumbleston JR, Quintanilla AL et al (2016) Layerless fabrication with continuous liquid interface production. Proc Natl Acad Sci U S A 113:11703–11708. https://doi.org/10.1073/pnas.1605271113
192. Tumbleston JR, Shirvanyants D, Ermoshkin N et al (2015) Continuous liquid interface production of 3D objects. Science 347:1349–1352. https://doi.org/10.1126/science.aaa2397
193. Yao H, Wang J, Mi S (2017) Photo Sprocessing for biomedical hydrogels design and functionality: a review. 10:11https://doi.org/10.3390/polym10010011
194. Eiríksson ER (2018) Computer vision for additive manufacturing, in DTU Compute. Technical University of Denmark: Kgs. Lyngby
195. Steyrer B, Busetti B, Harakály G et al (2018) Hot lithography vs. room temperature DLP 3D-printing of a dimethacrylate. Addit Manuf 21:209–214. https://doi.org/10.1016/j.addma.2018.03.013
196. Kim I, Kim S, Andreu A, et al. (2022) Influence of dispersant concentration toward enhancing printing precision and surface quality of vat photopolymerization 3D printed ceramics. 52:https://doi.org/10.1016/j.addma.2022.102659

197. Dulieu-Barton J, Fulton M (2000) Mechanical properties of a typical stereolithography resin. 36:81-87https://doi.org/10.1111/j.1475-1305.2000.tb01177.x
198. Luo X, Li J, Lucas M (2017) Galvanometer scanning technology for laser additive manufacturing. SPIE. https://doi.org/10.1117/12.2252973
199. Yang Q, Lu Z, Zhou J et al (2017) A novel method for improving surface finish of stereolithography apparatus. Int J Adv Manuf Technol 93:1537–1544. https://doi.org/10.1007/s00170-017-0529-1
200. Hui J, Yan Z, Lv J, et al. (2022) An investigation on energy consumption and part quality of stereolithography apparatus manufactured parts. 28:52-67https://doi.org/10.1108/RPJ-06-2020-0143
201. Mostafa KG, Nobes DS, Qureshi AJ (2020) Investigation of light-induced surface roughness in projection micro-stereolithography additive manufacturing (PμSLA). in Procedia CIRP. https://doi.org/10.1016/j.procir.2020.05.177
202. Shanmugasundaram SA, Razmi J, Mian MJ, et al. (2020) Mechanical anisotropy and surface roughness in additively manufactured parts fabricated by stereolithography (SLA) using statistical analysis. 13:https://doi.org/10.3390/ma13112496
203. Zhao J, Yang Y, Li L (2020) A comprehensive evaluation for different post-curing methods used in stereolithography additive manufacturing. 56:867-877https://doi.org/10.1016/j.jmapro.2020.04.077
204. Kazemi M, Rahimi A (2019) Improving the efficiency of fabrication of AM parts by segmentation design in DLP process. Rapid Prototyping J 25:1155–1168. https://doi.org/10.1108/RPJ-09-2018-0253
205. Kim N, Bhalerao I, Han D, et al. (2019) Improving surface roughness of additively manufactured parts using a photopolymerization model and multi-objective particle swarm optimization. Appl Sci. 9:https://doi.org/10.3390/app9010151
206. Milde J, Peterka J, Jurina F, et al. (2021) Influence of selected photopolymers on the resulting accuracy and surface roughness of the component in digital light processing technology. in Annals of DAAAM and Proceedings of the International DAAAM Symposium. https://doi.org/10.2507/32nd.daaam.proceedings.034
207. Reeves P, Cobb R (1997) Surface roughness investigation of Stereolithography ACES components. in Proceedings of the Second National Conference on Rapid Prototyping and Tooling Research.
208. Andrzejewska E, Andrzejewski M (1998) Polymerization kinetics of photocurable acrylic resins. J Polym Sci A Polym Chem 36:665–673. https://doi.org/10.1002/(SICI)1099-0518(199803)36:4%3c665::AID-POLA15%3e3.0.CO;2-K
209. Puebla K, Arcaute K, Quintana R et al (2012) Effects of environmental conditions, aging, and build orientations on the mechanical properties of ASTM type i specimens manufactured via stereolithography. Rapid Prototyping J 18:374–388. https://doi.org/10.1108/13552541211250373
210. Hague R, Mansour S, Saleh N, et al. (2004) Materials analysis of stereolithography resins for use in rapid manufacturing. 39:2457-2464https://doi.org/10.1023/B:JMSC.0000020010.73768.4a
211. Payami Golhin A, Srivastava C, Strandlie A et al (2023) Effects of accelerated aging on the appearance and mechanical performance of materials jetting products. Mater Design 228:111863. https://doi.org/10.1016/j.matdes.2023.111863
212. Baharnezhad S, Golhin A (2017) In-situ measurement and finite element simulation of thermo-mechanical properties of AA 6063 aluminum alloy for MIG weldment. Mater Phys Mech 32:222–236. https://doi.org/10.18720/MPM.3222017_15
213. Payami Golhin A, Strandlie A (2023) Appearance evaluation of digital materials in material jetting. Opt Lasers Eng 68:107632. https://doi.org/10.1016/j.optlaseng.2023.107632
214. Liravi F, Salarian M, Dal Castel C et al (2019) High-speed material jetting additive manufacturing of silicone structures: mechanical characterization. Prog Addit Manuf 4:479–495. https://doi.org/10.1007/s40964-019-00097-3
215. Suresh Babu A, Binish KM, Jaivignesh M et al (2018) Modelling of functional gradient porous structure and its fabrication using additive manufacturing process. Elsevier Ltd. https://doi.org/10.1016/j.matpr.2018.10.253
216. Tan WS, Suwarno SR, An J et al (2017) Comparison of solid, liquid and powder forms of 3D printing techniques in membrane spacer fabrication. J Membr Sci 537:283–296. https://doi.org/10.1016/j.memsci.2017.05.037
217. Holman RK, Cima MJ, Uhland SA et al (2002) Spreading and infiltration of inkjet-printed polymer solution droplets on a porous substrate. J Colloid Interface Sci 249:432–440. https://doi.org/10.1006/jcis.2002.8225
218. Yang H, Lim JC, Liu Y, et al. (2017) Performance evaluation of ProJet multi-material jetting 3D printer. 12:95–103. https://doi.org/10.1080/17452759.2016.1242915
219. Khoshkhoo A, Carrano AL, Blersch DM (2018) Effect of build orientation and part thickness on dimensional distortion in material jetting processes. Rapid Prototyping J 24:1563–1571. https://doi.org/10.1108/RPJ-10-2017-0210
220. Singh Tomar RP, Ulu FI, Kelkar A et al (2019) Investigation of process induced variations in polyjet printing with digital polypropylene via homogeneous 3D tensile test coupon. Am Soc Mech Eng (ASME). https://doi.org/10.1115/IMECE2019-11639
221. Liravi F, Toyserkani E (2018) Additive manufacturing of silicone structures: a review and prospective. Addit Manuf 24:232–242. https://doi.org/10.1016/j.addma.2018.10.002
222. Giorleo L, Stampone B, Trotta G (2022) Micro injection moulding process with high-temperature resistance resin insert produced with material jetting technology: effect of part orientation. 56:https://doi.org/10.1016/j.addma.2022.102947
223. Wei X, Bhardwaj A, Zeng L, et al. (2019) Experimental investigation of stratasys J750 polyjet printer: effects of finish type and shore hardness on surface roughness. in ASME 2019 14th International Manufacturing Science and Engineering Conference, MSEC 2019. https://doi.org/10.1115/MSEC2019-2998
224. Cheng YL, Huang KC (2020) Preparation and characterization of color photocurable resins for full-color material jetting additive manufacturing. Polymers (Basel) 12:650. https://doi.org/10.3390/polym12030650
225. Jabari E, Liravi F, Davoodi E et al (2020) High speed 3D material-jetting additive manufacturing of viscous graphene-based ink with high electrical conductivity. Addit Manuf 35:101330. https://doi.org/10.1016/j.addma.2020.101330
226. Furbank RJ, Morris JF (2004) An experimental study of particle effects on drop formation. Phys Fluids 16:1777–1790. https://doi.org/10.1063/1.1691034
227. Zhou W, Loney D, Degertekin FL, et al. (2013) What controls dynamics of droplet shape evolution upon impingement on a solid surface? 59:3071–3082. https://doi.org/10.1002/aic.14050
228. Raman KA, Birgersson E, Sui Y et al (2020) Electrically induced droplet ejection dynamics under shear flow. Phys Fluids 32:032103. https://doi.org/10.1063/1.5143757
229. Yap YL, Wang C, Sing SL et al (2017) Material jetting additive manufacturing: an experimental study using designed metrological benchmarks. Precis Eng 50:275–285. https://doi.org/10.1016/j.precisioneng.2017.05.015
230. Cheng YL, Chang CH, Kuo C (2020) Experimental study on leveling mechanism for material-jetting-type color 3D printing. 26:11–20. https://doi.org/10.1108/RPJ-09-2018-0227
231. Payami Golhin A (2021) Generation of micro-and nano-textured surfaces. European Commission: Brussels. 1–6. https://doi.org/10.5281/zenodo.7293168

232. Bussmann M, Chandra S, Mostaghimi J (2000) Modeling the splash of a droplet impacting a solid surface. Phys Fluids 12:3121–3132. https://doi.org/10.1063/1.1321258
233. Howland CJ, Antkowiak A, Castrejón-Pita JR et al (2016) It's harder to splash on soft solids. Phys Rev Lett 117:184502. https://doi.org/10.1103/PhysRevLett.117.184502
234. Mohammad Karim A, Suszynski WJ (2022) Physics of dynamic contact line: hydrodynamics theory versus molecular kinetic theory. 7:318https://doi.org/10.3390/fluids71003178
235. Tofan-Negru A, Barbu C, Stefan A, et al. (2021) Analysis and characterization of additive manufacturing processes. 13:167–180. https://doi.org/10.13111/2066-8201.2021.13.4.14
236. Miyanaji H, Momenzadeh N, Yang L (2019) Effect of powder characteristics on parts fabricated via binder jetting process. Rapid Prototyping J 25:332–342. https://doi.org/10.1108/RPJ-03-2018-0069
237. Gülcan O, Günaydın K, Çelik A (2022) Investigation on surface roughness of polyjet-printed airfoil geometries for small UAV applications. 9:https://doi.org/10.3390/aerospace9020082
238. Yuan J, Chen C, Yao D, et al. (2020) 3D printing of oil paintings based on material jetting and its reduction of staircase effect. 12:1–12. https://doi.org/10.3390/polym12112536
239. Pandey P, Nayak A, Taufik M (2022) Evaluation of mathematical models for surface roughness prediction of PolyJet 3D printed parts. https://doi.org/10.1080/2374068X.2022.2097416
240. Zmarzły P, Kozior T, Gogolewski D (2019) Dimensional and shape accuracy of foundry patterns fabricated through photocuring. Teh Vjesn 26:1576–1584. https://doi.org/10.17559/TV-20181109115954
241. Kechagias J, Iakovakis V, Giorgo E, et al. (2014) Surface roughness optimization of prototypes produced by polyjet direct 3D printing technology. In OPT-i 2014 - 1st International Conference on Engineering and Applied Sciences Optimization, Proceedings.
242. Cazón A, Morer P, Matey L (2014) PolyJet technology for product prototyping: tensile strength and surface roughness properties. 228:1664-1675https://doi.org/10.1177/0954405413518515
243. Udroiu R, Mihail L (2009) Experimental determination of surface roughness of parts obtained by rapid prototyping. 9:283-286
244. Velasco MA, Lancheros Y, Garzón-Alvarado DA (2016) Geometric and mechanical properties evaluation of scaffolds for bone tissue applications designing by a reaction-diffusion models and manufactured with a material jetting system. J Comput Des Eng 3:385–397. https://doi.org/10.1016/j.jcde.2016.06.006
245. Chand R, Sharma VS, Trehan R, et al. (2022) Investigating the dimensional accuracy and surface roughness for 3D printed parts using a multi-jet printer. https://doi.org/10.1007/s11665-022-07153-0
246. Tasch D, Schagerl M, Wazel B, et al. (2019) Impact behavior and fractography of additively manufactured polymers: laser sintering, multijet fusion, and hot lithography. Addit Manuf 29:https://doi.org/10.1016/j.addma.2019.100816
247. Raigar J, Sharma VS, Srivastava S, et al. (2020) A decision support system for the selection of an additive manufacturing process using a new hybrid MCDM technique. 45:https://doi.org/10.1007/s12046-020-01338-w
248. Gomez-Torrent A, Teberio F, Martinez A, et al. (2017) A study of the additive manufacturing technology for RF/microwave components. Institute of Electrical and Electronics Engineers Inc.https://doi.org/10.23919/EuCAP.2017.7928732
249. Bodaghi M, Mobin M, Ban D, et al. (2022) Surface quality of printed porous materials for permeability rig calibration. 37:548-558https://doi.org/10.1080/10426914.2021.1960994
250. Unkovskiy A, Spintzyk S, Kiemle T, et al. (2022) Trueness and precision of skin surface reproduction in digital workflows for facial prosthesis fabricationhttps://doi.org/10.1016/j.prosdent.2021.06.050
251. Hanon MM, Zsidai L (2020) Sliding surface structure comparison of 3D printed polymers using FDM and DLP technologies. in IOP Conference Series: Materials Science and Engineering. https://doi.org/10.1088/1757-899X/749/1/012015
252. Nazir A, Jeng JY (2019) A high-speed additive manufacturing approach for achieving high printing speed and accuracy. Proc Inst Mech Eng Part C J Mech Eng Sci. https://doi.org/10.1177/0954406219861664
253. Jiao F, Cheng K (2014) An experimental investigation on micro-milling of polymethyl methacrylate components with nanometric surface roughness. 228:790-796https://doi.org/10.1177/0954405413507251
254. Whitaker TA, Simões-Franklin C, Newell FN (2008) Vision and touch: independent or integrated systems for the perception of texture? Brain Res 1242:59–72. https://doi.org/10.1016/j.brainres.2008.05.037
255. Parraman C, Segovia MVO (2018) 2.5 D printing: bridging the gap between 2D and 3D applications. John Wiley & Sons.
256. Ansari N, Payami Z, Feghhi F (2020) Synthesis of iron/graphene composites with controlled magnetization by electrochemical exfoliation/deposition using sodium dodecyl sulfate as surfactant. J Magn Magn Mater 500:166398. https://doi.org/10.1016/j.jmmm.2020.166398
257. Ansari N, Payami Z (2020) Synthesis of magnetic graphene-Fe3O4 nanocomposites by electrochemical exfoliation method. J Nanostructures 10:39–43. https://doi.org/10.22052/JNS.2020.01.005
258. Rafiee F, Khavari P, Payami Z et al (2019) Palladium nanoparticles immobilized on the magnetic few layer graphene support as a highly efficient catalyst for ligand free Suzuki cross coupling and homo coupling reactions. J Organomet Chem 883:78–85. https://doi.org/10.1016/j.jorganchem.2019.01.014
259. Golhin AP, Kamrani S, Fleck C, et al (2022) Corrosion protection of Mg-SiC nanocomposite through plasma electrolytic oxidation coating process. Mater Corros 73:1813–1825. https://doi.org/10.1002/maco.202213118
260. Payami-Golhin A, Amrooni Hossaini M, Eslami-Farsani R, et al. (2014) Phosphate-free protective nanoceramic coatings for galvanized steel sheet with H2O2 additive. Adv Mater Res 29:436–440. https://doi.org/10.4028/www.scientific.net/AMR.829.436
261. Zindani D, Kumar K (2019) An insight into additive manufacturing of fiber reinforced polymer composite. Int j lightweight mater manuf 2:267–278. https://doi.org/10.1016/j.ijlmm.2019.08.004
262. Payami Golhin A, Srivastava C, Tingstad JF, et al. (2022) Additive manufacturing of multilayered polymer composites: durability assessment. In: Proceedings of the 20th European Conference on Composite Materials-Composites Meet Sustainability (Vol 1–6). Lausanne, Switzerland: EPFL Lausanne, Composite Construction Laboratory Switzerland. https://doi.org/10.5075/epfl-298799_978-2-9701614-0-0
263. Rafiee M, Farahani RD, Therriault D (2020) Multi-material 3D and 4D printing: a survey. Adv Sci 7:1902307. https://doi.org/10.1002/advs.201902307
264. González-Henríquez CM, Sarabia-Vallejos MA, Rodriguez-Hernandez J (2019) Polymers for additive manufacturing and 4D-printing: materials, methodologies, and biomedical applications. Prog Polym Sci 94:57–116. https://doi.org/10.1016/j.progpolymsci.2019.03.001